CRYSTAL CHEMISTRY AND PROPERTIES OF DOUBLE METAL NITRIDE IN THE TiN-AlN SYSTEM

The Institute of Scientific and Industrial Research

Osaka University

Suguru Inamura

Contents

CHAPTER I GENERAL INTRODUCTION

I-1. Metal nitrides

At present, the number of known chemical elements exceeds one hundred. Let us imagine that if each one had combined with each of the others to form a single binary compound, there would be approximately five thousand such compounds. In fact, although not all elements combine with all the others, some do combine to form more than one compound. This is true of many pairs of metals. Some examples chosen at random, include:

YB_2, YB_4, YB_6, YB_{12} and YB_{66};

$Mn_{23}C_6$, Mn_3C, Mn_5C_2 and Mn_7C_3;

Mn_2N_3, MnN, Mn_6N_5, Mn_3N_2, Mn_2N and Mn_4N;

Ti_3O, Ti_2O, TiO, Ti_2O_3, Ti_3O_5 and TiO_2.

Thus, the number of binary compounds alone is evidently considerable. Actually, there is an indefinitely large number of compounds built of atoms of three or more elements.

All elements and compounds can be solidified under appropriate conditions of temperature and pressure, and the properties and structures of resulting solids show that we must recognize four extreme types of bonding:

(a) the ionic bond in crystalline salts, such as NaCl or CaF_2,

(b) the covalent bond in non-ionizable molecules and in crystals such as diamond,

(c) the metallic bond in metals and intermetallic compounds (alloys),

which is responsible for their characteristic optical and electrical properties, and

(d) the much weaker van der Waals bond between chemically saturated molecules.

Many real crystals don't have only one bonding type, as described from (a) to (d), but do have a mixed bonding character of some types. Reflecting their bond natures, various properties can appear.

Most of the simple metal oxides structures can be built up on the basis of nearly close-packed oxygen ions, with cations placed in the available interstices, which are mainly octahedral or tetrahedral interstices. The structures of carbides and nitrides are characterized mainly by the small size of the carbon and nitrogen atoms which can readily fit into interstitial positions. Consequently, most of transition metal carbides and nitrides tend to have closed packed metal atoms with carbon and nitrogen atoms in the interstices. The metal-carbon and metal-nitrogen bonding in these structures is classified intermediate between covalent and metallic. The metal-nitrogen bonding is usually more covalent in nature than the metal-carbon bonds.

The number of oxides and sulfides found in the earth's crust is extremely large if compared to the case of nitrides. In earlier 19th-century, nitrides have been paid little attention in the field of basic science and technology. Recently, some nitrides, as Si_3N_4, BN, etc., have been spotlighted as important materials, since efficient methods to prepare them and other high quality performance nitrides have been developed. Therefor, nitrides is an interesting subject that is being systematically studied in many research laboratories.

Table 1-1. PERIODIC TABLE OF NITRIDES

Ia	IIa	IIIa	IVa	Va	VIa	VIIa	(VIII)			Ib	IIb	IIIb	IVb	Vb
Li_3N	Be_3N_2											BN		
Na_3N	Mg_3N_2											AlN	Si_3N_4	PN P_3N_5
—	Ca_3N_2 Ca_2N Ca_3N_4 $Ca_{11}N_8$	ScN	TiN Ti_2N	VN V_2N V_3N	CrN Cr_2N	Mn_3N_2 Mn_2N Mn_4N Mn_2N_3 Mn_6N_5 MnN	Fe_2N, Fe_3N, Fe_4N, Fe_8N,	Co_3N_2, Co_2N, Co_3N, Co_4N CoN	Ni_3N_2 Ni_3N Ni_4N	Cu_3N	Zn_3N_2	GaN	Ge_3N_4	
—	Sr_3N_2	YN	ZrN	NbN Nb_2N Nb_4N_3	Mo_2N MoN $Mo_{16}N_7$	TcN	—	—	—		Cd_3N_2	InN		
—	Ba_3N_2	LaN	HfN Hf_4N_3 Hf_3N_2	TaN Ta_2N Ta_3N_5	W_2N	Re_2N	—	—	—	—	Hg_3N_2	TlN		

— : non

Ceramic nitrides having good properties for special applications have been developed... Most elements combine with nitrogen as shown in Table 1-1. These nitride's list includes some stable compounds, such as aluminum nitride (a laboratory-use refractory material for melting aluminum), silicon nitride (a commercially important new refractory) and cubic boron nitride (a refractory in its most common form and a potential abrasive material) which is formed at extremely high pressures and temperatures.

I-1-1. Chemical bonding and crystal structure of nitrides

Metal nitrides have a wide range of chemical bond depending on kinds of metal atoms. We classify metal nitrides into three groups, i.e. ionic, covalent and metallic crystals, but it should be emphasized that there is no sharp boundary lines among the three bond natures. The characteristics of each group are description belows.

Ionic nitrides

Ionic nitrides which have intense ionic character are composed of the IA or IIA group elements and nitrogens, and their chemical formulas are represented as M_3N (M = element) or M_3N_2, respectively. Nitrides of the alkali metals other than Li do not appear to be known in a pure state. The simple structure assigned to Li_3N is peculiar to this compound. The coordination of Li^+ in Li_3N is related to the very small size of this ion compared with N^{3-}, i.e. a structure with tetrahedral coordination of Li^+ is geometrically impossible. One third of Li^+ ions have 2 nearest N neighbors (at 0.194nm) and the remainders have 3 nitrogen neighbors (at 0.211nm). The

N^{3-} ion is surrounded by 2 Li^{+} at 0.194nm and 6 more at 0.211nm, while Cu_3N has an anti-ReO_3 structure, in which Cu+ ions are coordinated with two nitrogens. This structure reflects a large contribution of covalent bonding in the Cu-N bond.

The nitrides M_3N_2 (M = Be, Mg, Zn, Cd), and α -Ca_3N_2 have the anti-Mn_2O_3 structure, in which the metal ions have 4 tetrahedral neighbors and N has two types of distorted octahedral coordination groups. The radius of the N^{3-} ion in these nitrides would appear to be close to 0.15nm, i.e., larger than most metal ions. These compounds are the analogous of the oxides, and form transparent colorless crystals. They are formed by direct reaction of the metal with nitrogen, or in some cases by heating the amide.

$$3\ Ba(NH_2)_2 \rightarrow\ Ba_3N_2 + 4\ NH_3$$

The nitrides have high melting points, ranging from 900℃ (Ca_3N_2) to 2200℃ (Be_3N_2) and are hydrolyzed by water to the hydroxides with liberation of ammonia.

Thus, Ca forms Ca_3N_2, one form of which (alpha) is anti-Mn_2O_3 structure, but there are also black and yellow forms of the same compound. Moreover, Ca also forms Ca_2N, Ca_3N_4, and $Ca_{11}N_8$. Ca_2N forms lustrous green-black crystals with the anti-$CdCl_2$ (layer) structure, in which the Ca-Ca distances within the layer (0.323 and 0.364nm) are much shorter than in metallic Ca (0.388 and 0.395nm). Nevertheless this is apparently an ionic compound, for the action of water produces NH_3+H_2. The luster and semiconductivity suggest formulation as $Ca^{2+}{}_2N^{3-}(e^-)$.

In addition to the binary nitrides described here, some ternary nitrides have been prepared, for example, Li_5TiN_3, Li_7NbN_4, and Li_9CrN_5, all with a fluorite type of structure (superstructure in most cases), and

alkaline-earth compounds with Re, Os, Mo, or W (e.g. $Sr_9Re_3N_{10}$, Ca_5MoN_5).

Covalent nitrides

In contrast to the ionic Zn or Cd nitrides, the chocolate-coloured explosive Hg_3N_2 made from HgI_2 and KNH_2 in liquid ammonia, is presumably a covalent compound. For the B, Al, Ga, In and Tl nitrides, the geometrical possibilities are the same as for carbides with average of 4 valence electrons per atom in MN.

Boron nitride has been known for a long time as a white powder of great chemical stability and high melting point with a graphite-like layer structure. It has been prepared with the zinc-blend structure by subjecting it most ordinary form to a pressure of 6GPa at 1400-1800℃ . This form, so called "borazon", is very much more dense, 3.47g/cm^3 as compared with 2.25g/cm^3 for the ordinary form. The structure of the Al, Ga, and In nitrides (Group III elements) are the zinc-blende type. While BN is presumably a covalent compound, the bonds in AlN, GaN and InN would have appreciable ionic character, and the compounds with a heavier Group V elements are essentially metallic compounds, such as InBi. The structure of $BeSiN_2$ is a superstructure of the wurtzite structure of AlN, etc..

The structure of several nitrides with chemical composition of M_3N_4 are known. For example, both Si_3N_4 and Ge_3N_4 have two polymorphous. The structure of both compounds is closely related to that of Be_2SiO_4 (phenacite); M has 4 tetrahedral, surrounded by 4 N neighbors and so, N forms coplanar bonds up to 3 M atoms. There is appreciable ionic character in the bonds in Ge_3N_4 and also in Th_3N_4. In particular, Si_3N_4 has potentially wide application via its good friction and wear resistance at

ambient temperatures or good thermal shock and oxidation resistance required for elevated temperature use[5].

Nitrides of transition metals

Some of these compounds are extremely numerous, because more than one nitride can be formed by many transition metals. For example, five distinct phases (apart from the solid solution in the metal) have been identified in the Nb-N system. On the other hand, within the so-called 'interstitial' nitrides the metal atoms are approximately, or in some cases exactly, close-packed (as in ScN, YN, TiN, ZrN, VN, and rare-earth nitrides with the NaCl structure), but the arrangement of metal atoms in these compounds is generally not the same as in the pure metal.

I-1-2. Properties of nitrides

Nitrogen has lower activity of ionization than oxygen, and so the chemical bonding state originated in nitrides is affected by alternating its partner element. Moreover, reflecting the chemical bonding state, the properties of nitrides are varied in many respects. In particular, most of the transition-metal nitrides of the forth and fifth groups in the periodic table have extremely high melting points (2000-4000℃) and these compounds are, therefore, frequently referred to as "refractory nitrides", which have plenty of useful applications. Beside, most of the transition-metal nitrides are metallic in electric conductivity. In contrast, ionic nitrides composed of the IA or IIA elements are insulators. Most of nitrides of IIIB and IVB elements are semiconductors.

I-2. Historical background of TiN and AlN

Both titanium nitride and aluminum nitride are attractive as high-temperature materials. Titanium nitride has already been applied as cutting tool and as coating material, due to both high hardness and high thermal conductivity at high temperature. Aluminum nitride has been intended for applications such as a substrate material for semiconductors because of the high insulating property and high thermal conductivity. AlN also has another possibility to be applied to window with high transmittance in the wide range of wavelength at high temperature. However, the properties of both titanium nitride and aluminum nitride are quite different each other because of the differences in crystal structure and in bond nature.

I-2-1. Titanium nitride

Metal nitrides have attracted considerable attention as engineering ceramics, i.e. for its application as high temperature structural materials, cutting tools, passivation films and so on. Among them, titanium nitride TiN, has been widely used as a hard coating material for cutting tools, good wear resistance materials and as a gold color film deposited on several accessories. However, a main disadvantage for TiN is that it rapidly oxidizes to TiO_2 above 550℃ , in the open air.

$TiN_{0.58}$ could be prepared[6] by heating Ti film to 750℃ for 1 hour, under nitrogen gas flow. Recently, many kinds of methods for preparation

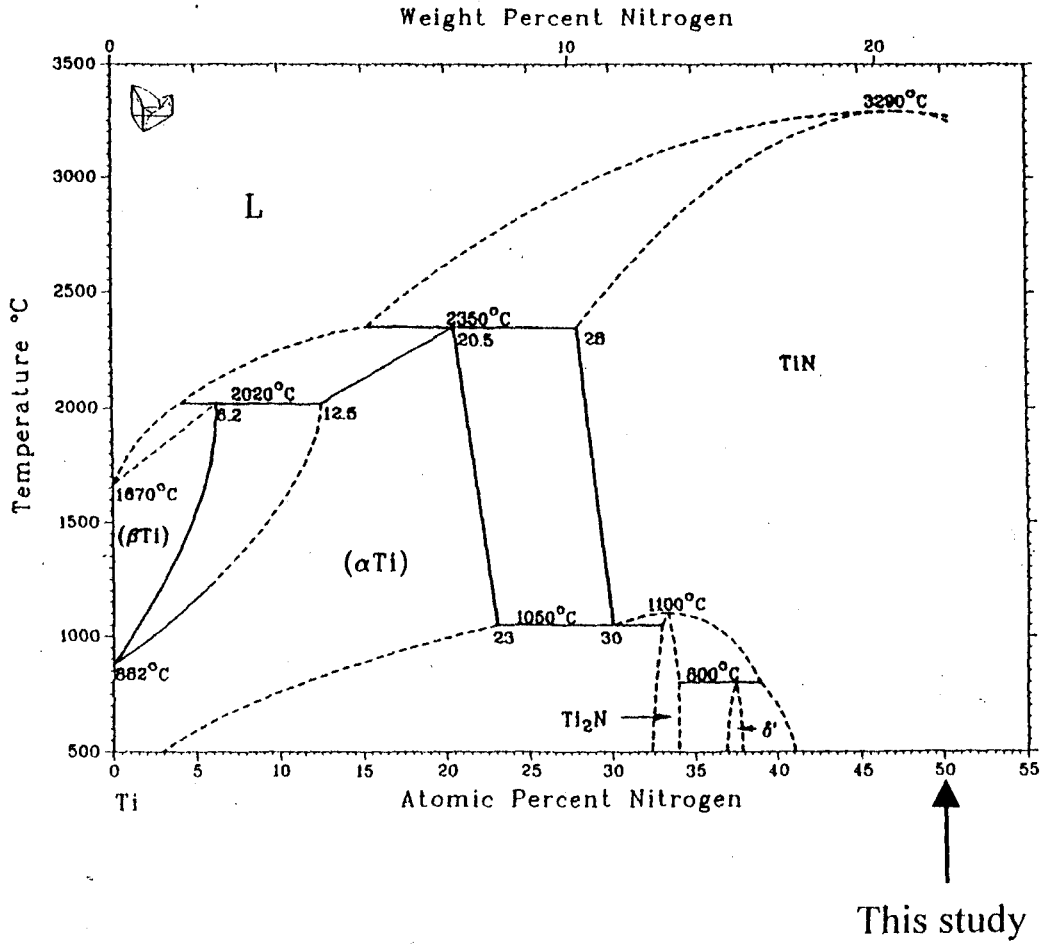

Fig.1-1. Part of the phase diagram in the Ti-N system

of TiN have been developed. For example, reactive sputtering methods[7], reactive evaporation methods[8], laser physical vapor deposition method [9], or chemical vapor deposition (CVD) methods such as plasma-CVD [10] and photo-CVD [11].

The equilibrium solid phases in the Ti-N system are: (A) the hexagonal closed packing (hcp) solid solution, α Ti(N); (B) the body centered cubic (bcc) solid solution, β Ti(N); (C) the tetragonal nitride, Ti_2N; (D) the face centered cubic (fcc) nitride, TiN and TiN_x; and (E) the body centered tetragonal (bct) nitride, ' δ ' as shown in Fig.1-1. TiN_x exists stably over an extensive composition range, which includes the stoichiometric compound, with a congruent melting temperature at 3290℃ [12].

TiN has NaCl-type crystal structure as shown in Fig.1-2 ; titanium atom is denoted as the larger ball, nitrogen atom as the smaller ball. The lattice is face centered cubic (f.c.c.). Nitrogen atoms occupy all octahedral holes in the cubic closest packing, that is f.c.c. lattice, composed of titanium atoms. The basis consists of one titanium and one nitrogen atom are separated by one-half the body diagonal of a unit cell, so that both atoms are arranged alternately at the lattice points of a simple cubic lattice. Each atom has as nearest neighbors six atoms of the other kind.

Deviations from stoichiometry in either direction cause the decrease of the lattice parameters a [13].

I-2-2. Aluminum nitride

The compound AlN was first made in 1862 by direct nitriding of Al-melt in N_2 gas by F.Briegleb et.al.[15], in accordance to the reaction:

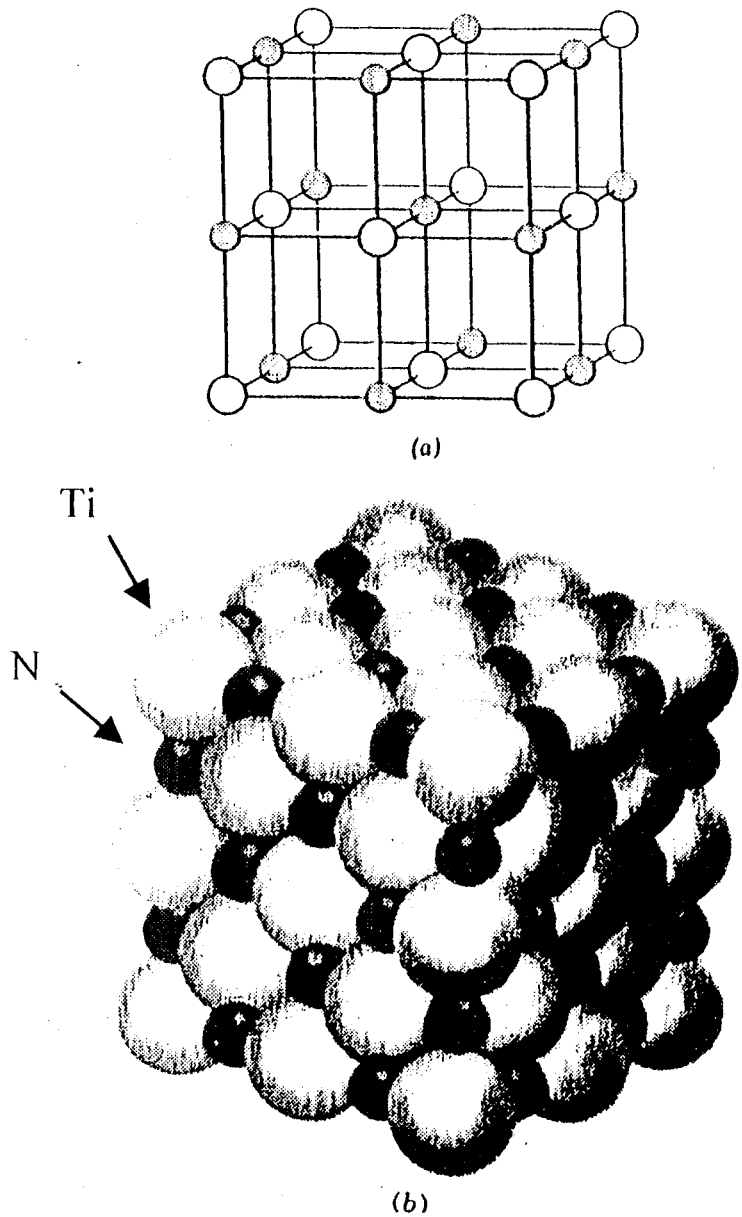

Fig.1-2. Crystal structure of TiN (sodium chloride like structure) Ti →Cl^-, N →Na^+

$$Al(liq.) + 1/2\ N_2 \rightarrow AlN(sol.)$$

The major difficulty in such a direct reaction method is that the surface film of AlN on the Al is very adherent and impedes further reaction. In 1957 E.Kauer et.al.[16] have shown that at 10^5 Pa pressure of N_2 gas the protective surface film on liquid Al begins to break down only at temperatures above 1500℃ .

Bulk single crystals of AlN have been grown by sublimation of AlN powder[17-21]. Thin films of AlN have been grown by several techniques: chemical vapor deposition (CVD)[22-28], metalorganic chemical vapor deposition (MO-CVD)[29-32], reactive sputtering[33-38], reactive evaporation[39-41], and reactive molecular beam epitaxy (MBE)[42,43]. The thin films were formed on silicon carbide, sapphire and silicon as substrates.

AlN has a wurtzite-type structure. A typical compound having such structure is ZnS. Similar to AlN, in the ZnS case, each zinc ion is placed at the center of a tetrahedral coordination with four sulfur. The bond strength is then equal to one-half, so that each sulfur must be coordinated with four cation. These requirements can be met with hexagonal packing of the large sulfur ions with half the tetragonal interstices filled up with zinc ions, so as to achieve maximum cation separation. This is shown in Fig.1-3.

On the other hand, by employing the optical absorption method, the band gap of AlN has been proposed to possess values ranging between 5-6eV. It is worth recalling that it is easy for AlN to introduce oxygen as an impurity. AlN including oxygen shows an optical absorption peak of 2.86eV[20]. The band gap is also affected by non-stoichiometry and often impurities, i.e. around 2.8eV for AlN with excess aluminum[17] and 3-6eV for

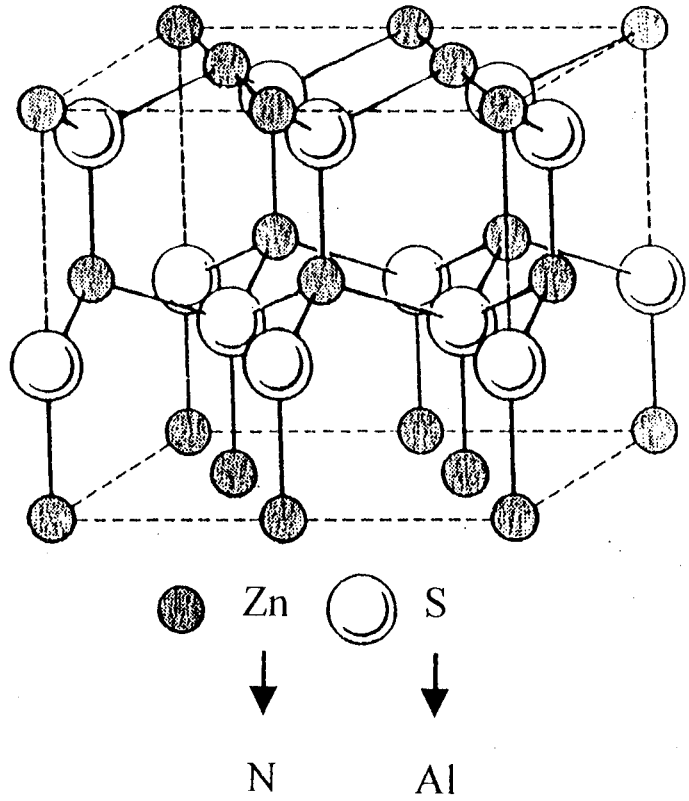

Fig.1-3. Crystal structure of AlN; wurtzite (ZnS) structure

AlN containing carbon impurity[21]. Yim et al[44] supposed that in contrast to GaN, AlN exhibits a direct transition between the energy levels with a band gap of about 6.2 eV at room temperature. He based his idea in an optical absorption measurement performed in AlN prepared by the CVD method. In 1978 Perry and Rutz confirmed by optical measurement the band gap data for AlN.

Several band-structure calculations have been made for AlN. An early calculation by Hejda and Hauptmanova was carried out using the orthogonalized plane wave (OPW) method[46] in 1969; followed by then an empirical pseudopotential calculation by Bloom[47]; next, a model potential calculation by Jones and Lettington[48]; later, an empirical tight-binding calculation by Kobayashi et al.[49], and more recently, the semi-ab initio linear-combination-of-atom-orbitals (LCAO) calculation of Haung and Ching[50]. Fig.1-4 is the band structure scheme and density of states of AlN calculated by Haung and Ching. The gamma point of the figure shows to exist the direct band gap with a value of 6.25eV. It is in good agreements with the experimental value, 6.28eV reported by Perry et al..

I-2-3. Metal nitride in the TiN-AlN system

The ternary system Ti-Al-N has been investigated by Schuster and Bauer(51) who prepared three different nitrides, Ti_2AlN, Ti_3AlN and $Ti_3Al_2N_2$, by the solid state reaction from TiN, AlN, Ti and Al in the temperature range from 1000 to 1400℃ . Ti2AlN was denoted as the H-phase (a=0.2994, c=1.361nm). Ti_3AlN had the perovskite-type structure (a=0.41120nm). $Ti_3Al_2N_2$ was included in the hexagonal system (a=0.29875,

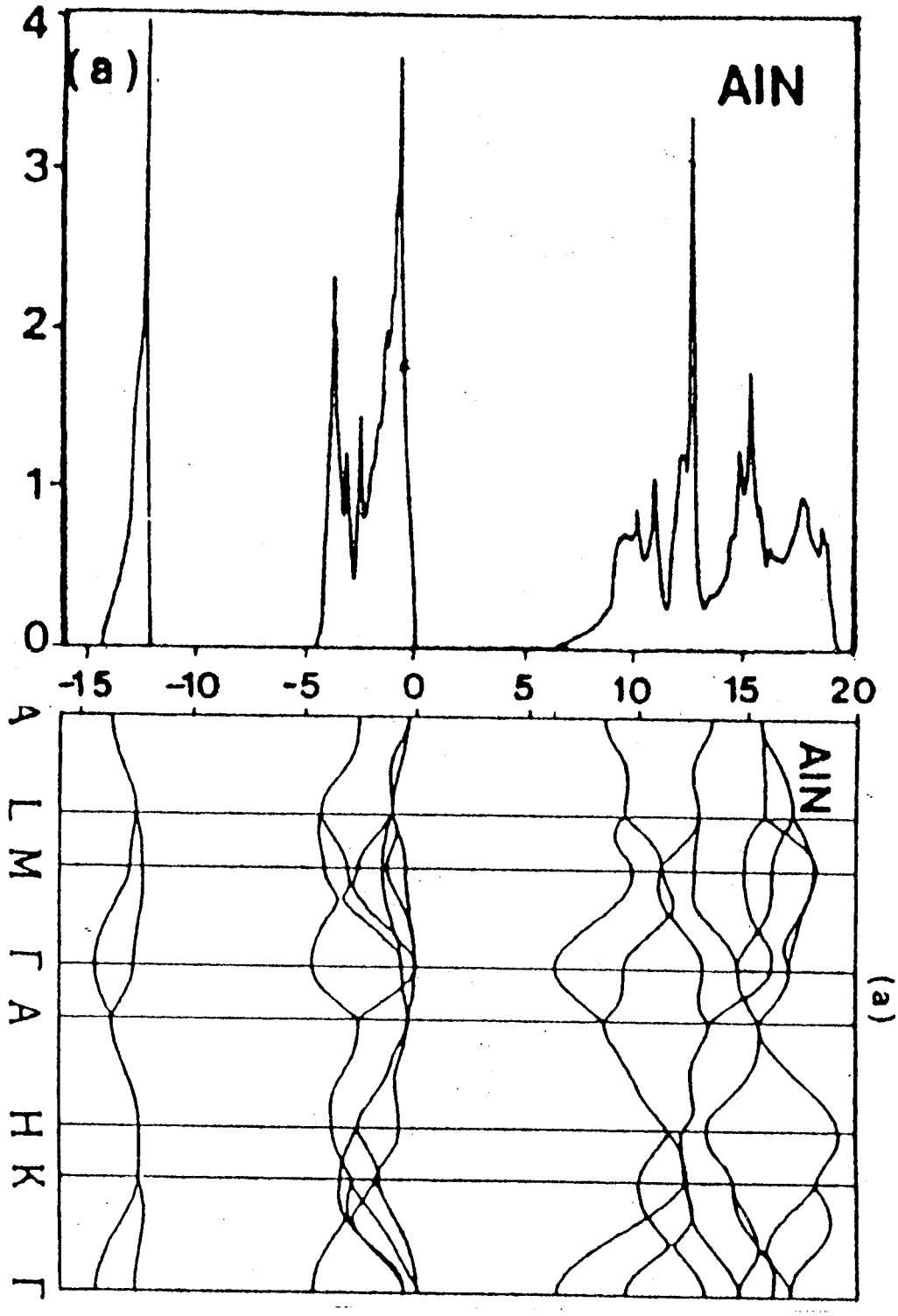

Fig.1-4. AlN band scheme

c=2.3350nm). In these nitrides, N/(Ti+Al) ratios of each nitride is smaller than unity.

On the other hand, the compounds in the binary TiN-AlN system prepared by a vapor-deposition method using a hot two- sectional electrode were investigated by A.Michalski[52]. The nitride films were deposited by using a electrode of Ti and Al rods connected in turn, and a $4x10^{-5}$s pulse discharge in a gas mixture of N_2 and H_2 (10:1)gas was employed. The coating films were deposited on carbon steel substrates at 200 mm apart from the plasma accelerator; substrate temperature during deposition was <500K. Depending on the composition of electrodes, the mixtures of TiN-AlN-Ti and TiN-Ti_3Al-Ti were obtained in the coating films.

The synthesis of compounds in the Ti-Al-N system by sputtering methods were also practiced by K.Wasa, et al.[53] and G.Beensh-Marchwicka, et al.[54]. K.Wasa, et al. reported that the sputtered Ti-Al-N films were chiefly composed of a mixture of polycrystalline TiN and amorphous AlN, although a small amount of Ti and Al oxides might be present due to their high affinity for oxygen.

G.Beensh-Marchwicka, et al. reported structural modifications of thin films prepared by co-sputtering Ti and Al in an N_2-Ar atmosphere. The nitrogen content of the sputtering atmosphere had the greatest effect on the composition and structure of the films. They did not observed AlN phase, but only observed TiN phase in the Ti-Al-N films. Moreover, the Ti-Al-N films produced in the range of nitrogen contents, where both TiN and AlN co-exist were almost completely amorphous. There were no reports that a single phase in the binary system TiN-AlN was obtained by vapor-deposition methods.

On the other hand, it is difficult to form solid solution in the TiN-AlN system because of large differences in both crystal structure and chemical bonds between TiN and AlN; both Ti and N atoms in TiN have coordination numbers of 6, while in AlN, the coordination numbers of Al and N atoms are 4. Recently, many kinds of vapor deposition method have been developed, especially sputtering method. Some single phases in the TiN-AlN system[55] by applying a reaction sputtering method have been produced. Thus three different crystal phases, namely one solid solution with NaCl-type structure[56], the other solid solution with wurtzite-type structure[57] and one new double nitride were obtained in the composition range of $0<x<0.6$, $0.8<x<1.0$ and $x=0.7$, respectively. Recently, the investigation in the system have proceeded in properties for example, hardness, and in particular durability against oxidation.

I-3. Purpose of this investigation

The properties of materials strongly depend on the chemical bonding states of them. Accordingly, various electrical properties are often discussed involving the factor of "ionicity"; for example, ionic conductivity, band gap of semiconductor, etc.

Nitrides can have wide chemical bonding states of the range over ionic, covalent and metallic bond, which depend on the kinds of metal elements as the counter atoms to nitrogen. The appearance of various properties are expected in nitrides because various chemical bonding states appear in selection of metal elements.

In the former processes, it was difficult to prepare metal nitrides.

Accordingly, the investigations of nitride solid solutions and double nitrides are very little. In oxides, however, investigations on solid solutions and multicomponent oxides have rendered great services in material science, material design, etc. It is also important to investigate the solid solution of nitrides and multicomponent nitrides because of the possibility to bring out new function in the wider range than oxides.

Recently, the development of vapor deposition techniques make the preparation of various nitrides easy. For example, the PVD (physical vapor deposition) method is used as a thermo non-equilibrium reaction process, to perform at low temperature. Using the PVD method, we can prepare a metastable compound having a chemical composition which can not be produced by the common equilibrium reaction at high temperature. It is also possible to change the chemical composition of products in wide range by utilizing the PVD method.

In this study, the rf-sputtering method which is a non-equilibrium reaction process was employed to produce new compounds in the TiN and AlN system. In Chapter II, the method of preparing these novel metastable crystal phases, i.e. synthesis of the NaCl-type and the wurtzite-type solid solution and a new crystal phase $Ti_{0.3}Al_{0.7}N$ is described. In Chapter III, a detailed structural study of these products was carried out by X-ray diffraction and X-ray absorption fine structure (XAFS) techniques. Chemical bond is studied by X-ray photoelectron spectrum (XPS) and auger electron spectrum (AES). The crystal structure and chemical bonding of the products are studied and discussed with relation to their chemical composition. In Chapter IV, the properties of the products, such as electric resistivity, optical band gap, and durability against oxidation and hydrolysis, as a

function of the chemical composition, are investigated. Physical and chemical properties of the sinthesized phases are discussed in connection to their chemical bonding. In particular, the effects in addition of Al and Ti on the durability against oxidation of TiN and the durability against water of AlN, respectively, are systematically discussed on the basis of DV-Xα MO calculation.

CHAPTER II PREPARATION OF FILMS IN THE Ti-Al-N SYSTEM.

II-1. Introduction

Metal nitrides have a great variety of chemical bond natures such as metallic, covalent and ionic bondings corresponding to the countermetals of transition metals, IA and IIA metals and IIIB and IVB metals, respectively. It is expected, therefore, to have metal nitrides with improved properties and also to bring about new operational functions by controlling the chemical composition in solid solutions of nitrides having different bond nature.

Titan nitride, having high hardness, has been spotlighted as a coating material. However, the durability against oxidation for TiN is much inferior to that of AlN with a strong covalent bond. In contrast, TiN has an unfilled d-d-band, resulting in metallic conductivity. Thus, AlN is then an insulator with a wide band gap. It should be expected that durability against oxidation for TiN might be improved by adding Al, and also that the existing band gap varies in the range from 0 to 6 eV, which is a function of the chemical composition between the solid solution of TiN and AlN. In practice, however, since there is large difference in their crystal structure, it is difficult to prepare the solid solution in the TiN and AlN system by conventional reaction processes, such as calcination of a mixture of TiN and AlN at high temperature.

In the present work, the rf-sputtering method, which is a non-equilibrium reaction process was applied to produce two types of solid solutions and a new crystal phase in the TiN and AlN system. Details of

their synthesis procedure and characterization of the products are described in this chapter.

II-2. Sputtering apparatus and experimental conditions

Preparation of thin films in the $Ti_{1-x}Al_xN$(Ti-Al-N) system.

The rf-magnetron sputtering equipment used for the preparation of $Ti_{1-x}Al_xN$ films was an ANELVA SPF-210H apparatus type, as shown in Fig.2-1. The face of substrate is parallel to the target's face, which is coupled to a concentric magnet on its back side. As shown in Table 1, the targets used for co-sputtering were composed of an Al disk (100 mmϕ) and Ti disk, and Ti chips (5x5mm^2) and Al chips geometrically distributed on the Al and Ti disks, respectively, for example, as shown in Fig.2-1-a. If Al chips were to be dispersed on the Ti disk, careful must be taken as to avoid the possibility of fusing the Al chips (with the lower melting point) because of a high temperature generated by an electric discharge. The substrates employed to fabricate nitride films were a slide glass and a fused silica with high transmittance (in the range up to the ultraviolet level) which are convenient to measure optical properties. Another substrate employed was a Mo sheet exhibiting high electric conductivity, which is of much importance in determining the electronic properties of several materials. Nitride films were prepared by reactive co-sputtering in an equimolar proportion of an Ar and N_2 gas mixture. Sputtering conditions are shown in Table 2-1. The chemical composition of the sputtered films was set by controlling the Ti deposit over the Al target as shown in Fig.2-1-b. In practice, thickness of the sputtered films were controlled by handling the

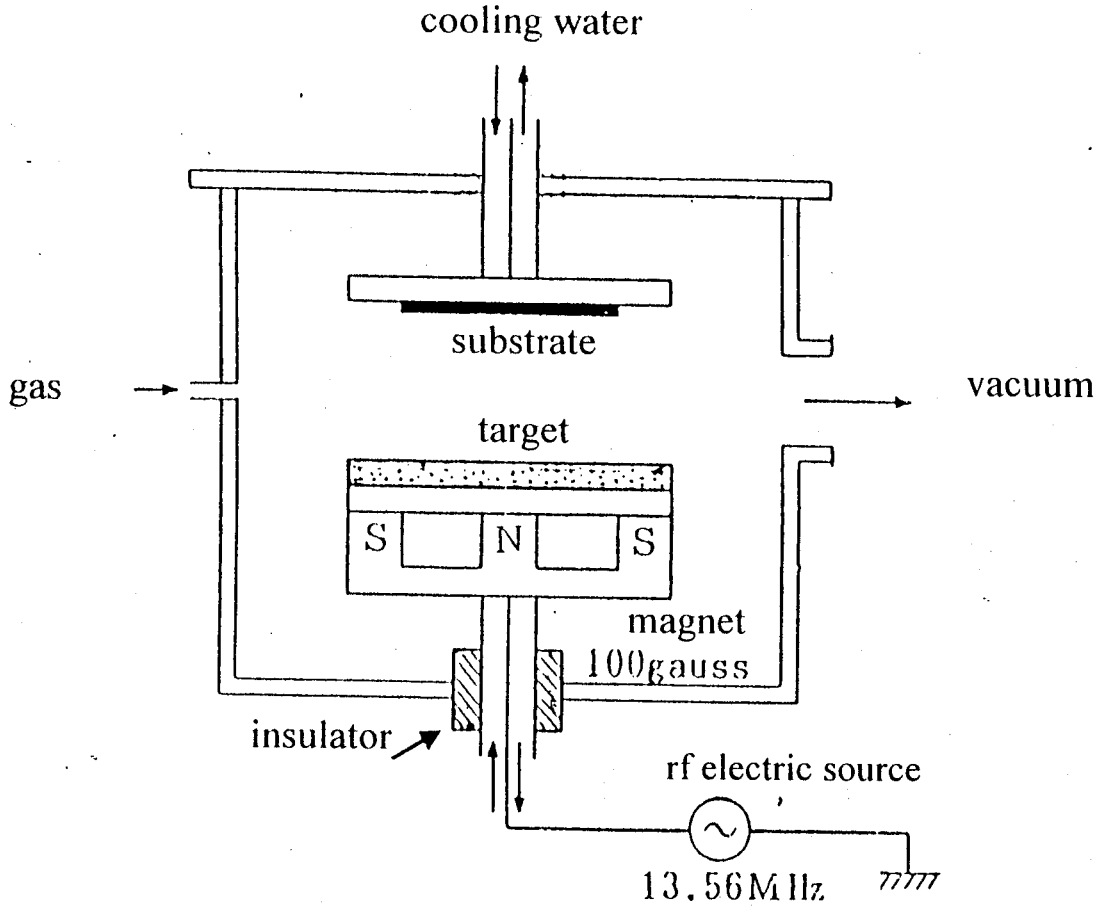

Fig.2-1. Rf-magnetron sputtering apparatus
ANELVA SPF - 210 H

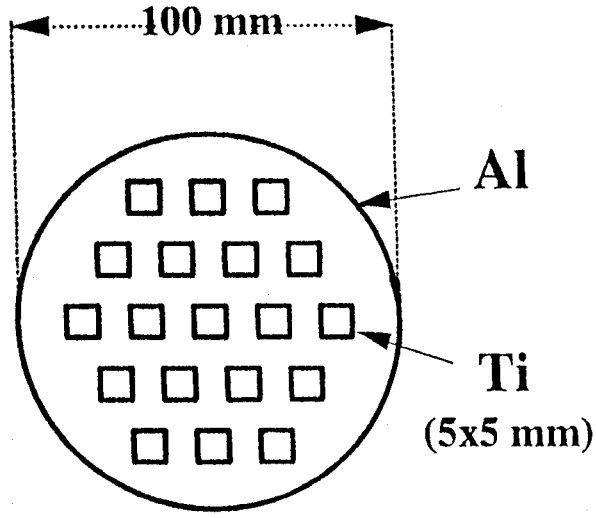

Fig. 2-1-a A target

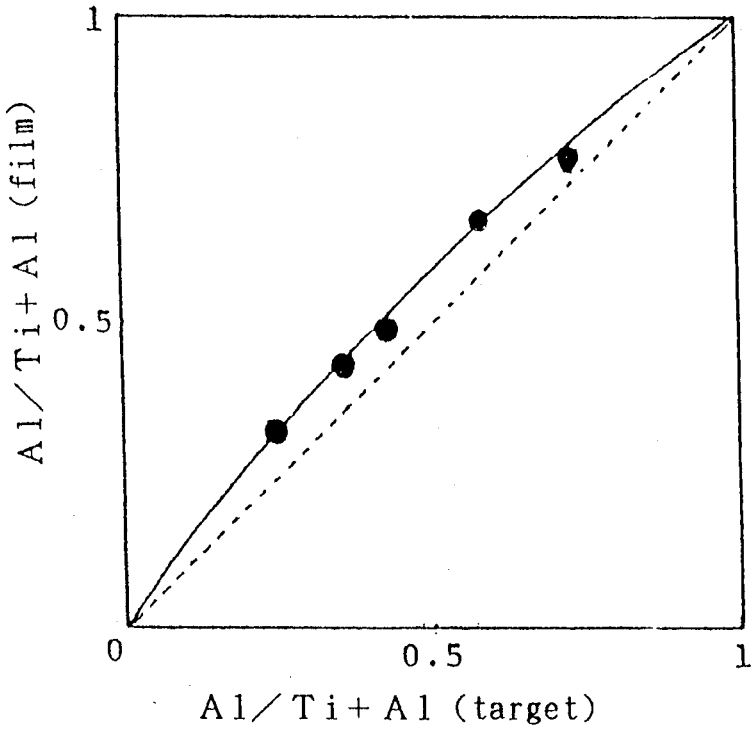

Fig. 2-1-b Relation between the chemical composition of film and the area ratio of target.

sputtering time and were measured by the ball polishing method and scanning electron microscopy.

Table 2-1. Rf-magnetron sputtering conditions for the films preparation

Target	Ti disk, Al disk,
	Ti chips on Al disk,
	Al chips on Ti disk
Substrate	slide glass, fused silica, Mo
Temp. of substrate	80～ 200℃
Sputtering gas	Ar + N_2
Gas pressure	1×10^{-3}～ 3×10^{-2}Torr
Rf-power	100 W
Rf-frequency	13.56 MHz
Magnetic field	100 gauss
Deposition time	15 min.～ 12 hrs.

II-3. Characterization of the nitride film

Double-metal nitride films in the TiN-AlN system were fabricated on slide glass substrates by using a reaction rf-sputtering method with composite targets consisted of titanium and aluminum metals. A gas mixture of Argon and nitrogen gases were employed as sputtered gases. The chemical composition of the sputtered films was controlled by varying the Ti coverage on the Al plate. A different nitride phase came out when the gas pressure of sputtering was varied. For example, the X-ray diffraction patterns of the films obtained using a target of Al/Ti=1 are shown in Fig.2-2. In the film sputtered at a gas pressure of $1x10^{-3}$ Torr, a diffused and very wide open pattern was revealed, which can be observed in Fig.2-2(a). It is doubtlessly associated to an amorphous phase. In the film sputtered at a gas pressure of $3x10^{-3}$ Torr, shown in Fig.2-2(b), both diffraction lines (200) and (111) are easily identified even though they are broad. From such broadened planes one can deduce the presence of particles whose crystallite size is considerably small. On the other hand, in the film sputtered at a higher gas pressure, shown in Fig.2-2(d) the diffraction peak became sharp because at that pressure conditions the crystal grain growth took place, and a preferred orientation running up from the (100) plane to the surface was observed.

The Ti/Al ratio in the sputtered films, which was determined by AEM measurements after sputter etching the film surface with Ar gas ($1x10^{-2}$Torr) was found to be lower by a factor of 1.4 ± 0.3 than the area-ratio of Al to Ti on the target. The ratio of N to metal atoms, $[(1-x)Ti+ xAl]$, was estimated to be almost unity by means of ESCA spectroscopy. In order to check oxygen contamination, Auger electron spectros-

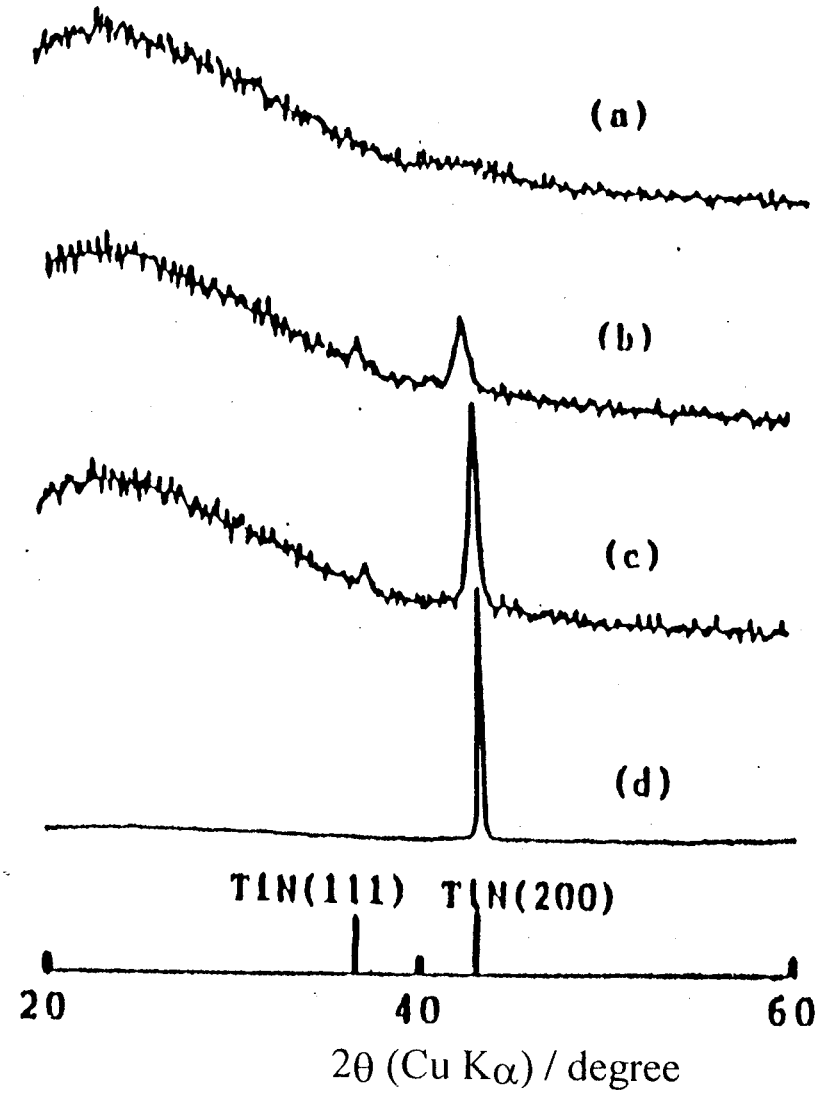

Fig.2-2. X-ray diffraction patterns of the as-sputtered films on slide glass substrate
(Al:Ti = 1:1 Target, 100w)
(a) $1x10^{-3}$Torr (b) $3x10^{-3}$Torr
(c) $1x10^{-2}$Torr (b) $3x10^{-2}$Torr

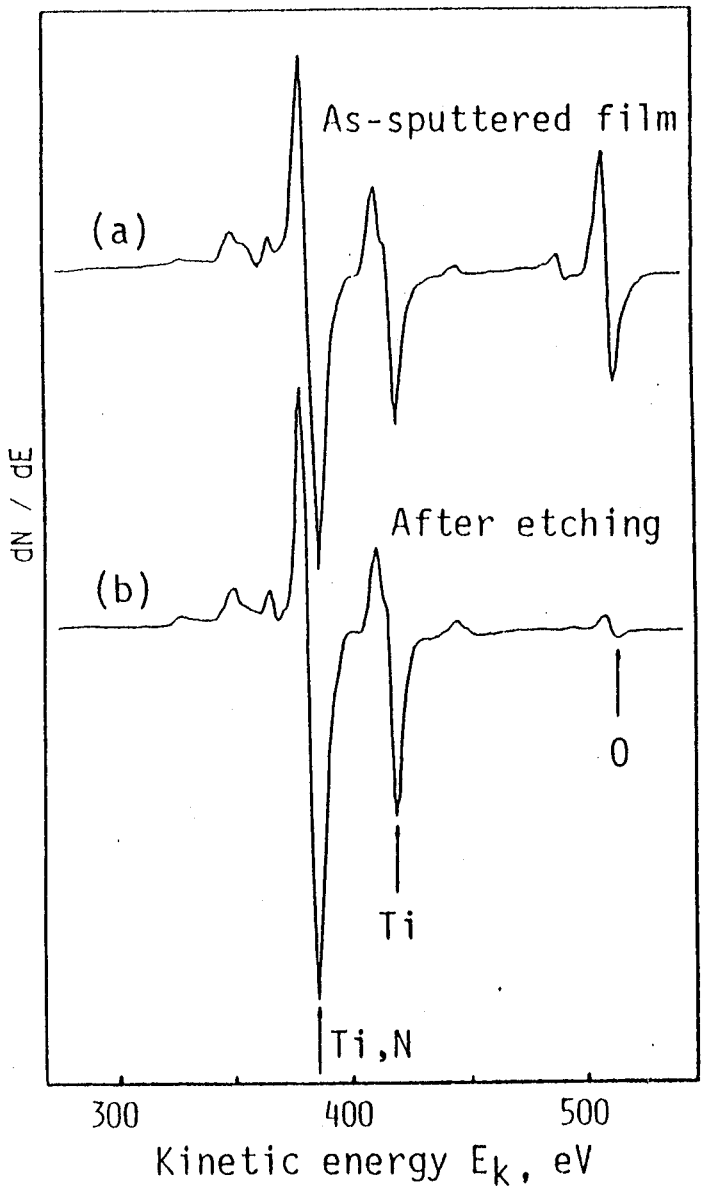

Fig. 2·3. Auger electron spectroscopy of the TiN film.

copy was carried out on the sputtered films. An example of the analysis is given below. Auger electron spectra for the TiN film are displayed in Fig.2-3(a) and (b). The spectrum (a) suggests that the surface of the sputtered film is appreciably oxidized. Once the film's surface has been etched by an argon ion beam, a little oxygen signal is observed as shown in Fig.2-3(b). This fact indicates that oxygen contamination had not occurred during film deposition. These results are described in detail in a latter chapter (CHAPTER IV). Oxygen contamination does not exist inside the films, even though the surface of the TiN film was heavily oxidized in air.

Polycrystalline compounds were also found in the $Ti_{1-x}Al_xN$ films prepared under the above-mentioned conditions. Three different crystal phases, two kinds of solid solution and one new double nitride, were obtained as a function of the target composition, i.e., in connection to the coverage ratio of Ti to Al on the target. The thickness of the film was controlled by handling the deposition time and the rf-power. For example, a film with thickness of 1μ m was prepared by sputtering for about 5 hours, under the gas pressure of $1x10^{-2}$ Torr and the rf-power of 100W.

The most typical X-ray diffraction patterns for the three kinds of phases are shown in Fig.2-4. In turn, Fig.2-5 shows the resulted traces of AEM for the each case samples. One of the solid solutions was produced in the composition x=0.5, which was determined by using AEM, and had NaCl-type structure, this is shown in Fig.2-4.(a). The NaCl-type solid solution is obtained at a composition range of $0 \leqq x \leqq 0.6$. The other solid solution was produced at the composition of x=0.95 and had wurtzite-type structure, as shown in Fig.2-4(c). The wurtzite-type solid solution had a composition ranged between $0.8 \leqq x \leqq 1.0$. The new double nitride phase yielded in the

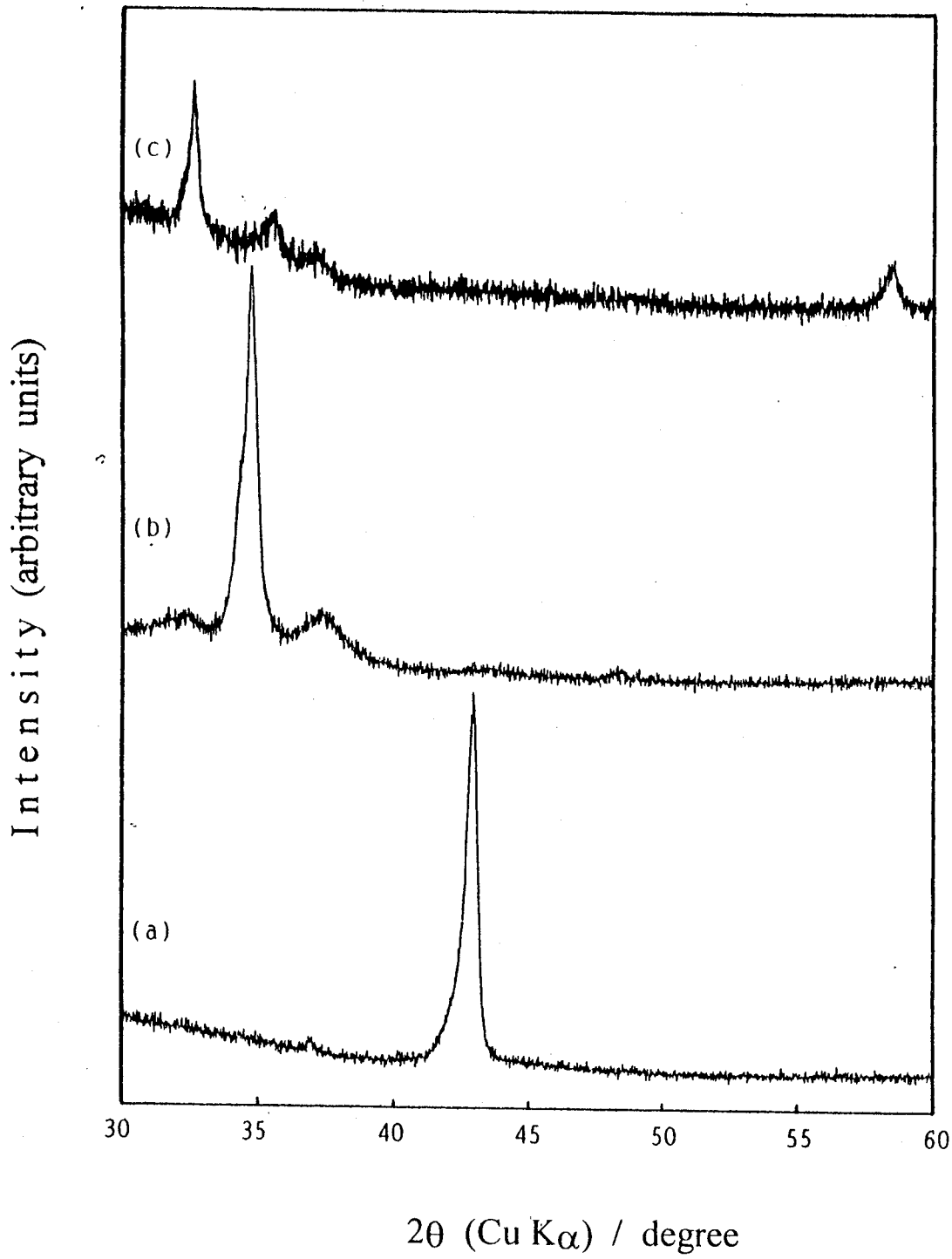

Fig.2-4. X-ray diffraction patterns of $Ti_{1-x}Al_xN$ solid solutions:
a) NaCl- type solid solution (x = 0.5)
b) New double nitride (x = 0.7)
c) Wurtzite- type solid solution (x = 0.85)

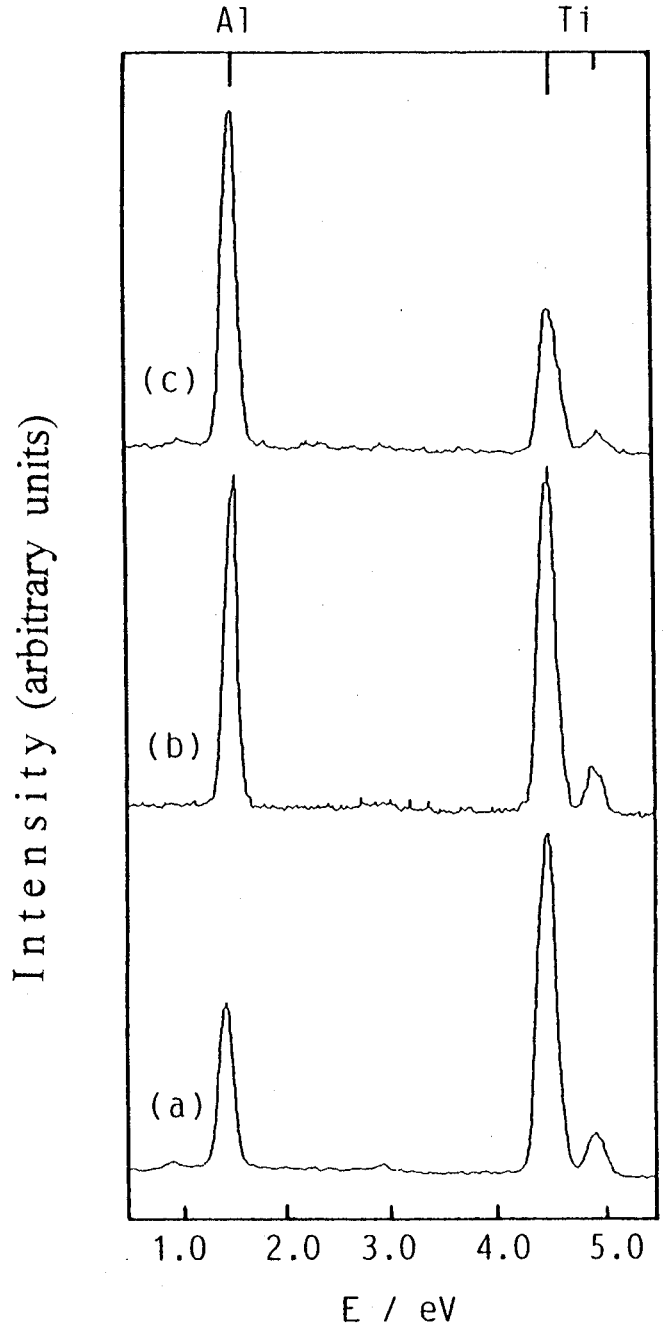

Fig.2-5. Analytical electron microscope traces of $Ti_{1-x}Al_xN$ solid solutions:

a) x = 0.5

b) x = 0.7

c) x = 0.85

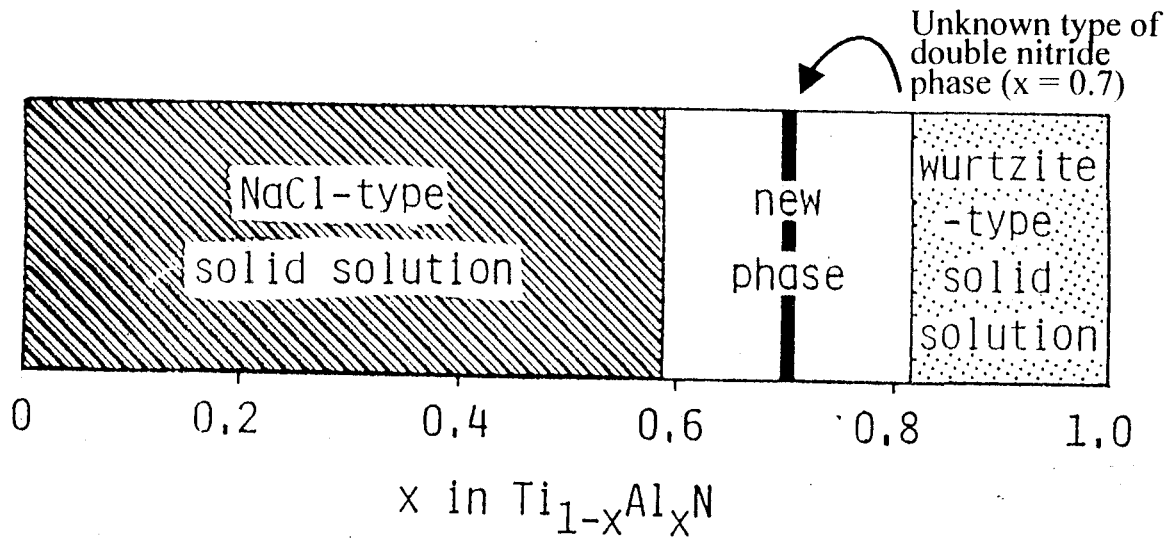

Fig.2-6. Concentration range of several $Ti_{1-x}Al_xN$ phases

vicinity of x=0.7 as shown in Fig.4(b), and its crystalline phase was calculated to belong to the orthorhombic system. This will be described in the later part of the next chapter.

Fig.2-6 displays the relationship between the sputtered films phases and the chemical composition x in the $Ti_{1-x}Al_xN$ system. Results of AEM and EM measurements confirmed that the $Ti_{1-x}Al_xN$ films of each phase had good homogeneity in both chemical composition and texture. Thus, wide range solid solutions between TiN and AlN were successfully prepared for the first time by employing the vapor deposition method. As shown in Fig.6 the films whose composition range stands between $0.6<x<0.7$ were mixtures of the NaCl-type solid solution (x=0.6) and the new double nitride, $Ti_{0.3}Al_{0.7}N$. Moreover, those of $0.7<x<0.8$ were mixtures of the wurtzite-type solid solution (x=0.8) and $Ti_{0.3}Al_{0.7}N$.

II-4. Conclusion

Titanium nitride has a NaCl-type structure and exhibits metallic conductivity. AlN is insulator with a wurtzite-type structure and has intense covalent character. Their crystal structure and chemical bond are quite different among each other. In principle, it is therefore, crystallographically very difficult to prepare the solid solution in the TiN and AlN system by the conventional reaction processes at high temperatures. That is the reason why few reports dealing on the synthesis of double nitrides in the TiN and AlN system have been done so far (exceptions are Ti_3AlN, Ti_2AlN and $Ti_3Al_2N_2$). In the present study, synthesis of the double nitride, in which the atomic ratio of metal (Ti,Al) to nitrogen is in unity,

was examined by a reaction sputtering method. Three crystal phases, two solid solutions and one new identified crystal phase, were prepared.

One of the solid solutions, $Ti_{1-x}Al_xN$, has NaCl-type structure and is produced in the composition range of $0<x\leq0.6$. Another solid solution with the chemical composition in the range of $0.8\leq x<1.0$ has Wurtzite-type structure. The new double nitride, which is the unknown double nitride belongs to orthorhombic lattice, was produced in the vicinity of x =0.7. The two solid solutions and $Ti_{0.3}Al_{0.7}N$ are considered to be metastable phases, because they easily decompose to both end members, TiN and AlN, above 900 in N_2 atmosphere. Therefore, the present results indicate that a reaction sputtering method, which is a non-equilibrium reaction process, is a powerful synthesis method for preparation of metastable crystal phase.

CHAPTER III. CRYSTAL CHEMISTRY OF $Ti_{1-x}Al_xN$ ($0 \leqq x \leqq 1$)

III-1. Introduction

The ternary system Ti-Al-N has been investigated by Schuster and Bauer(51) who prepared three different nitrides (Ti_2AlN, Ti_3AlN and $Ti_3Al_2N_2$), by inducing the solid state reaction between TiN, AlN, Ti and Al at temperatures from 1000 to 1400℃ . Ti_2AlN was denoted as the H-phase (a=0.2994, c=1.361nm). Ti_3AlN had the perovskite-type structure (a=0.41120nm). $Ti_3Al_2N_2$ was included in the hexagonal system (a=0.29875, c=2.3350nm). Thus, the N/(Ti+Al) ratio for each nitride is smaller than unity.

The synthesis of nitrides in the Ti-Al-N system by sputtering methods was also studied by K.Wasa.(53) and G.Beensh-Marchwicka.(54). K.Wasa, et al. reported that the sputtered Ti-Al-N films are chiefly composed of a mixture of polycrystalline TiN and amorphous AlN, although a small amount of Ti and Al oxides might be present due to their high affinity for oxygen. In turn, G.Beensh-Marchwicka, et al. reported structural modifications of thin films prepared by the co-sputtering Ti and Al in an N_2-Ar atmosphere. The nitrogen content of the sputtering atmosphere had the greatest effect, as reflected on the composition and structure of the films. They couldn't observe, however, the formation of the AlN phase, but only TiN phase in the Ti-Al-N films.

The ordering of the TiN phase depends on the Al content in the target. The existence of the TiN phase perturbs the formation of polycrystalline phases of other components. Moreover, the Ti-Al-N films produced

within the range of nitrogen contents as the atomic ratio of N/(Ti+Al)=1 were almost amorphous. So far no one have reported on the formation of crystal phases in the pseudo binary system TiN-AlN.

Both titanium nitride and aluminum nitride are attractive as high-temperature materials. Titanium nitride has already been applied to cutting tool and coating material due to its high hardness and high thermal conductivity at high temperature. Aluminum nitride has been intended to applying as substrate material of semiconductor because of the high insulating property and high thermal conductivity. AlN also has another possibility to be applied to window with high transmittance in the wide range of wavelength at high temperature. These two nitrides are similarly simple metal nitrides with a composition MN (M:Ti,Al). However their properties are quite different each other because of the differences in crystal structure and in bond nature. Titanium nitride is a interstitial nitride, accordingly exhibits metallic conductivity. While AlN is an insulator with a wide band gap.

It have been considered that the difficulty of forming solid solutions in the TiN-AlN system is due to large differences in both crystal structure and chemical bonds between TiN and AlN; both Ti and N atoms in TiN have coordination numbers of 6, while in AlN the coordination numbers of Al and N atoms are 4. In the present study, we succeeded to prepare new nitrides in the TiN and AlN system by applying a reaction sputtering method as described in chapter II. There were formed three different crystal phase, i.e., two kinds of solid solutions and one new double nitride. One of solid solutions had NaCl-type crystal structure. The other had wurtzite-type crystal structure. It was clarified that both solid solutions

exit in the appreciably wide range.

On basis of crystal data obtained by X-ray diffraction and X-ray absorption fine structure, the crystal structure and coordination states of solute atoms in solid solution are described. The change of chemical bonding are examined by X-ray photoelectron spectroscopy and X-ray induced Auger electron spectroscopy.

III-2. Experimental

The rf-magnetron sputtering equipment used for the preparation of $Ti_{1-x}Al_xN$ films was an ANELVA SPF-210H apparatus type. Nitride films were fabricated on glass and Mo metal substrates by reactive co-sputtering. which condition described in detail in chapter II. Heat treatments under a reducing atmosphere was carried out in N_2 gas mixed with 10% H_2. The phase identification of the samples was made by X-ray diffractometer with graphite monochromatized CuKα radiation. The chemical composition of films was determined by an analytical electron microscope (AEM), Hitachi HU-12SE, and aluminum titanate was used as a standard for a quantitative analysis. Auger electron spectrum (AES), X-ray photoelectron spectrum (XPS) and X-ray induced Auger electron spectrum (XAES) were measured for investigations on the electronic states by using PERKIN-ELMER PHI 5100, Shimadzu HIPS-70 and Shimadzu ESCA-850. MgKα X-ray (1253.6 eV) was used as the excitation source. The C 1s line, contaminated on sample surface and the Au $4f_{7/2}$ were used as reference level, the binding energy, Eb, of which were taken to be 285.0 and 84.0 eV, respectively. Argon ion etching for film surface was performed to obtain the depth profiles of the individual elements. The ion etch rate was 2.5± 0.5nm/min.

Low energy electron loss spectra(EELS) data were taken with a PHI single-pass cylindrical mirror analyzer (CMA) equipped with coaxial electron gun with primary-beam voltages of 170eV and beam currents of <1 μ A in the high vacuum of $<1x10^{-10}$. The spectra were obtained as negative second derivative of energy distribution N(E) of electrons backscattered since derivative spectra revealed much finer structures than nonderivative ones. The X-ray absorption near the Ti K-edge was measured with using a synchrotron radiation and a XAFS (X-ray absorption fine structure) facilities installed at the beam line of the 2.5-GeV storage ring of Photon Factory in KEK, Tsukuba.

III-3. Results and discussion

III-3-1. Structural characterization of $Ti_{1-x}Al_xN$ solid solution

(1) NaCl-type solid solution

The TiN film prepared at a gas pressure of $1x10^{-2}$Torr, which had the characteristic golden color of the stoichiometric TiN phase[61], exhibited an X-ray diffraction pattern corresponding to NaCl-type structure as shown in Fig.3-1-1(a). A remarkable preferred orientation with (100) plane being parallel to the film surface was observed. The lattice constant of this compound was a= 0.4258 nm slightly larger than the value 0.4240 nm[62] reported for the bulk TiN. This large value is a typical feature of thin films and has been reported for TiN film by Sundgren et al.[4]. It is probably affected by the small grain size, existing stresses and possible defect structure of TiN in the thin films.

The TiN films were prepared at higher gas pressure of $3x10^{-2}$ Torr (A), and at lower that of $2x10^{-3}$ Torr (B). Both of them were confirmed to have NaCl-type structure from X-ray diffraction patterns, which show the preferred orientation similar as the stoichiometric TiN although they had dark bluish brown in color. The lattice constant of (A) and (B) were 0.4235 and 0.4240 nm, respectively. In the system TiN_{1-B} ($0<B<<1$), it seemed generally that the lattice parameter increases with increasing nitrogen content[61,63], but in the system TiN_{1+B} some confusion has occurred: the lattice parameter increases[61] (1) and decreases[65] (2) with increasing nitrogen content. In this work it seemed to agree with the case

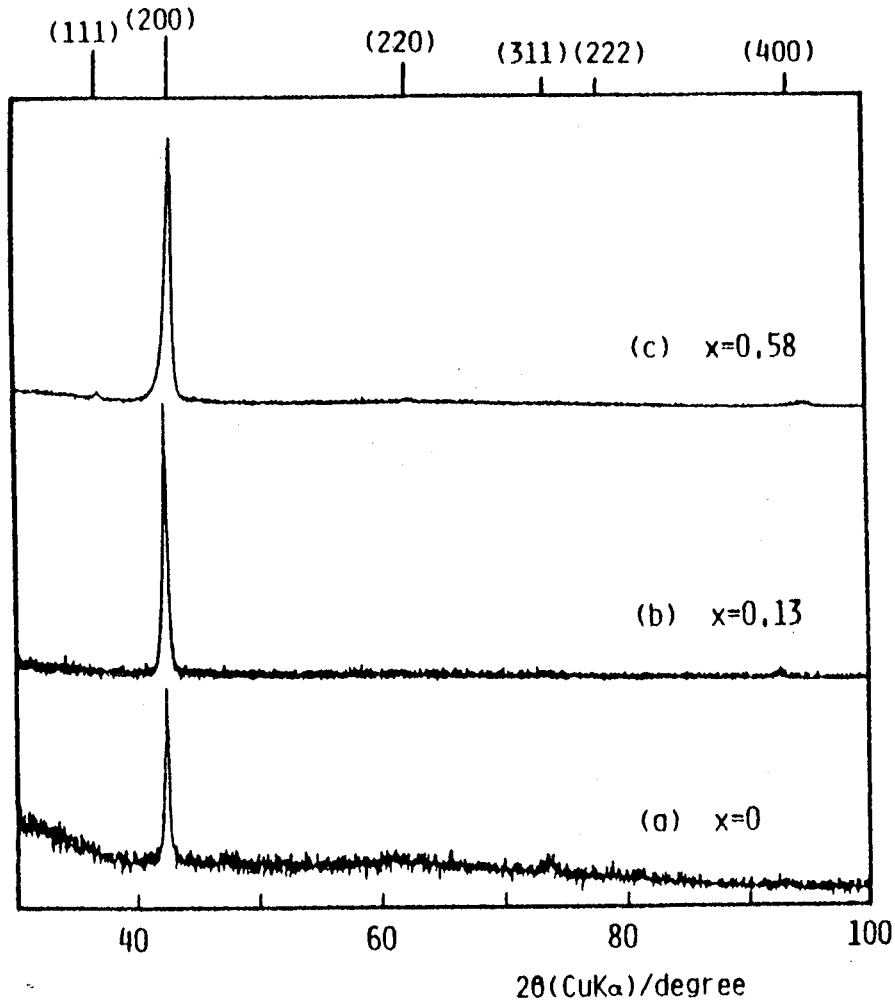

Fig. 3·1·1. X-ray diffraction patterns of $Ti_{1-x}Al_xN$ with NaCl-type structure (sputtered at gas pressure 1×10^{-2} Torr).

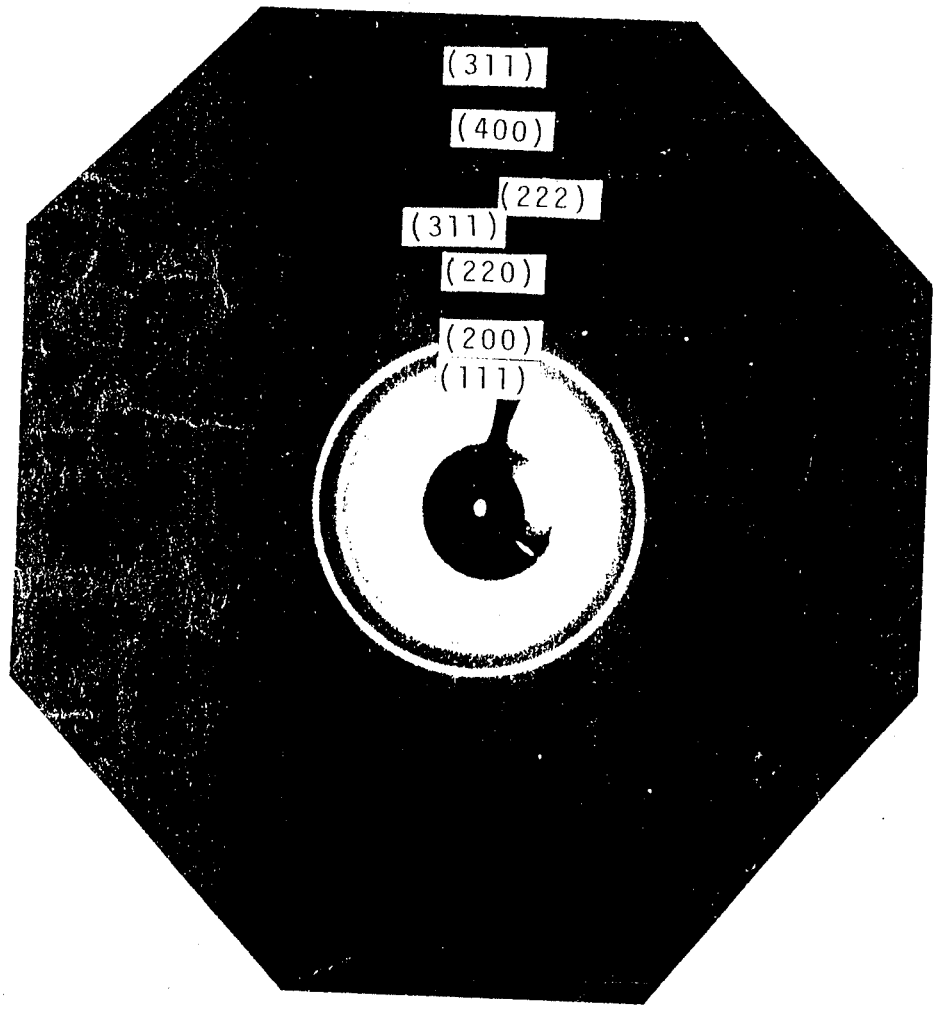

Fig. 3·1·2. X-ray diffraction pattern of the NaCl-type solid solution with x=0.58.

(2) as the lattice parameter of stoichiometric TiN was maximum and that of over- and under-stoichiometric TiN became smaller value.

The thin films with the composition range of $0.13<x<0.58$ were dark greenish brown in color and the X-ray diffraction patterns of them are similar to one of the TiN film and show remarkable preferred orientation as shown in Figs.3-1-1(b) and (c), where only 200 reflection is observed for each sample. Therefore, the X-ray diffraction patterns are insufficient to identify the samples as NaCl-type compounds.

To confirm the structure type of the $Ti_{1-x}Al_xN$ film with the composition of $x=0.58$, X-ray powder photograph as shown in Fig.3-1-2 was taken for the powder sample scrapped off from slide glass substrate and set into glass capillary. All diffraction lines observed was indexed with NaCl-type lattice. On the base of these results, the $Ti_{1-x}Al_xN$ films were identified as the NaCl-type phase in the very wide range of $0<x<0.58$.

Fig.3-1-3 displays rocking curves of 200 reflections of the $Ti_{1-x}Al_xN$ solid solutions with NaCl-type structure, which were prepared under the gas pressure of $1x10^{-2}$Torr. The 200 diffraction peak shifts toward higher Bragg angle with increasing Al content. For the films with $x=0.61$, a new double nitride was crystallized with the presence of NaCl-type phase. The relationship between chemical composition, x, and lattice constant of the NaCl-type solid solution calculated by using the 200 and 400 reflections is represented in Fig.3-1-4. As mentioned above, the lattice constant of the as-deposited TiN was slightly higher than that of bulk TiN. The lattice constant of the NaCl-type solid solutions linearly decreases with increasing Al content. That is seemed to be due to the replacement of Ti by Al, atomic radius of which is smaller

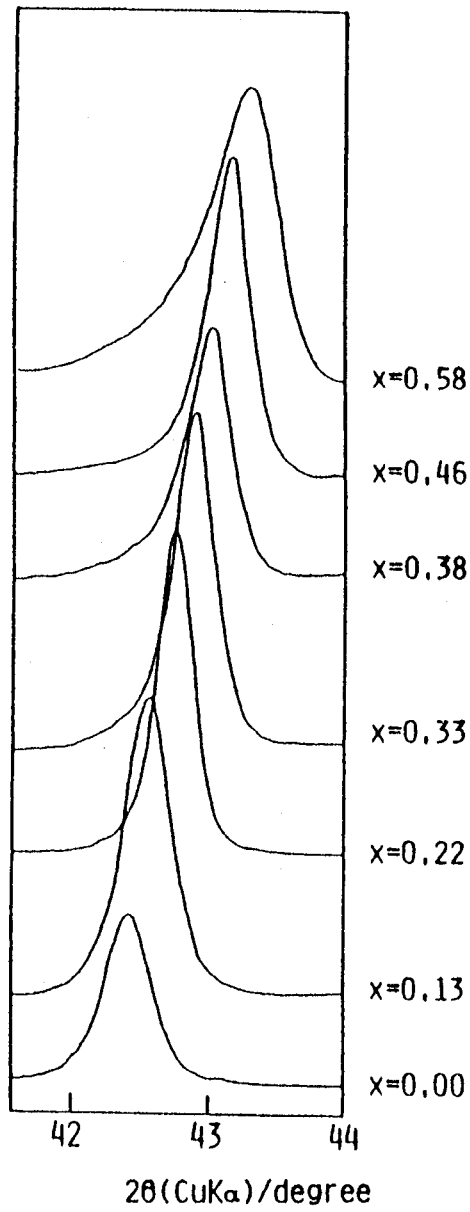

Fig. 3·1·3. X-ray diffraction profiles near (200) reflection of the NaCl-type phase.
($Ti_{1-x}Al_xN$; x = 0.00, 0.13, 0.22, 0.33, 0.38, 0.46, 0.58)

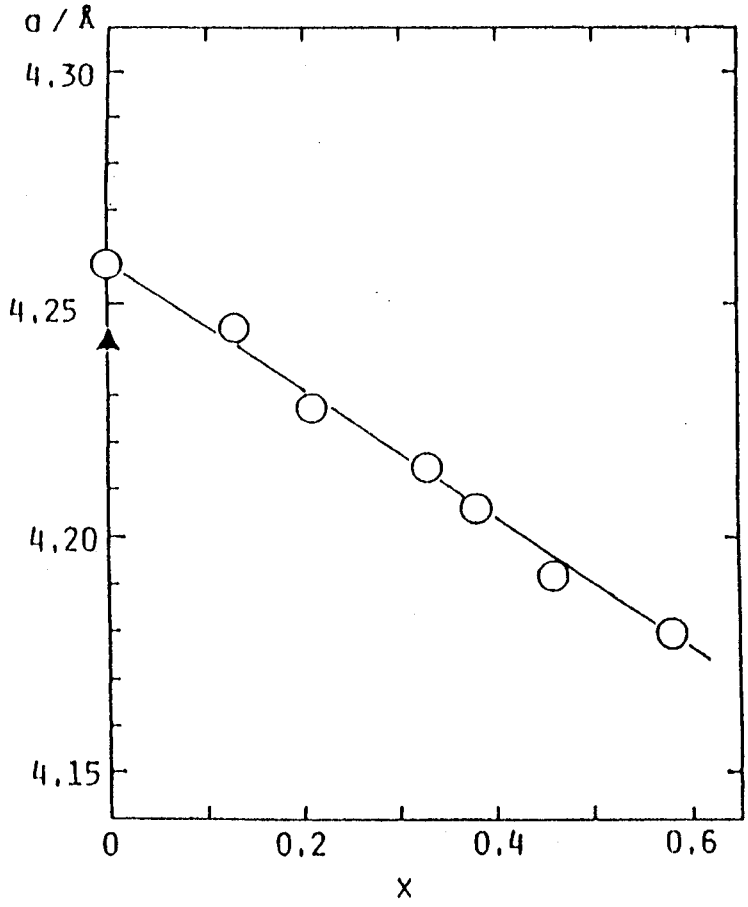

Fig. 3·1·4. Relationship between lattice constant and composition of $Ti_{1-x}Al_xN$ with NaCl-type structure. ○: sputtered films at gas pressure 1×10^{-2} Torr, ▲: reported value at ASTM card 6-0644.

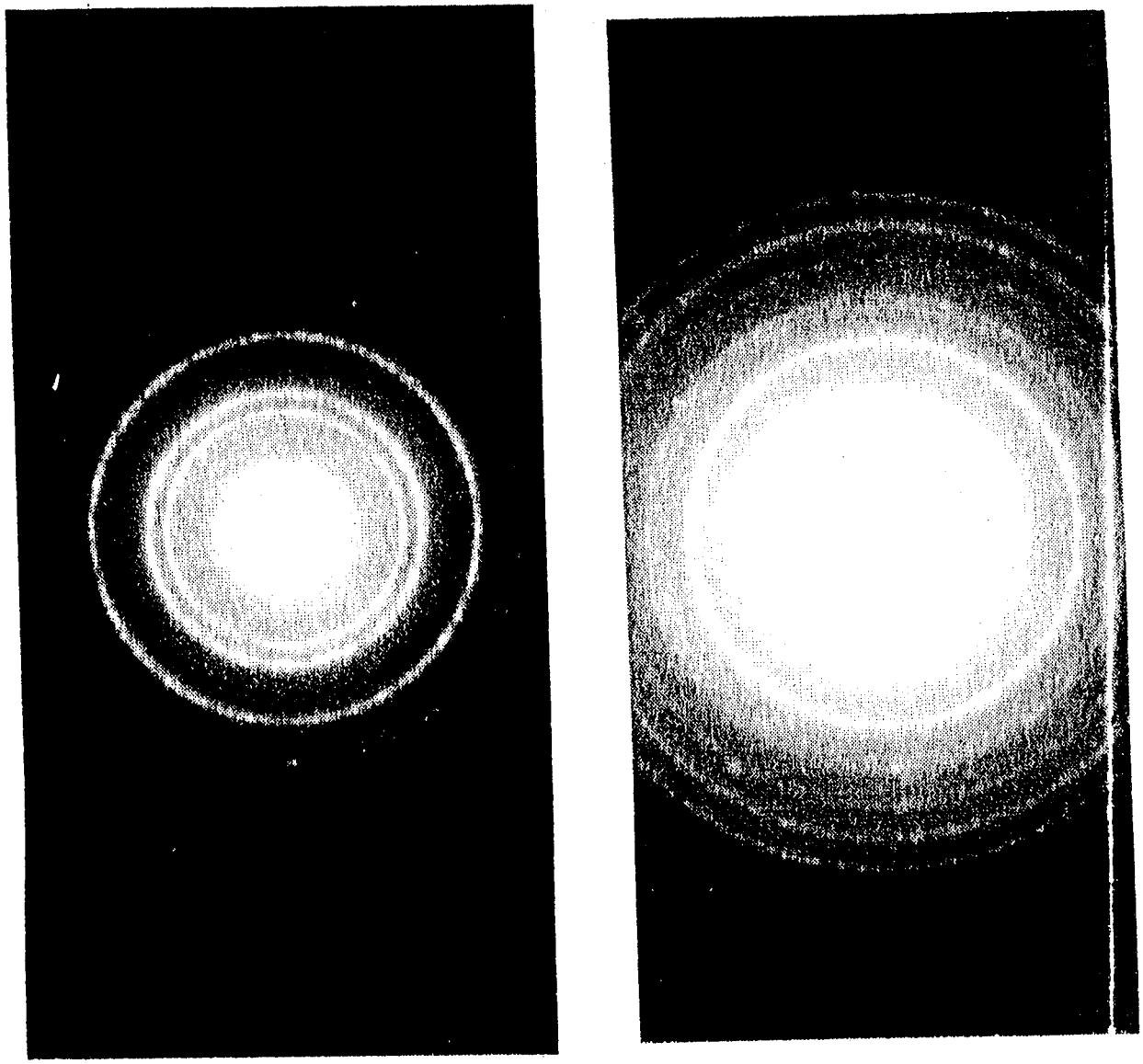

(a) x = 0.38

$Ti_{0.62}Al_{0.38}N$

(b) x = 0.58

$Ti_{0.42}Al_{0.58}N$

Fig. 3-1-5. Electron diffraction photograph of NaCl- type solid solution

than that of the former.

The very thin films were prepared to observe microstructure of the film by TEM. The sputtered films were prepared for the short deposition time of 15 min. on the slide glass coated by carbon. The film was too thin to be identified by X-ray powder diffraction method. It is assumed that the thickness of the films are 50nm from the deposition time in sputtering. The films peeled from the substrate were observed by TEM. Electron diffraction was measured for the films with the composition of x=0.38 and 0.58 as shown in Fig.3-1-5. For both of them, good homogeneities in texture were confirmed and all diffraction lines observed was indexed with NaCl-type lattice.

To examine the crystal phase at early stage of deposition, the film with the composition of x=0.38 was prepared by sputtering for only 5 minutes on the carbon coated substrate and was peeled off. The electron diffraction pattern of the thin film was similar to ones of the sample with x=0.58 appeared in Fig.3-1-5 and was indexed with NaCl-type lattice. It is thought that the sputtered film is deposited as polycrystal even at first stage of sputtering.

The 200 line profile of the as-sputtered film with a composition of $Ti_{0.42}Al_{0.58}N$, which is slightly rich in aluminum, is broad and asymmetric as shown in Fig.3-1-6(b). After annealing the films at 550℃ in N_2 contained H_2 gas up to 10 %, the 200 reflection shifts toward higher angle, and its rocking curve becomes sharper and more symmetric than that of the former as-sputtered film as shown in Fig.3-1-6(a).

Most of the NaCl-type solid solution were easily stripped off from substrates. That is thought to be caused by the difference in the expan-

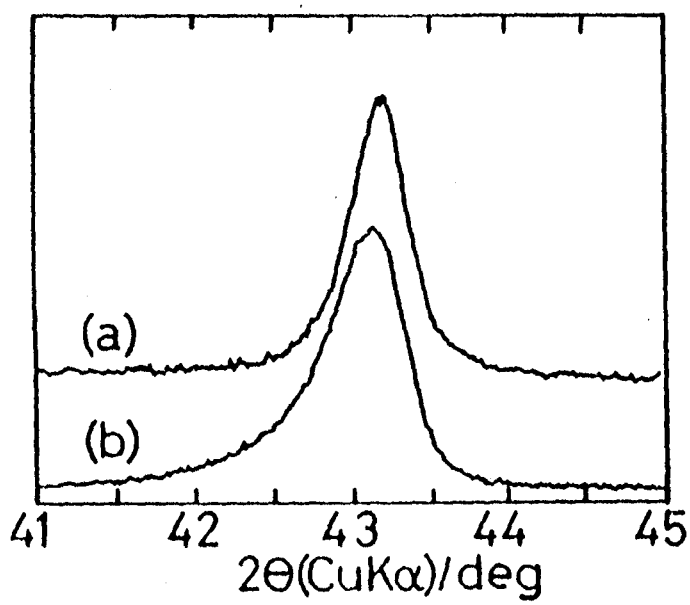

Fig. 3·1·6. XRD line profiles (200 reflection) of $Ti_{0.42}Al_{0.58}N$ films. (a); annealed at 550°C and (b); as-sputtered films.

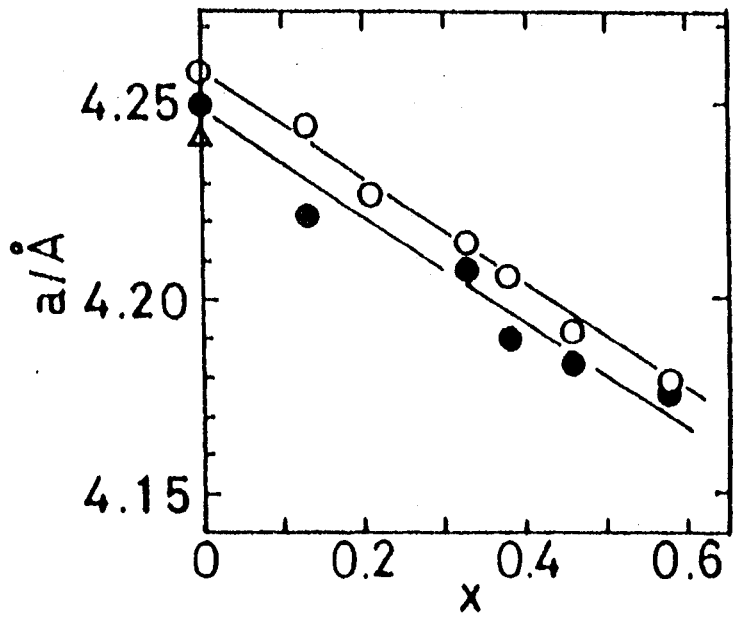

Fig.3-1-7. Lattice constant, a, to composition, x, relationship displayed from the NaCl- type solid solution. Open and closed circles denotes both as-sputtered films and those annealed at 550^{0}C, respectively. Triangle is TiN data, taken from ASTM cards.

sion coefficient between the products and the substrates. As mentioned above, the results of AEM and EM measurements on the as-sputtered film showed that the film had good homogeneity in both chemical composition and texture. Annealing experiment for the as-sputtered film with x=0.58 indicated to be also a single phase with NaCl-type structure. Therefore one can deduce that the broad and asymmetric X-ray reflection peak of the as-sputtered film is caused by not the coexistence of particles having different chemical composition, but the lattice strain induced during sputtering process.

The NaCl-type solid solutions except x=0.58 were also annealed in the reducing atmosphere similar to the case of $Ti_{0.42}Al_{0.58}N$. The lattice constant of the samples after annealing them were shown as a function of x in comparison with the a vs x curve appeared in Fig.3-1-7. The lattice constant of the annealed film decreases linearly with an increase of x as similar to that of the as-sputtered films. But the lattice constants of the annealed films are smaller than those of the as-sputterd film.

The as-sputtered TiN had slightly larger lattice constant compared to the lattice constant of bulk TiN reported[62] so far, but after annealing, the lattice constant approached to the reported value.

These findings confirm that the as-sputtered films have the lattice strain and the strain is reduced by annealing the films at 550℃ .

The relationship between the lattice constant a and chemical composition x is represented as follows;

$$a\ (nm) = 0.425 - 0.014x \qquad (1)$$

The lattice constant a of TiN was 0.425nm. The atomic radius of N is 0.070

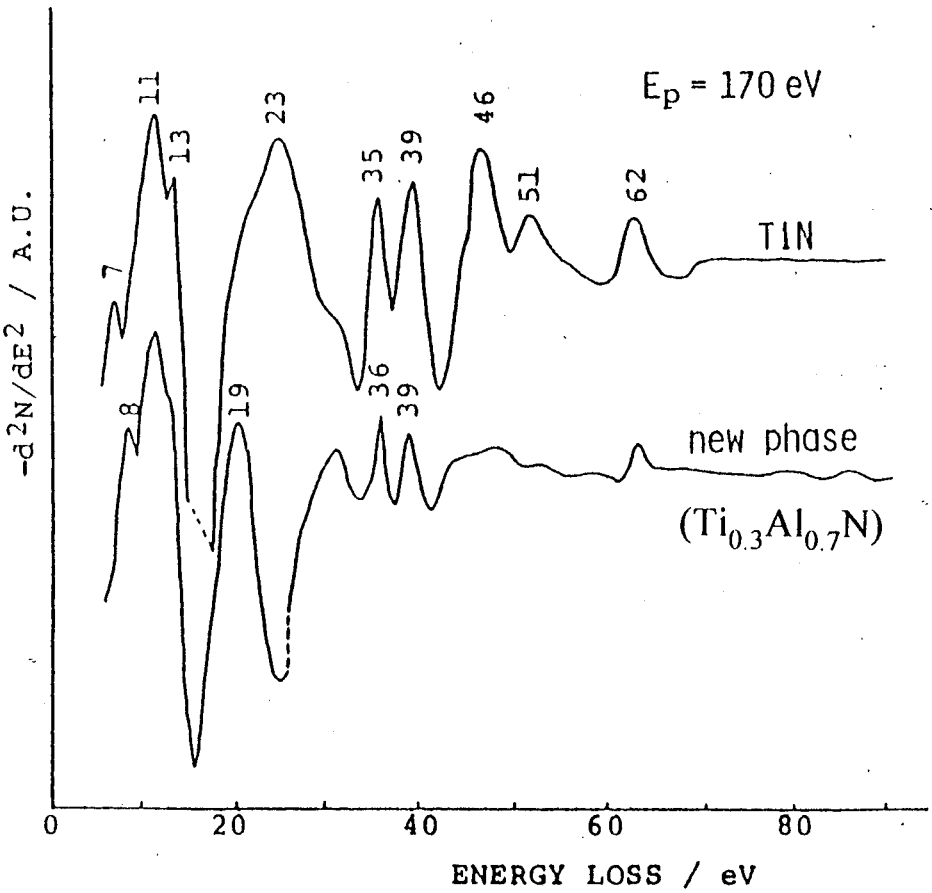

Fig.3-1-8. EELS of TiN and the new double nitride phase

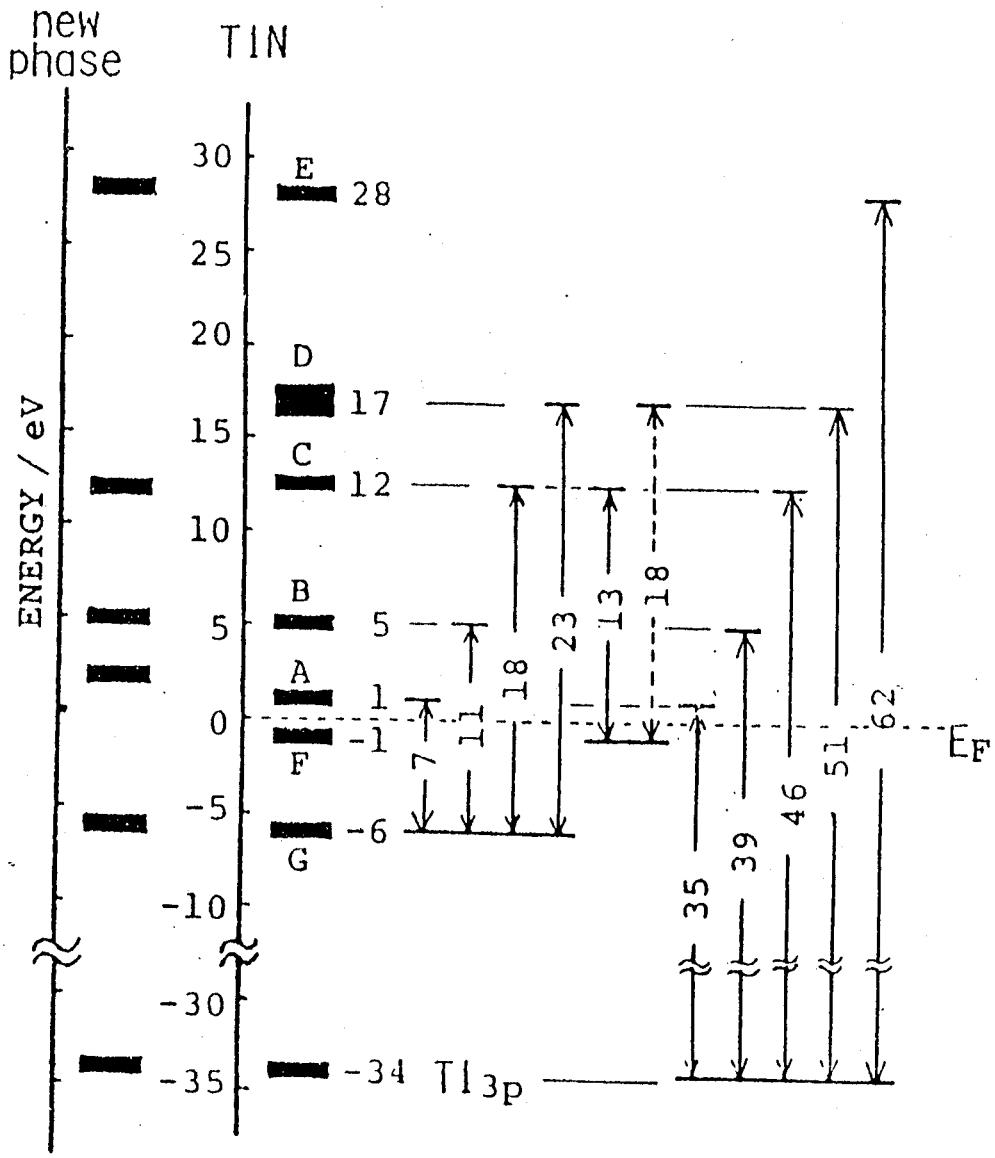

Fig.3-1-9. EELS assignment spectrum for TiN

nm[6]. While the atomic radius of Ti is 0.140 nm[67] and the atomic radius of Al in tetrahedral covalent bond is 0.126 nm[66] The difference of Ti and Al is 0.014 nm which is good agreement with the coefficient in the equation (1), indicating that Vegard's law is applicable for the NaCl-type solid solution in the composition range of $0<x<0.58$.

The low energy electron loss spectroscopy (EELS) were measured on TiN and $Ti_{0.3}Al_{0.7}N$ films. Both spectra are shown in Fig.3-1-8. The assignment of the loss peak, except for collective excitations, may yield informations on the empty levels through the knowledge about the filled states. In the case of the transition-metal dichalcogenides with layer structures, the final levels can be associated with the electronic states of the bulk bands because of the fact that the compounds have no surface states [68]. The loss data on core-electron excitations are expected to indicate directly the electronic structure of the empty states, since the initial states of the transitions populate in narrow energy regions [69,70]. The binding energy of Ti 3p was determined to be about 34 eV by XPS measurement. On the basis of this value 34 eV, the energy levels of TiN were assigned from the EELS spectrum as shown in Fig.3-1-9, which is in good agreement with the results of calculation by LAPW method [71].

The EELS spectrum of new double nitride was assigned on the base of that of TiN. The density of states of the energy level corresponding to D of TiN is very low, so the peaks at 23 and 51 eV in EELS was not observed. The energy level corresponding to A in TiN shifts from 1 to 2 eV, so the peak 7 and 35 eV originated to A, shifts to 8 and 36 eV, respectively. As the density of states of energy level corresponding to F in TiN was lower, the peak at 13 eV was not observed. Thus, the difference of energy level

with TiN and new double nitride suggests to bring to the difference of properties between metallic and semi-conductive.

(2) Wurtzite-type solid solution

In the TiN-AlN system it is difficult to synthesize a solid solution by the usual solid reaction at high temperature. In the present investigation, the reactive sputtering which is a non-equilibrium reaction process was employed for preparation of the solid solution. The synthesized nitride had three crystal phase which were wurtzite-type solid solution, NaCl-type solid solution and the new double nitride, with the ranges of contents $0.8 \leq x \leq 1.0$, $0 \leq x \leq 0.6$ and $x=0.7$ respectively as shown in Fig.2-6.

Fig.3-2-1 shows X-ray diffraction patterns of the $Ti_{1-x}Al_xN$ films in the range of $0.64 \leq x \leq 1.0$. These films were confirmed to have good homogeneity from the results of AEM and EM measurements. The pattern of AlN, $x=1.0$ shows that the AlN film exhibits a remarkable preferred orientation with the (002) plane parallel to the film surface, and that the preferred orientation diminishes with increasing x, Ti content. Then it was observed the preferred orientations with the (100) or (110) plane parallel to the films surface in the range of $0.09 \leq x$. The peak position of the both 100 and 110 diffraction of the films with chemical composition of $0.83 \leq x \leq 1.0$ were shifted to lower angle side with decreasing x, indicating that the a-axis expands with the Ti content. Whereas no shift for the 002 diffraction was observed.

Fig.3-2-2 showed the relationship between lattice constant calculated from 100 and 110 diffraction peak position and composition x of wurtzite-type $Ti_{1-x}Al_xN$. The a-parameter of the AlN film was 0.3136nm, the value of

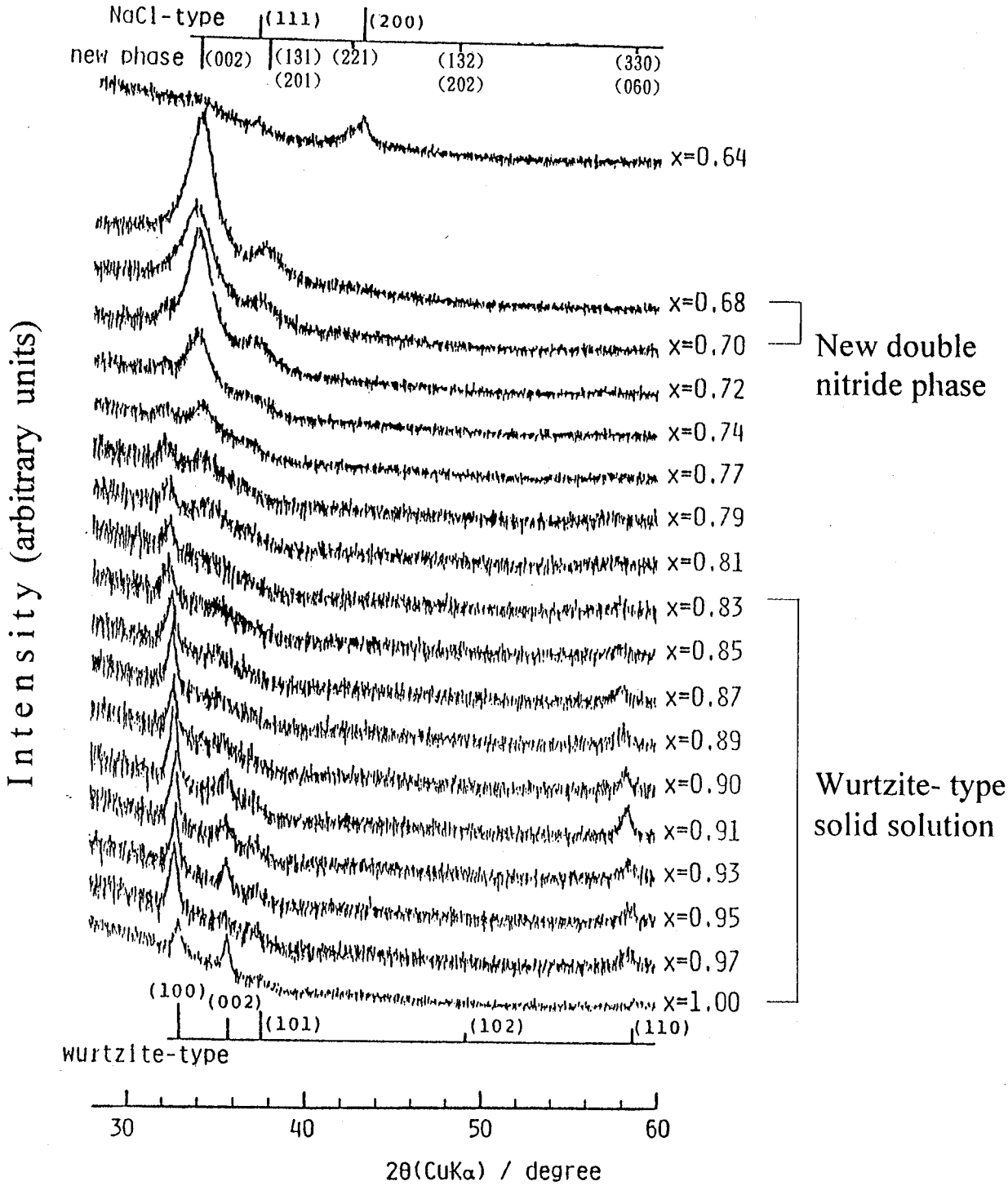

Fig.3-2-1. X-ray diffraction patterns of $Ti_{1-x}Al_xN$ films in the $0.64 \leqslant x \leqslant 1.00$ range

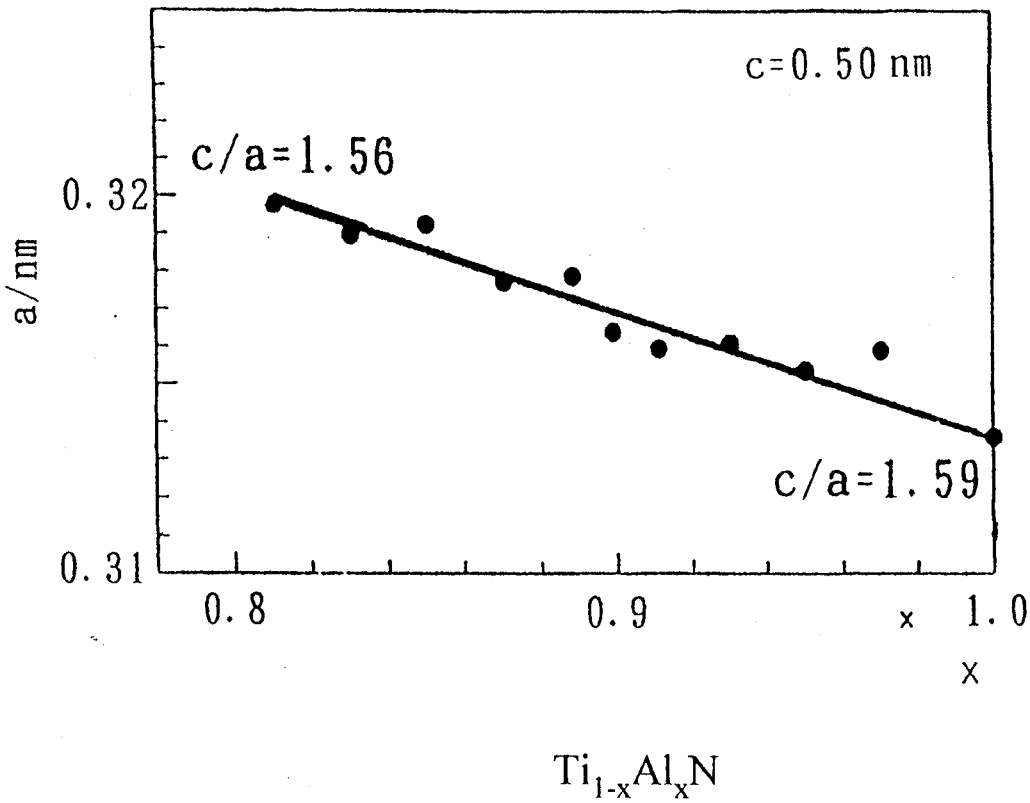

Fig.3-2-2. Lattice parameter of wurtzite-type solid solution

which was larger by 0.0025nm than that of AlN reported in ASTM. This discrepancy was thought to be due to the nonstoichiometry of nitrogen or the impurity of oxygen etc..

In the range of $0.83 \leq x \leq 1.0$ the length of c-axis kept the constant value of 0.50nm, whereas the length of a-axis increased from 0.314 to 0.319nm with increasing TiN content. The dependence of unit cell volume on composition agrees with the expected one based on different between the covalent bond radii of Al atom and the atomic radii of Ti atom. It is therefore, proved that the wurtzite-type solid solution was formed in this range. The axial ratio, c/a, was reported to be the value of 1.60 for AlN[72], whereas the value of 1.59 was obtained by this measurement. This discrepancy may be caused by nonstoichiometry of the sputtered samples. Anyhow, the axial ratio by this experiment is smaller than that for the ideal wurtzite-type structure, 1.63. This tendency becomes larger with increasing TiN content.

(3)New double nitride phase

The X-ray diffraction patterns of the sputtered films with x=0.5, 0.7, and 0.85 are displayed in Fig.2-4 (a), (b) and (c), respectively, which show remarkable preferred orientations. The patterns of the samples with x=0.85 and 0.5 showed wurtzite-type and NaCl-type crystal structure, respectively. The pattern of the sample with x=0.70 was different from wurtzite-type or NaCl-type structure and suggested that the sample was a new crystal phase. Fig.3-3-1 showed the X-ray diffraction pattern of the sample with x=0.70 which was peeled off from the substrate and milled to eliminate the effect of preferred orientation. The peak around 2θ =34° (d=0.26nm) is

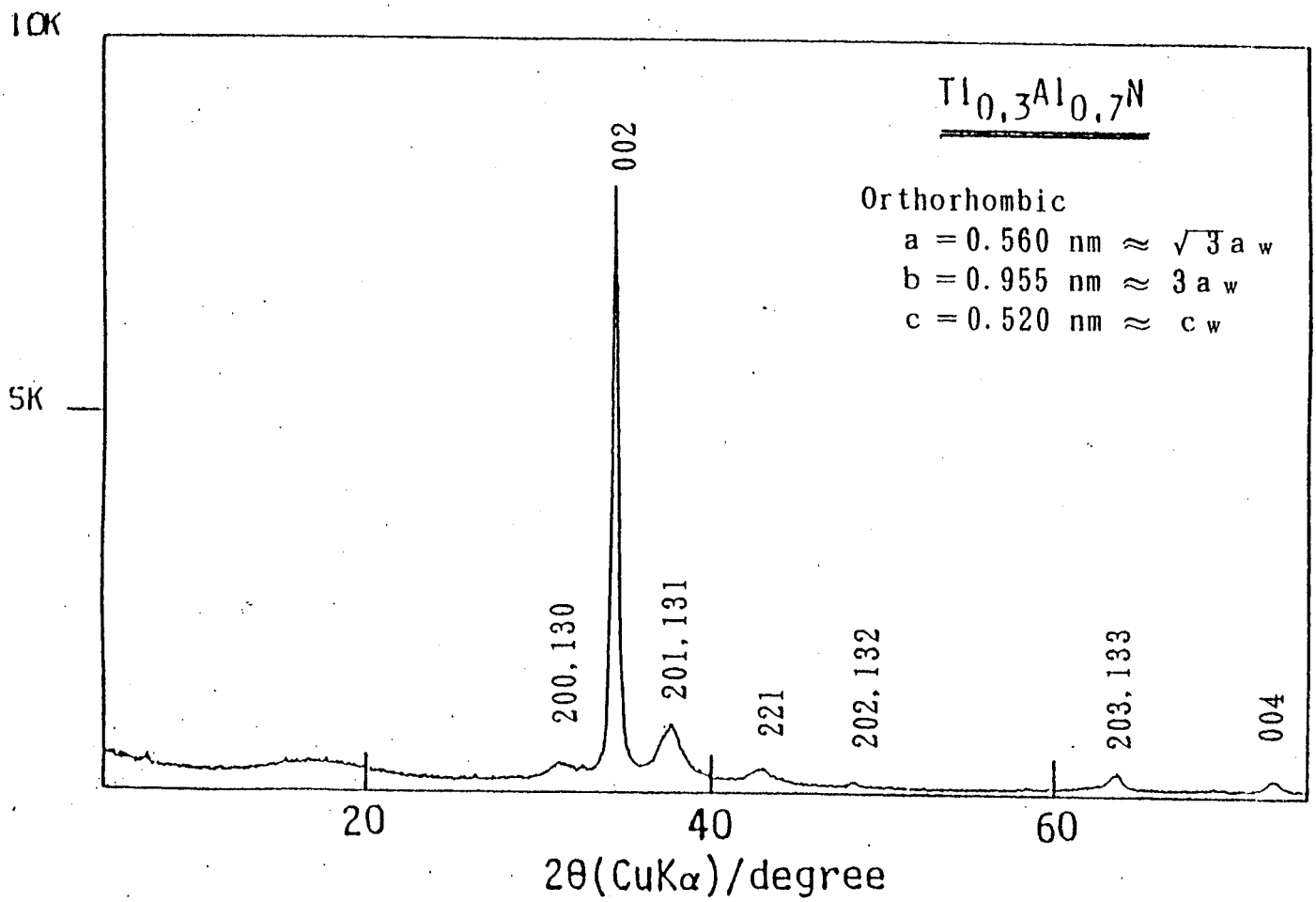

Fig. 3-3-1 X-ray diffraction pattern of the new double nitride.

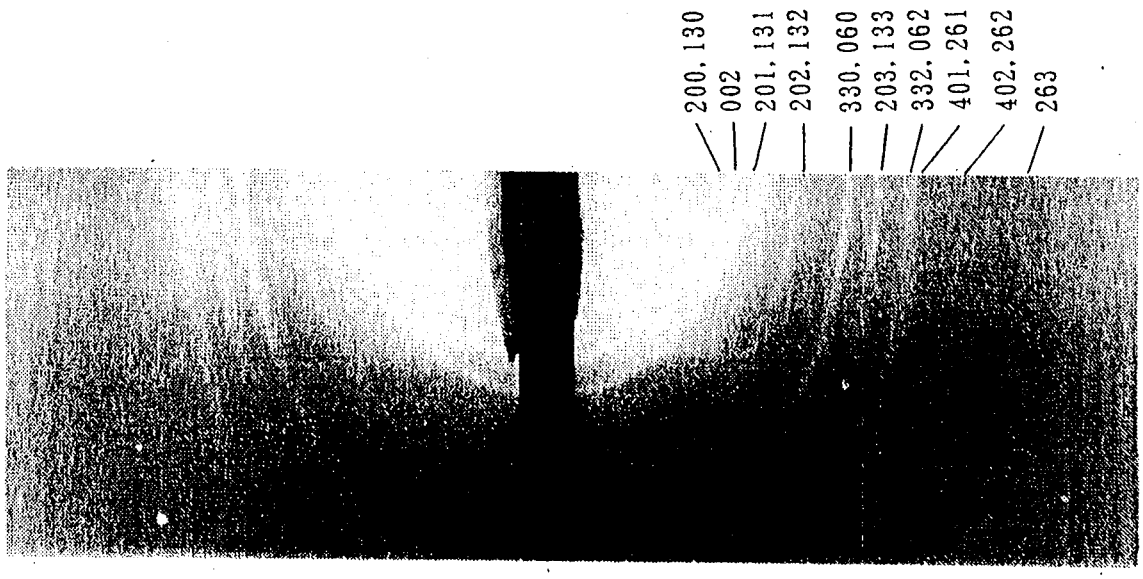

Fig. 3-3-2 X-ray diffraction photograph of the new double nitride. ($Ti_{0.3}Al_{0.7}N$)

Table 3-1. X-ray diffraction data of $Ti_{0.3}Al_{0.7}N$

observation		calculation		
d(nm)	Int.	d(nm)	h k l	Int(%)
--	--	0.483	1 1 0	7
--	--	0.478	0 2 0	13
--	--	0.354	1 1 1	19
		0.280	2 0 0	42
0.278	V.S.	0.277	1 3 0	80
0.260	S.	0.260	0 0 2	78
		0.247	2 0 1	52
0.245	V.S.	0.244	1 3 1	100
		0.191	2 0 2	14
0.190	M.	0.189	1 3 2	28
		0.161	3 3 0	51
0.161	S.	0.159	0 6 0	24
		0.147	2 0 3	24
0.148	M.	0.147	1 3 3	48
		0.137	3 3 2	35
0.136	M.	0.136	0 6 2	17
		0.135	4 0 1	8
0.135	M.	0.134	2 6 1	15
--	--	0.130	0 0 4	3
		0.123	4 0 2	3
0.123	W.	0.122	2 6 2	6
--	--	0.109	4 0 3	8
0.108	W.	0.108	2 6 3	17

(S.:strong, M.:medium, W.:weak, V.:very)

very strong in comparison with all the others.

To confirm the relative intensity, the X-ray diffraction was measured also on the peeled sample set into glass capillary by Debye-Scherrer method as shown in Fig.3-3-2. The peak position and intensity appear in Table 3-1. The peak of d=0.278 and 0.245nm are very strong, but the peak of 0.260 nm reflection is highest in intensity in Fig.3-3-1. In comparison between the results of diffractometer and Debye-Scherrer camera method, the peak position is in a good agreement each other but the relative intensity is very different. The difference of relative intensity means that a week preferred orientation remained yet in the diffraction pattern shown in Fig.3-3-1, because the samples on the glass plate are the form of sheet in micro-vision. Diffractometer provides precise values in the peak position, and Debye-Scherrer photograph provides good data in the relative intensity.

In order to examine coordination number of Ti in the new double nitride XAFS of $Ti_{0.3}Al_{0.7}N$ was measured and analyzed in comparison with the both solid solutions. Fig.3-3-3 is XAFS data of $Ti_{1-x}Al_xN$ with x= 0, 0.4, 0.7 and 0.9, corresponding to TiN, NaCl-type solid solution, new double nitride and wurtzite-type solid solution, respectively.

In XAFS of Ti in the wurtzite-type solid solution, the obvious peak around 4.966 keV was observed, which corresponds to coordination number of 4 for Ti. In contrast with the wurtzite-type solid solution, in TiN and the NaCl-type solid solution, a weak peak is observed at 4.968 keV, which corresponds to coordination number of 6 for Ti.

In the XAFS of new double nitride, a obvious peak was observed at 4.966 keV which is same as in wurtzite-type solid solution. These results indicate

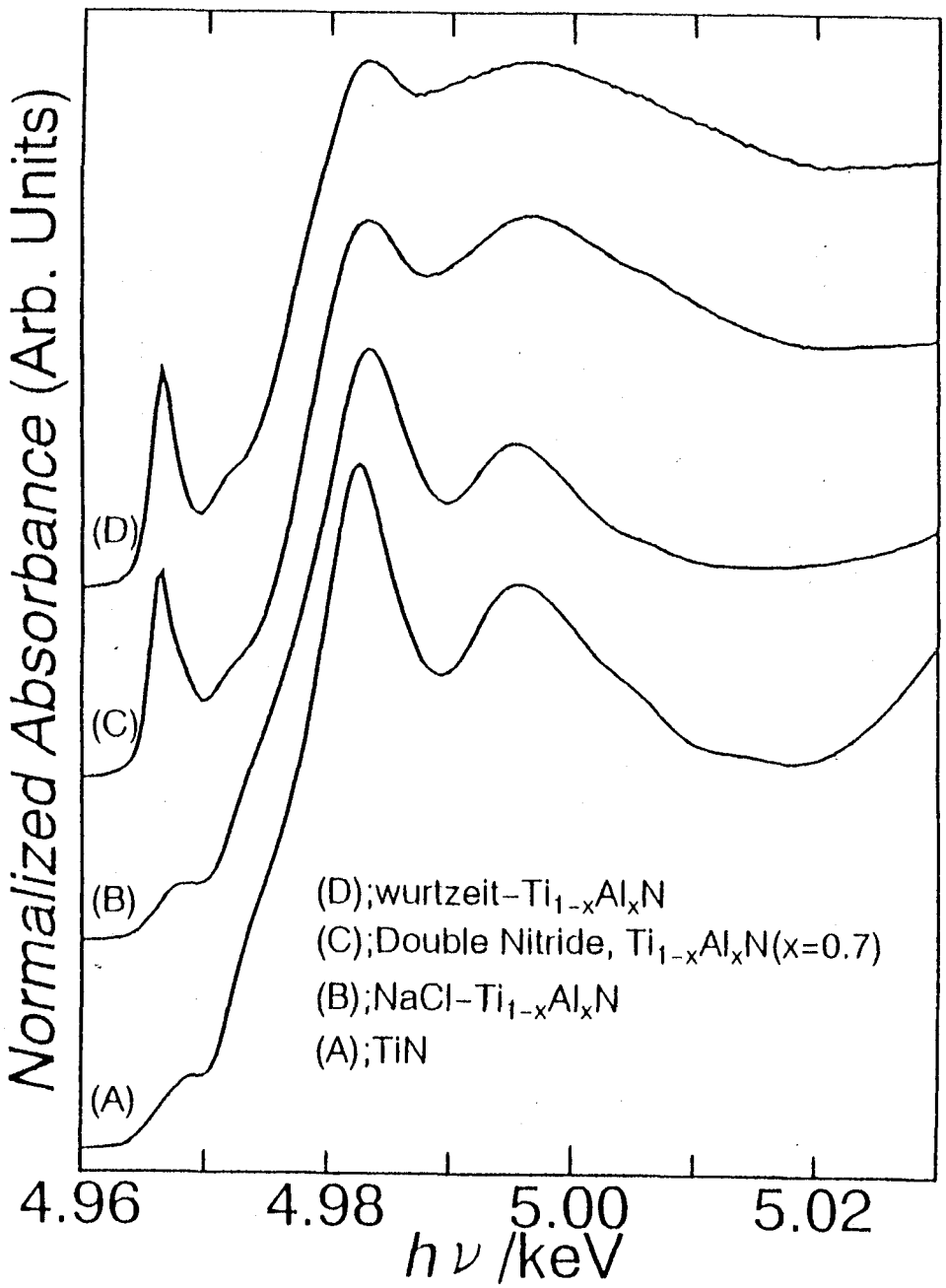

Fig.3-3-3. XANES of $Ti_{1-x}Al_xN$.

(A) x = 0.0, TiN

(B) x = 0.4, NaCl- type solid solution

(C) x = 0.7, New double nitride phase

(D) x = 0.9, Wurtzite- type solid solution

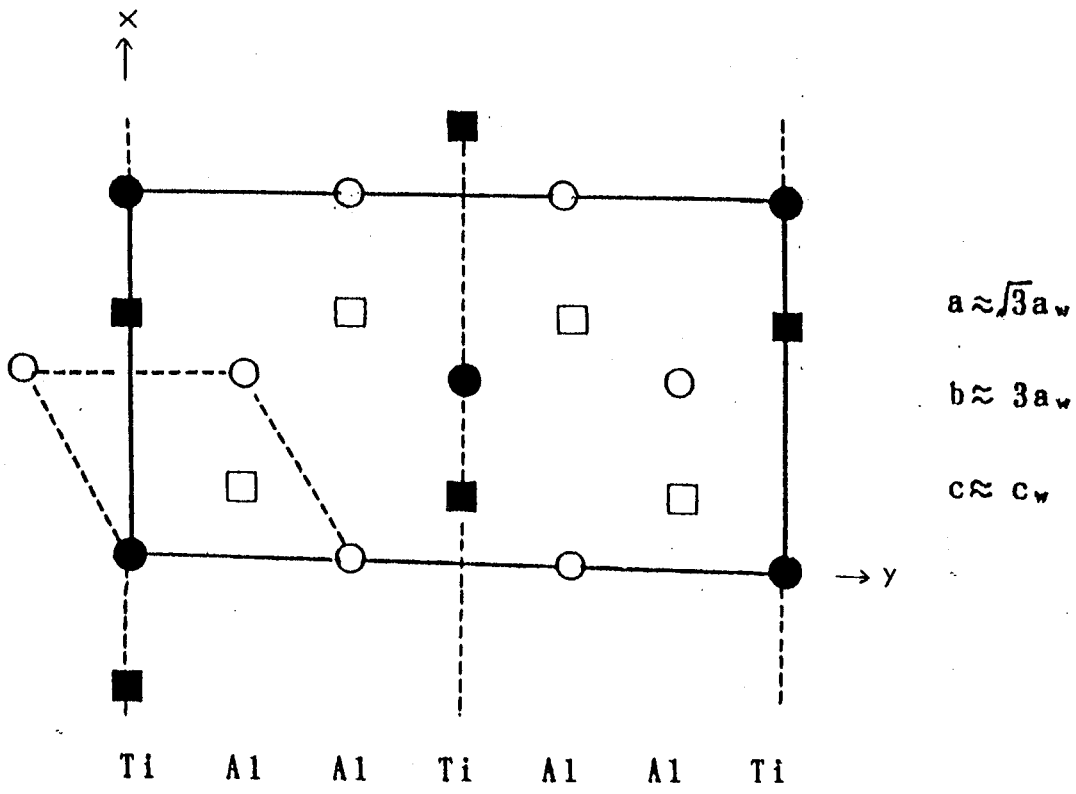

Fig. 3-3-4 Structure of $Ti_{0.3}Al_{0.7}N$

●, ■ Ti, z = 0, z = 1/2

○, □ Al, z = 0, z = 1/2

Orthorhombic

a = 0.560 nm

b = 0.955 nm

c = 0.520 nm

that in the new double nitride, Ti atoms have the coordination number of 4. On the basis of these findings, the analysis of crystal structure in $Ti_{0.3}Al_{0.7}N$ was performed. The observed diffraction lines of the $Ti_{0.3}Al_{0.7}N$ are indexed on a orthorhombic cell with the lattice constant a=0.560, b=0.955, c=0.520 nm as shown in Fig.3-3-4. A lozenge is the unit cell in wurtzite-type structure. A rectangular in line is the orthorhombic cell of $Ti_{0.3}Al_{0.7}N$. The atoms of Ti, Al, Al are ordered along y-axis. The relationship between d-value in observation and calculation is described in table 3-1. The both of d-values have a good agreement. The relations of lattice constants between the new crystal phase and AlN are as follows;

$$a=\sqrt{3}\,a(AlN),\ b=3a(AlN),\ c=c(AlN).$$

These relationships suggest a ordered structure of Ti and Al atoms in the wurtzite-type structure. Fig.3-3-4 shows the structure model of $Ti_{0.3}Al_{0.7}N$, where the doted lozenge indicates the unit cell corresponding to wurtzite-type structure, and N atoms are eliminated to simplify the figure. The observed values of relative intensity of $Ti_{0.3}Al_{0.7}N$ is in good agreements with the calculated ones as shown in table 3-1.

III-3-2. Chemical bonding

(1) X-ray photoelectron spectra

In order to investigate the chemical bonding states of the both solid solutions and double nitride, X-ray photoelectron spectroscopy (XPS) was measured. Fig.3-5-1 is the Ti 2p spectra of $Ti_{1-x}Al_xN$ film's whose surface partially oxidized by exposing to air. Each sample with x = 0, 0.4, 0.7 and 0.9 is corresponding to TiN, NaCl-type solid solution, double nitride and wurtzite-type solid solution, respectively. The peak shapes of Ti 2p of each phase after removing oxide layer, by ion etching are shown in Fig.3-5-2. A detailed comparison of XPS in Fig.3-5-1 with those in Fig.3-5-2 suggests that TiN is oxidized vigorously on the film surface. Binding energy of Ti $2p_{3/2}$ for TiN was observed at 455.0eV after ion etching for 300 min., the value of which is in good agreement with the data reported for TiN[-15].
Ti 2p peak position of TiN before etching for 15 min. is about 459 eV which is corresponding to TiO_2[-14]. The Ti 2p peak shape had the shape corresponding to a mixture of TiO_2, TiN and others. Saha et al.[-14] reported spectral features for oxidized TiN which are intermediate between TiN and TiO_2. In similar studies Bertoti et al.[??] separated Ti 2p peak into those of TiN, TiN_xO_y, Ti_2O_3 and TiO_2 in the system of TiN-TiO_2. In the present work, we also could not explain the Ti 2p spectra as a mixture of TiN and TiO_2. In Fig.3-5-2 the Ti $2p_{3/2}$ peak position of $Ti_{1-x}Al_xN$ shifts to higher energy side with increasing x. Ti 2p peak position of wurtzite-type solid solution before etching was 457.6 eV. In Fig.3-5-1 also except TiN, Ti 2p peak shape of each phase before etching consists of nitride observed in Fig.3-5-2 and oxide which is higher energy side than nitride. The Ti $2p_{3/2}$

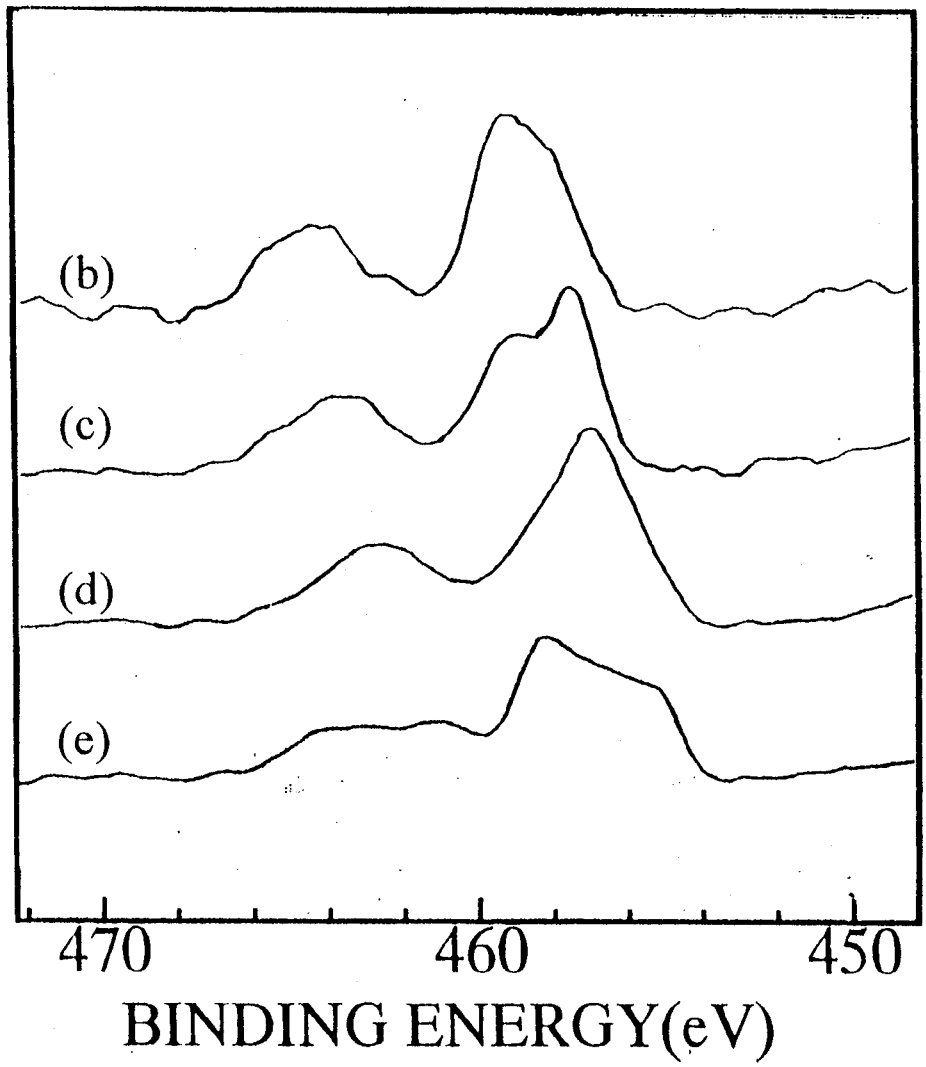

Fig.3-5-1. Ti 2p, XPS of $Ti_{1-x}Al_xN$ surface

(b) Wurtzite- type solid solution (x = 0.9)

(c) New double nitride phase (x = 0.7)

(d) NaCl- type solid solution (x = 0.4)

(e) TiN (x =0.0)

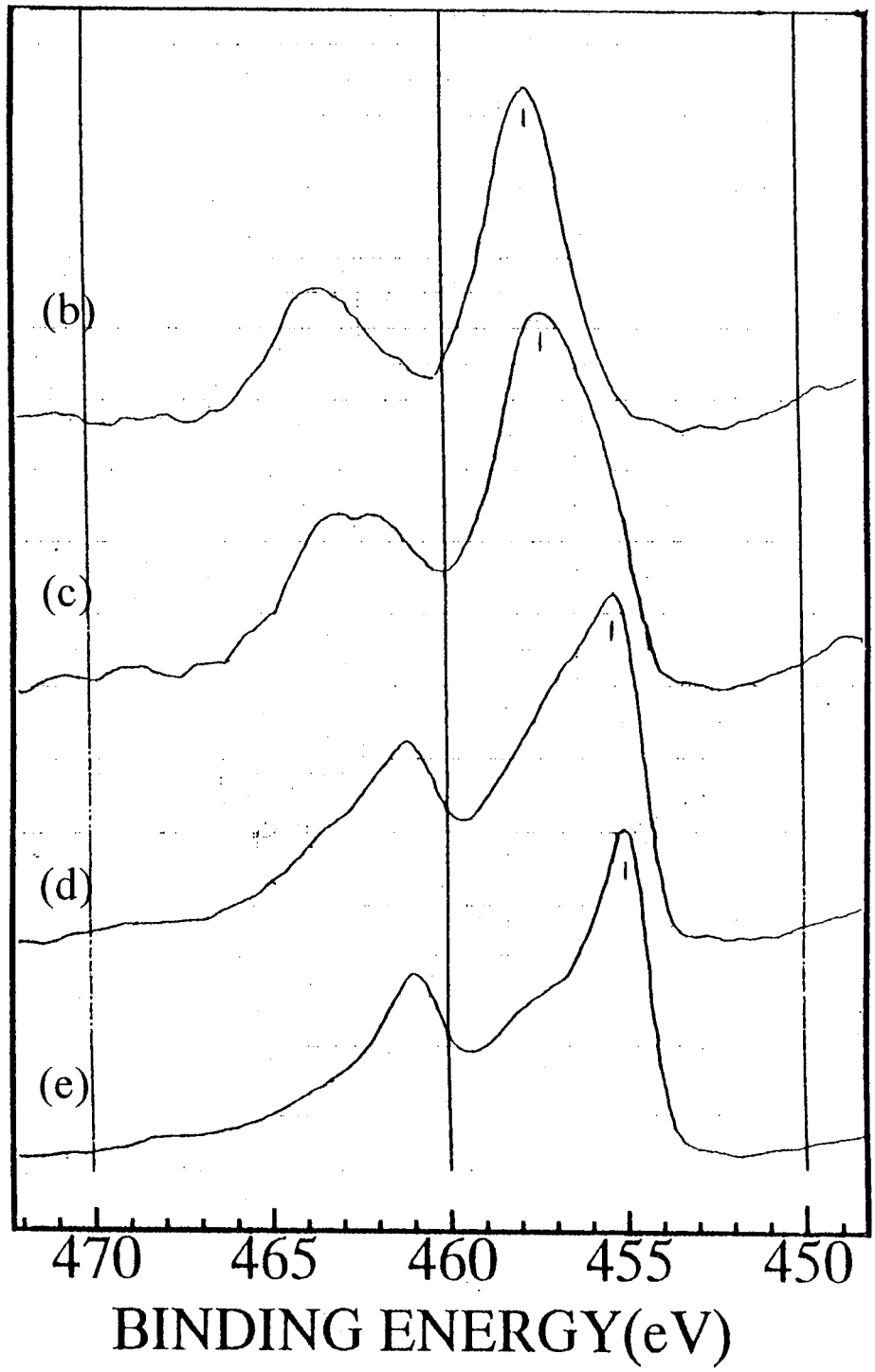

Fig.3-5-2. Ti 2p, XPS of $Ti_{1-x}Al_xN$ after 15 min. etching.

(b) Wurtzite- type solid solution (x = 0.9)

(c) New double nitride phase (x = 0.7)

(d) NaCl- type solid solution (x = 0.4)

(e) TiN (x =0.0)

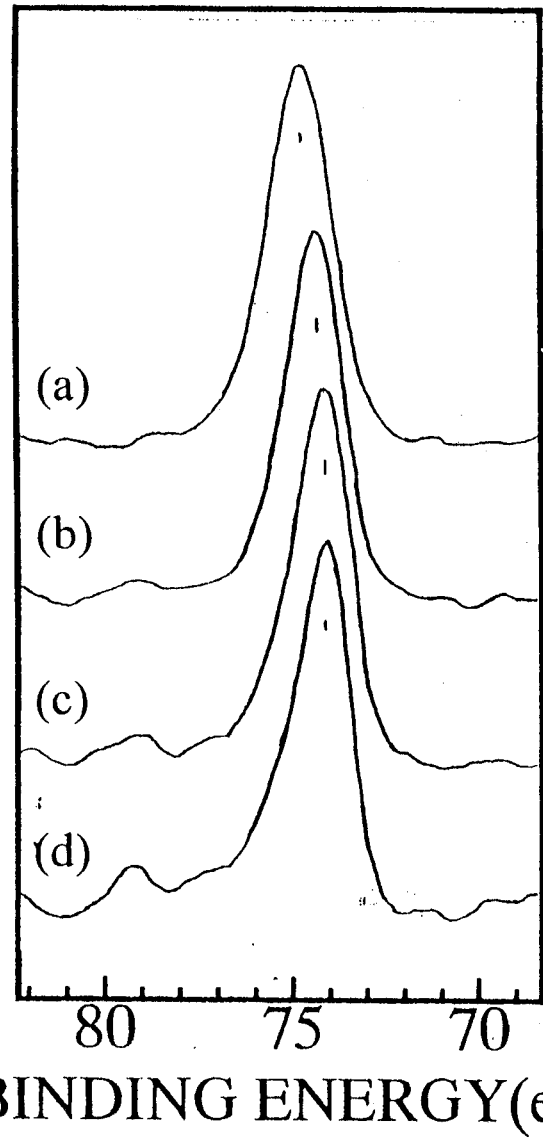

Fig.3-5-3. Al 2p, XPS of $Ti_{1-x}Al_xN$ after 15 min. etching

(a) AlN (x = 1)

(b) Wurtzite- type solid solution (x = 0.9)

(c) New double nitride phase (x = 0.7)

(d) NaCl- type solid solution (x = 0.4)

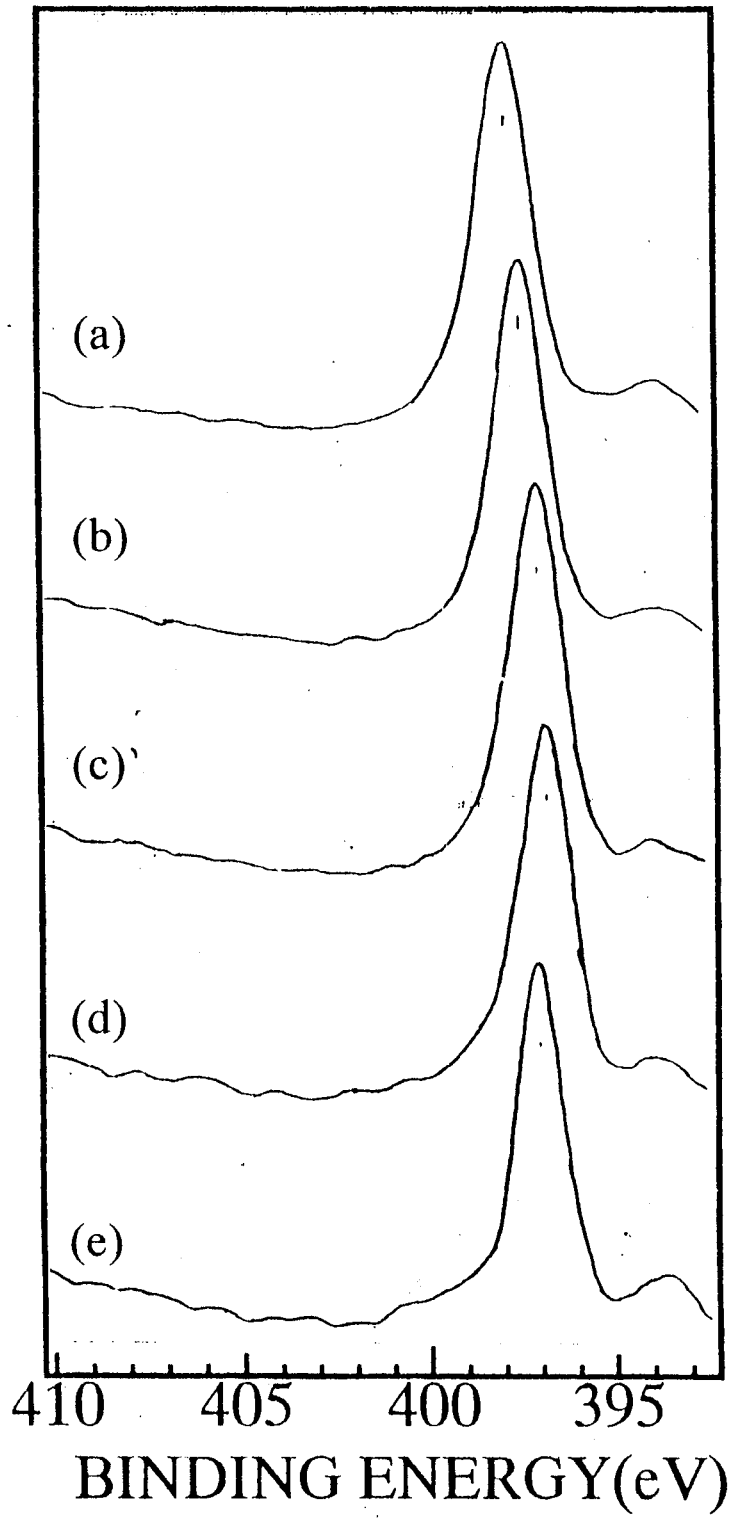

Fig.3-5-4. N 1s, XPS of $Ti_{1-x}Al_xN$ after 15 min. etching

(a) AlN (x = 1)

(b) Wurtzite- type solid solution (x = 0.9)

(c) New double nitride phase (x = 0.7)

(d) NaCl- type solid solution (x = 0.4)

(e) TiN (x = 0)

peak position of oxide shifts higher energy side with increasing x, similarly to nitride. This suggests to existing of chemical bonding in the complex oxides between Ti and Al, described in next chapter.

Al 2p spectra for each phase after etching for 15 min. to remove the oxide layer at the surface are shown in Fig.3-5-3. Binding energy for the Al 2p peak in AlN film was determined to be 74.8eV, and decreases with increasing Ti content, because of transfer a part of d-electrons from Ti atom to N and Al atoms. Binding energy for the Al 2p peak in the NaCl-type solid solution was 74.2 eV. In Fig.3-5-4 Binding energy for the N 1s peak in AlN after etching for 15 min. was determined to be 397.9 eV. Binding energy of the N 1s in the wurtzite-type solid solution and the new double nitride were 397.5 and 397.2 eV, respectively, i.e. the binding energy of N 1s in the wurtzite-type solid solution decreases with increasing Ti content, while, the binding energy of N 1s was not so much different among the new double nitride, NaCl-type solid solution and TiN films. These results indicate that the bond strength of Al-N increases with increase Ti content because of a partial electron transfer from Ti atom to Al atom via N atom.

The XPS's in the valence band energy region for $Ti_{1-x}Al_xN$ film are shown in Fig. 3-5-5. Spectra were measured after cleaning the sample surface by the ion beam etching. The Fermi edge are clearly observed in the spectra for both TiN and the solid solution with x=0.2. Whereas there is no sign for the Fermi level for both AlN and the solid solution with x=0.8. According to the preliminary study for the XPS measurement of $Ti_{1-x}Al_xN$, the Fermi edge was not detectable for $Ti_{1-x}Al_xN$ (x=0.3). These findings indicate that $Ti_{1-x}Al_xN$ with $x<0.3$ is expected to show the metallic electric conductivity.

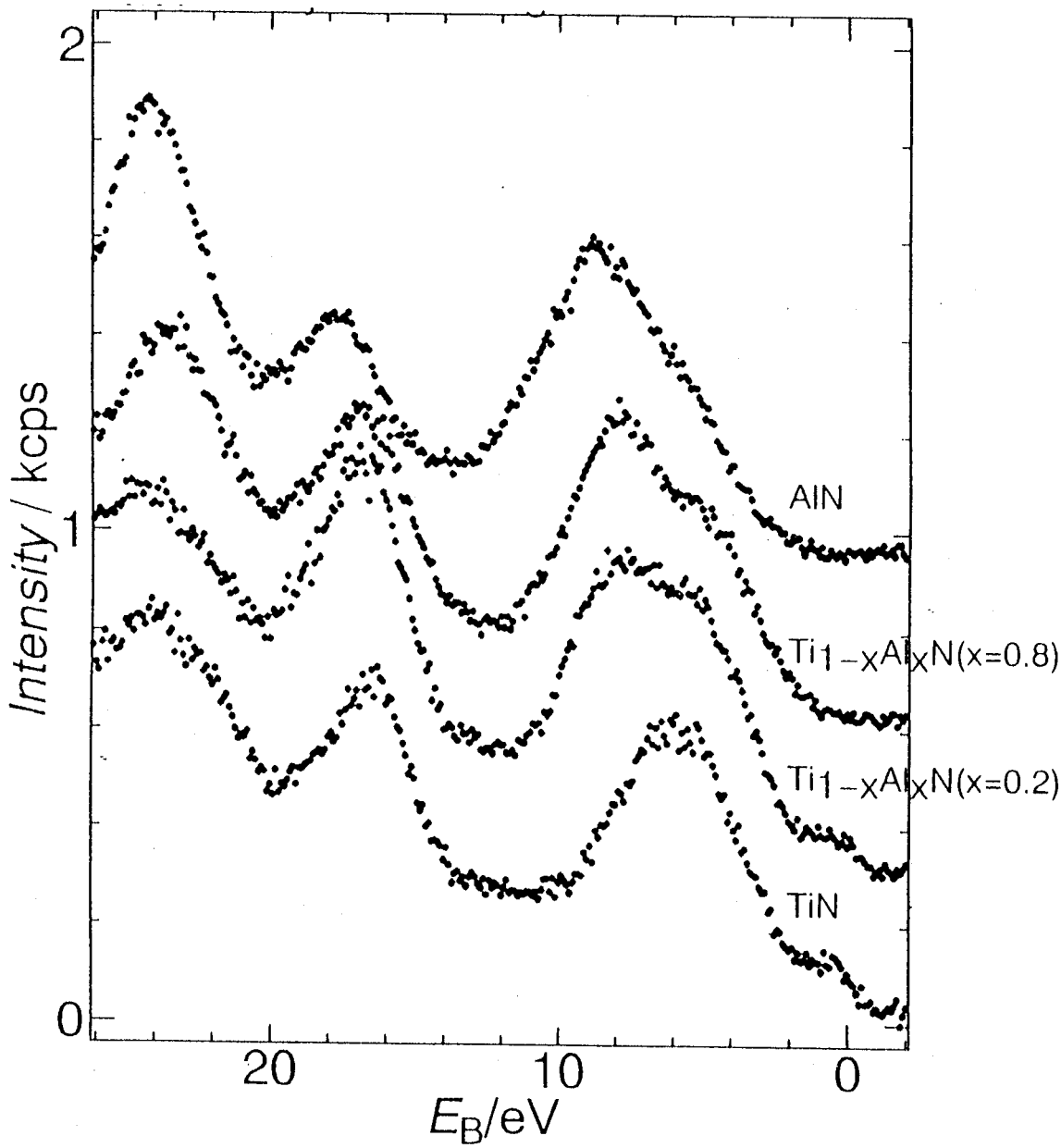

Fig.3-5-5. VB region of XPS for $Ti_{1-x}Al_xN$ thin film cleanned up by means of Kr^+ etching

The maximum intensity of the first band for AlN is around Eb (binding energy) of 9eV and the intensity of the spectrum around 9eV decreases with a decrease of x, i.e., decreasing of Al content. The DV-Xα MO calculations for several models for $Ti_{1-x}Al_xN$ lead to the following assignment of the spectra. The Fermi level for TiN consists of mainly Ti 3d and the broad band around 6eV is so-called 'p-d band' which is composed of both Ti 3d and N 2p. The numbers of 3d electrons which contribute to the construction of the Fermi level for TiN, decrease with an increment of x. Concurrently the levels composed of Al 3p appears at about 9eV below the Fermi level. The Al 2p electrons also take part in so-called 'p-d band', indicating the 'p-d band' is thought to be the band spread over Ti, N and Al atoms. Further increment of x results in the decrement of the level consisting of Ti 3d. The offset of the first band in the low Eb side shifts to higher Eb side with x, compared AlN and $Ti_{1-x}Al_xN$ (x=0.8) as seen in Fig.3-5-5. These make us inferred that the band gap for $Ti_{1-x}Al_xN$ increases with an increment of x.

(2) Auger measurement

X-ray induced Auger electron spectrum(XAES) of Al KLL were measured as shown in Fig.3-6-1. The kinetic energy of AlN after 5 min. etching was estimated to be about 1388.0 eV. The kinetic energy shifts to higher energy side and the peak intensity decreases with increasing Ti content. XAES's of O KLL (oxygen) are shown in Fig.3-6-2. The electronic state of surface oxide for each solid solution and new double nitride is different from both end member, but is, if anything, like that for AlN. Hereupon, the surface oxidation of Ti metal is easier than that of Al metal since both me-

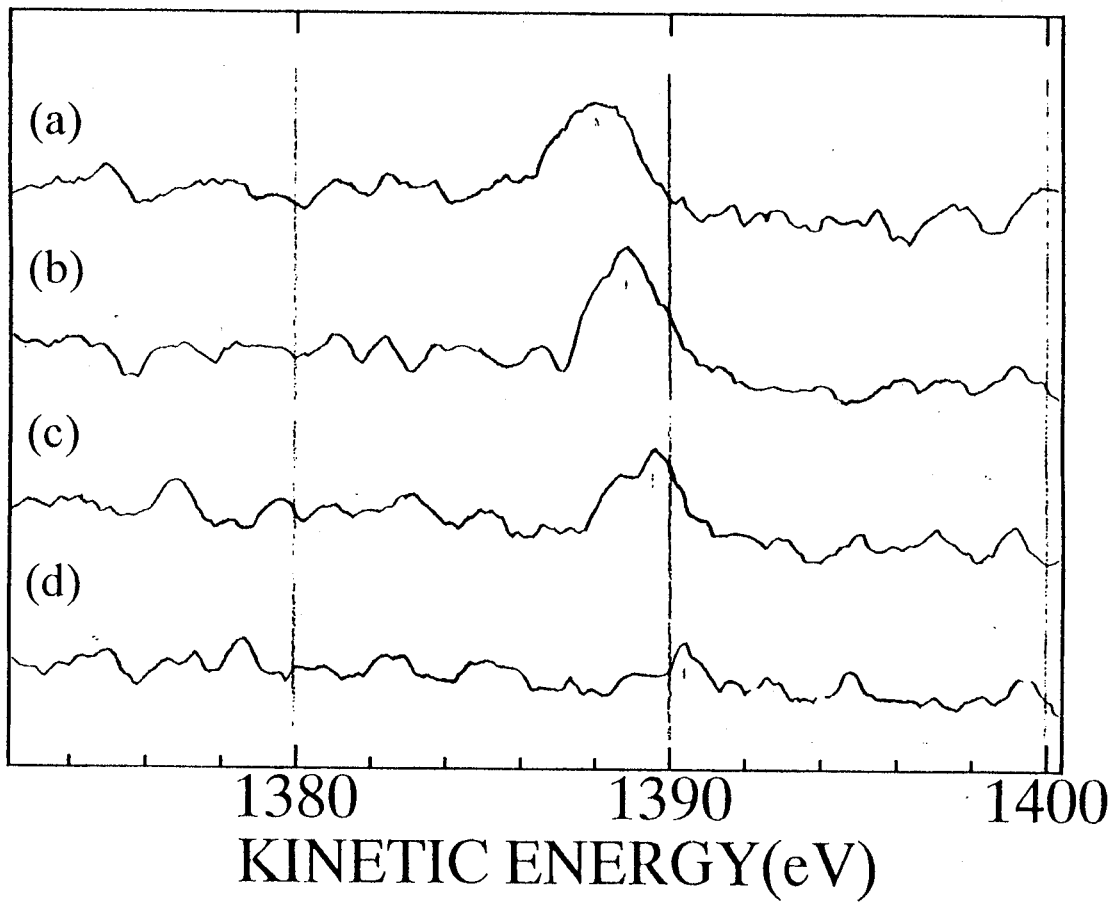

Fig.3-6-1. X-ray induced Auger electron spectra of Al KLL for:

(a) AlN (x = 1)

(b) wurtzite-type solid solution (x = 0.9)

(c) new double nitride (x = 0.7)

(d) NaCl-type solid solution (x = 0.4)

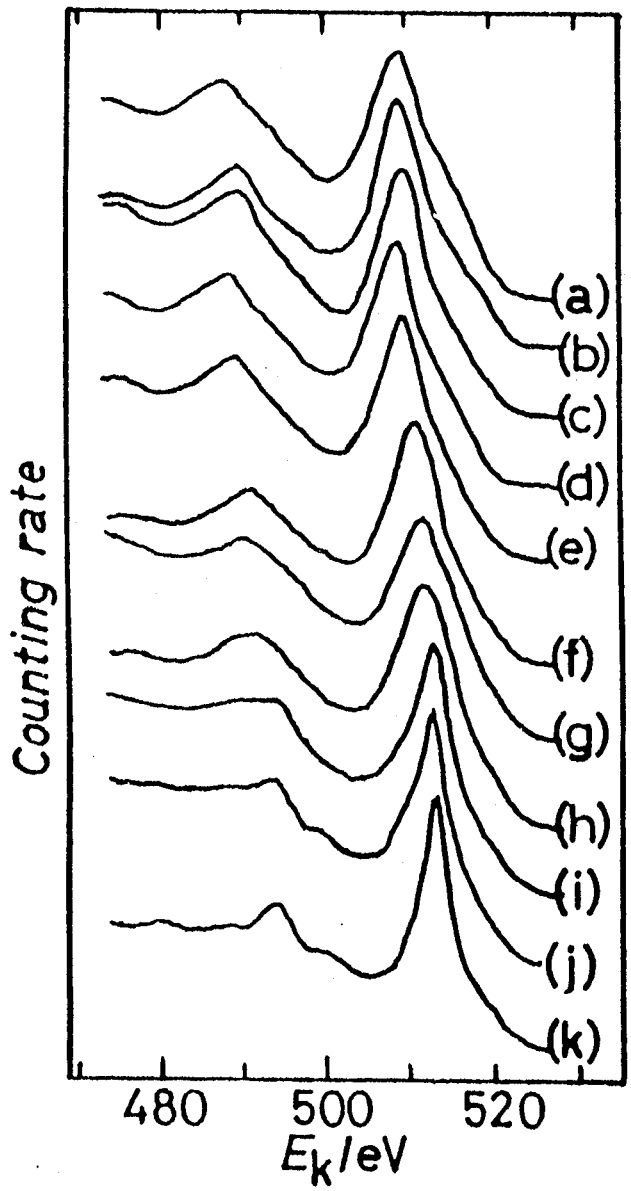

Fig.3-6-2. X-ray excited 0 KLL Auger spectra of:

(a) $Al(OH)_3$

(b) Al_2O_3

(c) Al film

(d) AlN

(e) Wurtzite- type solid solution (x = 0.95)

(f) New double nitride phase (x = 0.7)

(g) NaCl- type solid solution (x = 0.6)

(h) NaCl- type solid solution (x = 0.3)

(i) TiN

tal and oxide peaks for corresponding Al 2p peak are observed in the XPS of a sputter-deposited aluminum film, while metal peak for Ti 2p peak is hardly seen in the XPS of a sputter-deposited titanium film. As for the present solid solution and new double nitride, d electron of titanium is partially transferred into nitrogen and/or aluminum, and then the reactivity of titanium against oxygen becomes lower.

III-4. Conclusion

Titanium nitride has NaCl-type structure in which both Ti and N atoms have coordination number of 6 and exhibits metallic conductivity. While, aluminum nitride has wurtzite-type structure with coordination number of 4 for both Al and N atoms and is an insulator with wide band gap. There are serious difference in structure type and chemical bond between TiN and AlN. Therefore, it is very difficult to form solid solution in the TiN and AlN system by applying conventional solid state reaction. Little investigations of double metal nitrides in the TiN and AlN system have been done so far expect Ti_2AlN, Ti_3AlN and $Ti_3Al_2N_2$, in which the atomic ratio of N to metal (Ti+Al) is not unity.

In the present work, a reactive sputtering method as a thermally non-equilibrium reaction process was applied to prepare the double metal nitrides in the TiN-AlN system, and we succeeded first in forming two kinds of solid solutions and new double metal nitrides with an atomic ratio of N/(Ti+Al)=1 . Characterization of crystal structure and bond nature of the nitrides were carried out as follows.

1. In the TiN-AlN system, new crystal phases, i.e., two kinds of solid solutions and one new double nitride, were prepared by applying reaction sputtering process. One of solid solutions had NaCl-type crystal structure. The other solid solution had wurtzite-type crystal structure. It was clarified that both solid solutions exit in the appreciably wide range.

2. NaCl-type solid solution was produced in the range of $0 < x < 0.6$

in $Ti_{1-x}Al_xN$. The lattice constant linearly decreases with increasing Al content. For sample with x greater than 0.5, a remarkable lattice distortion was observed but disappeared by annealing at 550℃ in the reduction atmosphere. The coordination number of Al was estimated as 6 by the crystal data.

3. Wurtzite-type solid solution was produced in the range of $0.8 \leq x < 1.0$. The lattice constant a of wurtzite-type solid solution linearly increases with increasing Ti content although the lattice constant c is almost constant. The coordination number of Ti in the solid solution was estimated to be 4 by the measurement of XAFS and the crystal data.

4. The coordination number of Ti in the new double nitride was estimated to be 4 by the measurement of XAFS. The X-ray diffraction pattern of new double nitride $Ti_{0.3}Al_{0.7}N$ was indexed on a orthorhombic cell with a=0.560, b=0.955 and c=0.520 nm, consisting of a super lattice of the wurtzite-type structure, in which Ti and Al atoms takes an ordered arrangement.

5. The measurements of valence band in each phase suggested that the valence band of AlN consist mainly of Al 3p and N 2p, and the valence band of TiN consist mainly of Ti 3d and N 2p. Fermi level observed in TiN disappeared in the composition of $x \geq 0.3$ because of decreasing d electron in the t_{2g} band (d-d band) of Ti.

6. The XPS and XAES measurement shows that the Ti $2p_{3/2}$ peak shifted

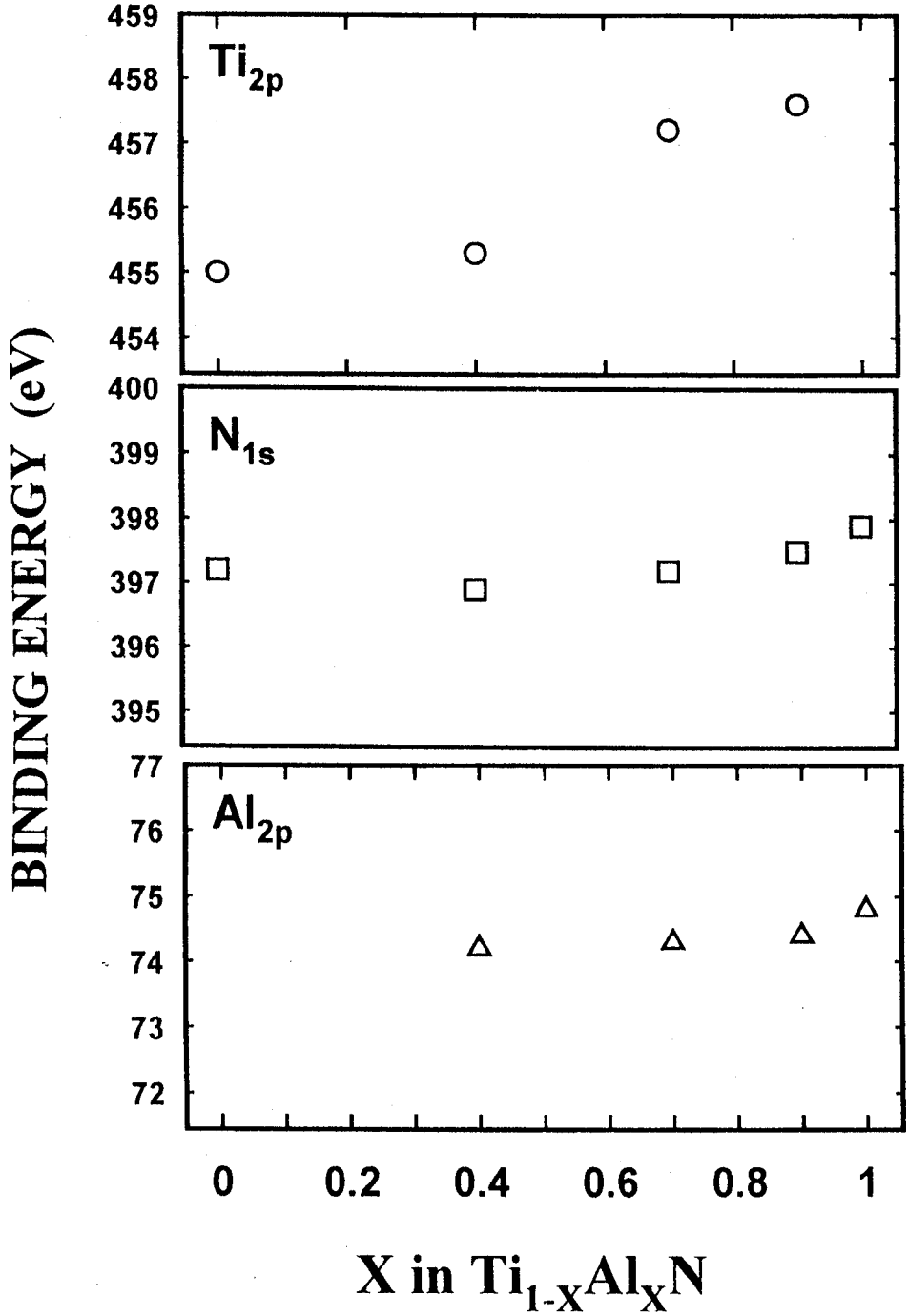

Fig.3-7-1. Binding energy of Ti 2p, N 1s and Al 2p at different concentration

toward higher energy side by adding Al to TiN, and that the Al 2p and N 1s peaks, on the contrary, shifted to lower energy side, compared with those of AlN in Fig.3-7-1. These findings indicate that a part of d electrons (in t_{2g} band) of Ti in TiN transferred to Al through N in the NaCl-type solid solution with increasing AlN content.

7. The electron transfer resulted in the increase of the bond orders for the Ti-N and the Al-N bonding, and also in the improvement of durability against oxidation and hydrolysis of $Ti_{1-x}Al_xN$.

CHAPTER IV. ELECTRONIC AND CHEMICAL PROPERTIES OF THE $Ti_{1-x}Al_xN$ SOLID SOLUTION

IV-1. Introduction

Nitrides can have wide chemical bonding states of the range over ionic, covalent and metallic bond, which depend to the kinds of metal element as the partner with nitrogen. The appearance of various properties are expected in nitrides because various chemical bonding states appear depending upon combination of different metal elements.

In the past process it was difficult to prepare metal nitrides. Accordingly the investigations of nitride solid solutions and double nitrides are very little. But, in oxides, the investigations of solid solutions and multicomponent oxides have rendered great services in material science, material design and etc. It is also important to investigate the solid solution of nitrides and multicomponent nitrides.

Recently the developments of vapor deposition techniques make the preparation of various nitrides easy. Furthermore, PVD (physical vapor deposition) methods are used as one of the thermo non-equilibrium reaction in low temperature process, and we can prepare often the metastable compound with the chemical composition which don't occur by common equilibrium reactions at high temperature. It is, therefore possible to change the chemical composition in wide range.

The band gap of AlN has been proposed as various values ranging from 5 to 6 eV on the base of the results of optical absorption measurements. It is easy for AlN to introduce oxygen as an impurity. AlN including oxygen shows optical absorption peak of 2.86eV(20); Furthermore, other impurities affect on the band gap of AlN as follows, around 2.8eV the sample

with excess aluminum(17) and 3-6eV in the case of carbon impurity(21). Yim et al.[44] supposed that AlN exhibits a direct transition between the energy-gap with a band gap of about 6.2 eV at room temperature. In 1978, Perry and Rutz clarified the band gap of AlN to be 6.2 eV.

While, (Ti,Al)N solid solution films are rapidly oxidized above 800℃ regardless of crystallochemical factors such as the Al concentration and their crystal structure, resulting in formation of TiO_2, Al_2TiO_5, Al_2O_3 and AlN[80]. McIntyre [81] indicated the formation of an Al-rich oxide layer located in the outermost surface followed by a Ti-rich oxide layer on the $(Ti_{0.5}Al_{0.5})N$ film. They could not identify the crystal phases of the oxide layers because of few reflections available in their electron diffraction patterns. These findings put a question whether the outermost oxide layer is useful to prevent oxidation of the film consists of a pure Al_2O_3 layer or not.

In the TiN-AlN system, polycrystallines which have never been reported were prepared. There were three different crystal phase, i.e., two kinds of solid solutions and one new double nitride. One of solid solutions had NaCl-type crystal structure. The other had wurtzite-type crystal structure. It was clarified that both solid solutions exit in the appreciably wide composition range.

In previous chapter, crystal structure and chemical bonding of three crystal phases produced in the TiN-AlN system, were investigated in connection with chemical composition. These results have revealed that the solid solutions and the double nitride have a different chemical bonding and electronic structure in comparison with TiN and AlN. Accordingly it is possible to appear new functions, for example in electric conductivity,

band structure, optical nature, hardness and durability against environment, etc.. It is also expected that the durability against oxidation of TiN is improved by addition of AlN.

In this chapter, the physical and chemical properties of $Ti_{1-x}Al_xN$ solid solutions are discussed in relation with the chemical bonding and structure which described in chapter III.

IV-2. Experimental

$Ti_{1-x}Al_xN$ films were deposited on the substrates such as glass slide, fused silica slide and Mo sheet with using an rf-magnetron sputtering equipment, ANELVA SPF-210H.

X-ray diffraction patterns of the films were taken by a powder diffractometer, employing graphite monochromatized CuKα radiation, and the Bragg angle was calibrated using Si powder as a standard. The film's chemical composition was determined by an analytical electron microscope (AEM), Hitachi HU-12SE. Aluminum titanate Al_2TiO_5, was used as a standard for quantitative analysis.

The electric resistivity was measured by four terminal method in the temperature range from room temperature to liquid helium temperature. The temperature of sample film was determined using a silicon diode sensor, model Si-400.

In order to investigate optical band gap, the optical absorption of wurtzite-type solid solution and the new double nitride was measured by Shimadzu MPS-5000 in the range of wave length from 210 to 740 nm. The band gap was evaluated on the basis of the position of absorption edge and absorption curve shape. Corresponding to the compositional dependence on

the band gap of wurtzite-type solid solution, molecular orbital (MO) calculation by DV-Xα method was performed for various kind of model cluster.

In order to investigate the durability against oxidation of the $Ti_{1-x}Al_xN$ solid solution, heat treatments were carried out under reducing and oxidizing atmospheres in N_2 gas containing 10% H_2, and in O_2 gas, respectively. A differential thermal balance, SINKU-RIKO TGD-5000RH, was used for isothermal oxidation measurements. X-ray photoelectron spectrum (XPS) was measured for investigations on the electronic state by using a Shimadzu ESCA-850 apparatus. The $4f_{7/2}$ line (Eb; 84.0 eV) of Au deposited on the sample's surface was used as a reference level. Argon ion etching for the samples was performed to obtain depth profile of each elements. The ion etch rate was 2.5± 0.5nm/min.

In order to investigate durability against water of the $Ti_{1-x}Al_xN$ solid solution, the measurement of XAES's of Al KLL was performed for the sample exposed in distilled water for 6 hours. Comparing with the spectra of $Al(OH)_3$ and Al_2O_3, the durability against water was evaluated.

IV-3. Results and discussion

IV-3-1. Electron resistivity of NaCl-type solid solution

Fig.4-1-1(a) shows the electrical resistivity-temperature variation of the $Ti_{1-x}Al_xN$ solid solution with NaCl-type structure in the temperature range from 6 to 300 K. The end member TiN was reported to have electrical resistivity of about $3x10^{-5}$ Ω cm in room temperature [85]. As shown in Fig.4-1-1, in room temperature the electrical resistivity of $Ti_{1-x}Al_xN$ increase by about three orders of magnitude with increasing Al content x. This trend reflects that AlN has high electrical resistivity.

The electrical conductivity of the solid solution with x=0.13 at room temperature is about $4x10^{-4}$ Ω cm and its temperature dependence is like metallic one with a positive temperature coefficient of electrical resistivity (TCR). However, the conductivity of solid solution with x=0.38 shows negative temperature coefficient of resistivity, indicating that the compound is a semiconductor. In the case of x=0.58, the electric resistivity changes further by about three orders of magnitude from $3x10^{-2}$ to $2x10^{1}$ Ω cm in this temperature range. On the basis of Fig.4-1-1(b), the values of activation energy for the solid solutions of x=0.38 and 0.58 were 0.2 and 0.5 eV, respectively. These findings indicate that the band gap of NaCl-type solid solution, exhibiting semiconduction, increases with increasing Al content.

Fig.4-1-2 shows the detailed relationship between composition x and binding energy of Ti $2p_{3/2}$, N 1s and Al 2p for $Ti_{1-x}Al_xN$ with the composition of $0<x<0.6$. The Ti $2p_{3/2}$ peak shifted toward higher energy side by adding Al. The Al 2p and N 1s peaks, on the contrary, shifted to lower energy

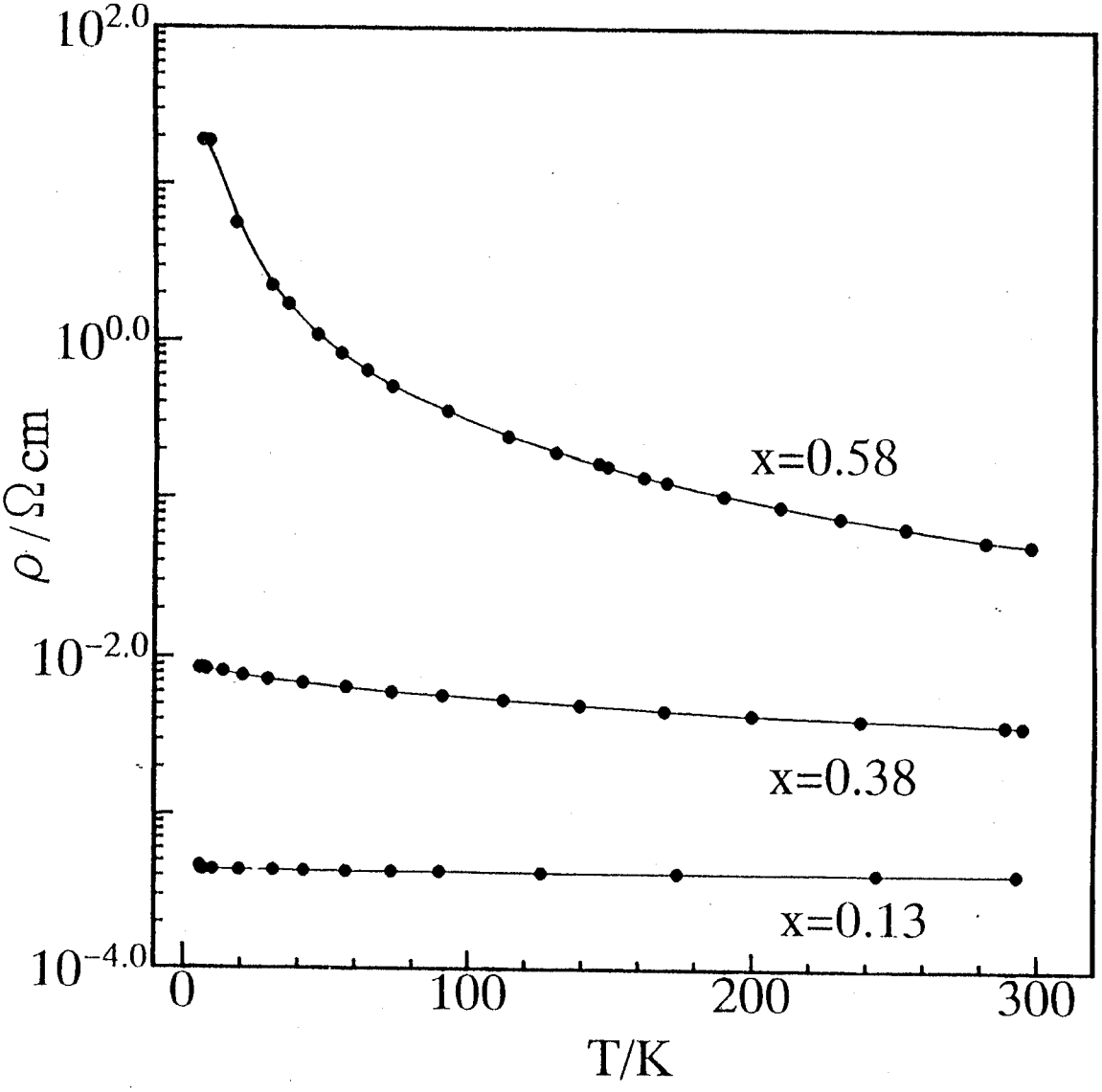

Fig.4-1-1 (a). Electric resistivity of NaCl-type solid solutions as a function of temperature

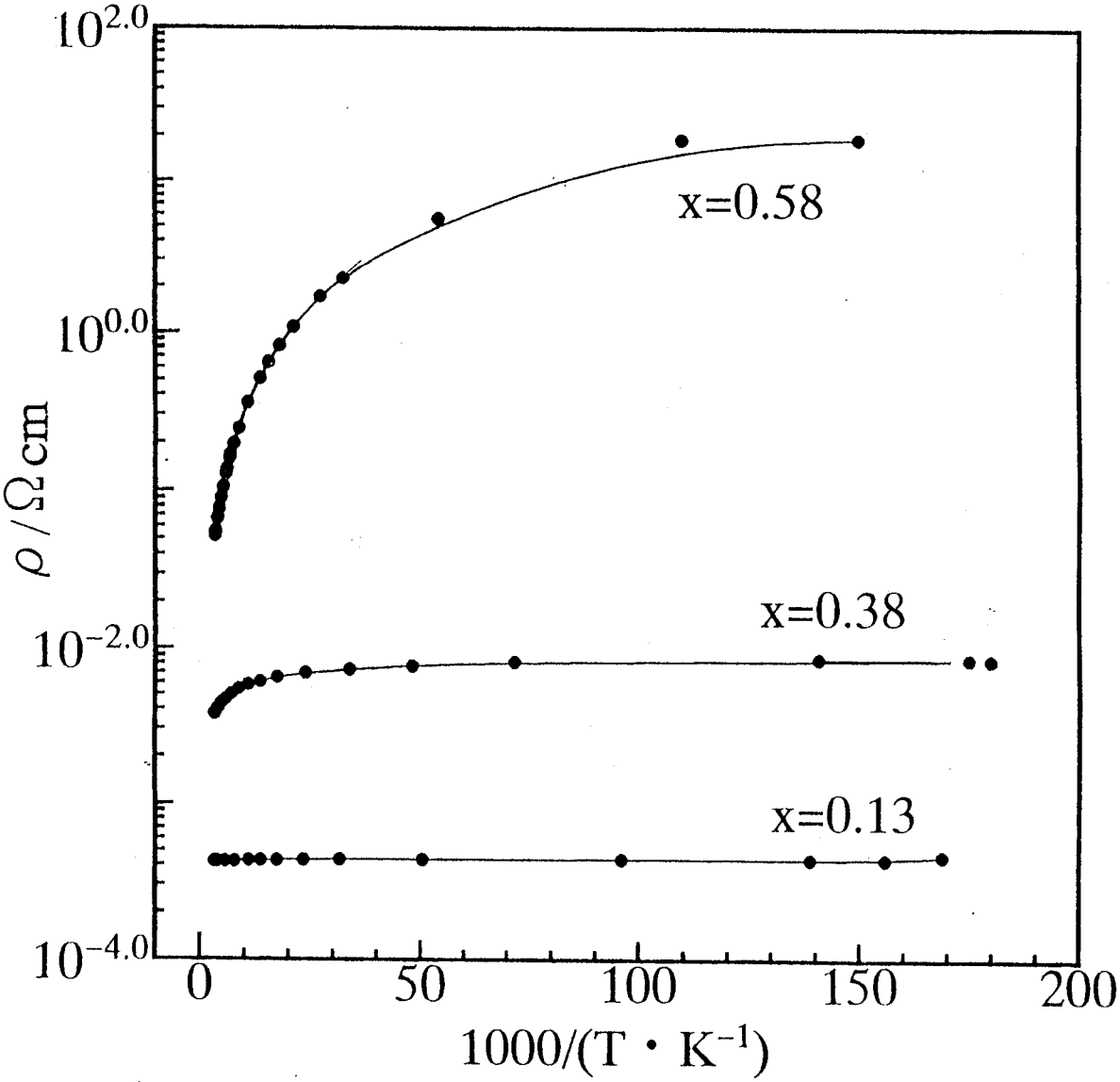

Fig.4-1-1 (b). Electric resistivity of NaCl-type solid solutions as a function of temperature

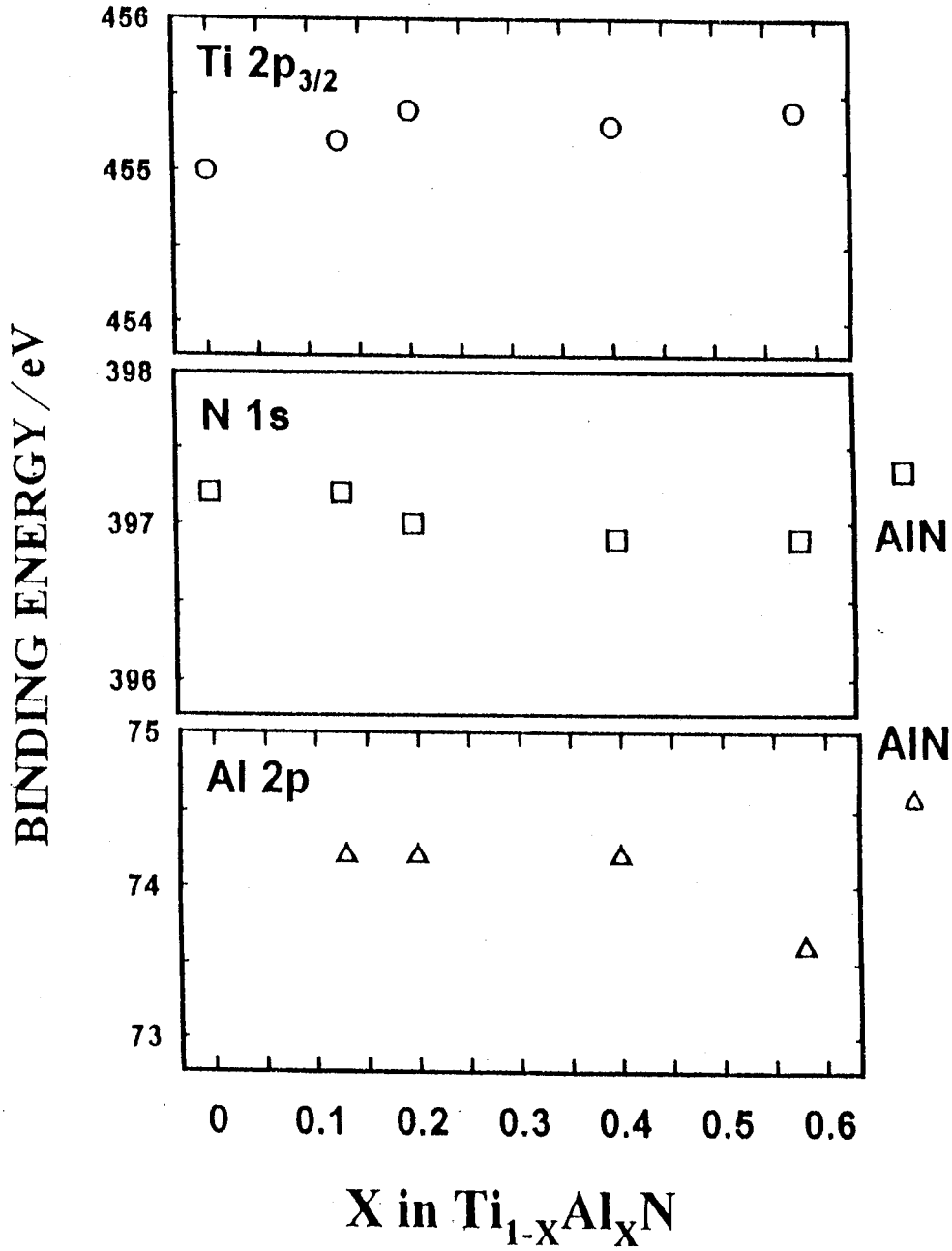

Fig. 4-1-2 **XPS of NaCl- type solid solution**

side, compared with those of AlN. These facts suggest that electrons in the d-d band in the solid solution become to be bound as valence electrons in the Ti-N and Al-N bonds by increasing Al content.

While, the spectra of XPS in the valence band of TiN mainly consists of N 2p and Ti 3d, containing e_g and t_{2g}, and a Fermi level is clearly observed at Eb=0 in Fig.4-1-3. The intensity of Ti 3d near the Fermi level, that is t_{2g}, decreased with increasing Al content, and the Fermi level disappeared in the composition range more than x=0.3 though the level was observed for the sample with x=0.2, suggesting that the NaCl-type solid solution exhibits metallic conductivity in the composition range less than x=0.2, but semiconducting behavior in the composition range more than x=0.3. These results of XPS are consistent with those of electric measurement of the NaCl-type solid solution.

Noting density of states (DOS), in order to investigate the change from metallic to semiconducting behavior between the composition of x=0.2 and 0.3. Fig.4-1-4 consists of total and partial density of states for CrN with NaCl-type structure. The tight band theory indicates that the DOS pattern is similar in same crystal structure. Accordingly it is suggested that the DOS of TiN is similar to one of CrN. The valence electrons of TiN are 4 for Ti and 5 for N, i.e. 9 for total. Accordingly the Fermi level of TiN is lower energy level than one of CrN which has 11 valence electrons. The number of electron in conduction band, T_{2g} band, for TiN is fewer than one for CrN. Addition of Al which has 3 valence electrons, reduce the Fermi level, resulting in that the NaCl-type solid solution with $x \geq 0.3$ become semiconductor because the t_{2g} electrons in conduction band disappear in the range of $x \geq 0.3$.

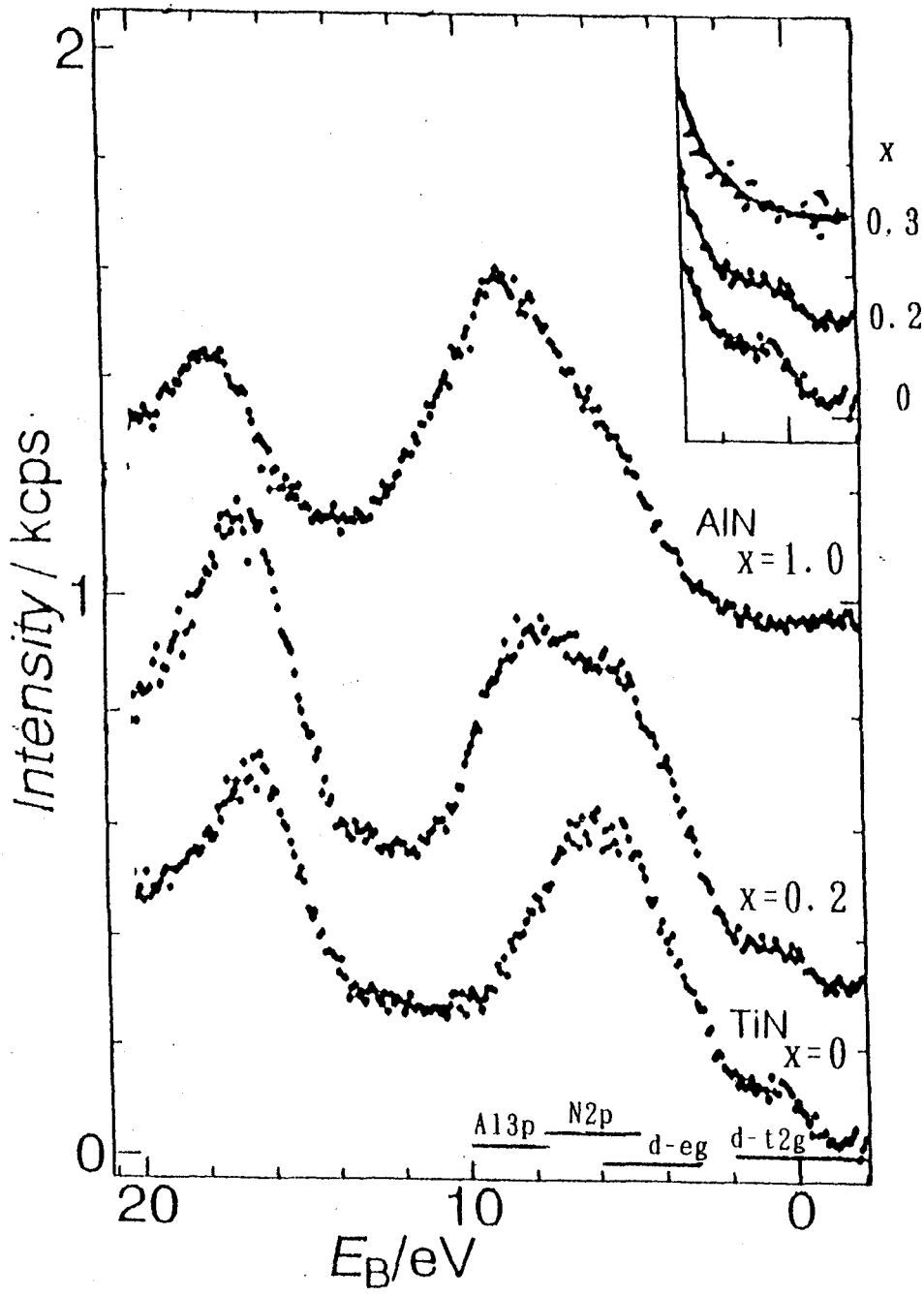

Fig. 4-1-3 VB region of XPS for $Ti_{1-x}Al_xN$ thin film

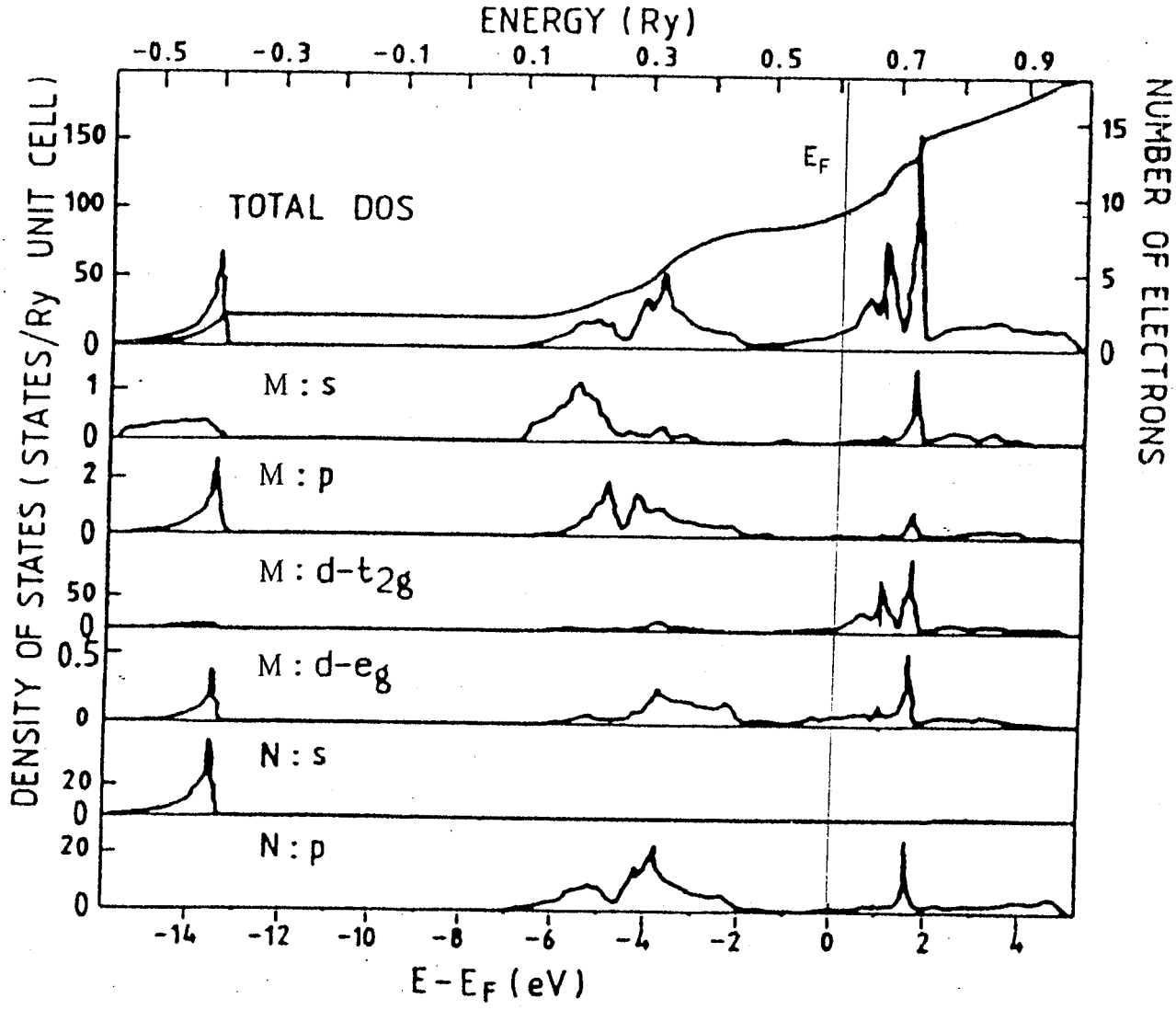

Fig. 4-1-4 Total and partial densities of states for MN with NaCl-type structure

IV-3-2. Optical band gap of the wurtzite-type solid solution and $Ti_{0.3}Al_{0.7}N$

The color of the wurtzite-type solid solution, is changed to dark brown via light yellow from colorless, depending on the amount of Ti-addition. Moreover the color of new double nitride was dark brown. The absorption edge of the wurtzite-type solid solution shifts to shorter wave length side with decreasing x in $Ti_{1-x}Al_xN$ as shown in Fig.4-2-1. This result indicates that the band gap decreases with increasing Ti content. The absorption coefficient is denoted as a function of transmittance T by equation (1)

$$\alpha\, l = -\ln(T/100) \qquad (1)$$

where, l is the thickness of sample. The transmittance vs $h\nu$ curves of the wurtzite-type solid solution are shown in Fig.4-2-2. The band gap energy Eg of AlN is evaluated to be 5.5 eV from the edge of the transmittance curve. However, in the case of the solid solution, broad tailing near the edge of the curve is observed, and so it is hard to evaluate directly Eg from the curve. Because of this difficulty, the band gap was evaluated by extrapolation of the line in the $(\alpha\, h\nu)^2$ vs $h\nu$ plot which is used for amorphous silicon. Fig.4-2-2 shows the dependence of x on band gap of $Ti_{1-x}Al_xN$ film with wurtzite-type structure. The band gap of AlN was 5.5 eV which was lower than the reported value because of the lattice distortion inside film induced by rf-sputtering. The band gap of $Ti_{1-x}Al_xN$ solid solution with wurtzite-type structure was decreasing with decreasing x. The change of band gap is suggested to depend on the change of local interatomic distance and of chemical bonding states which is due to moving partially electron from Ti to Al-N, by adding Ti.

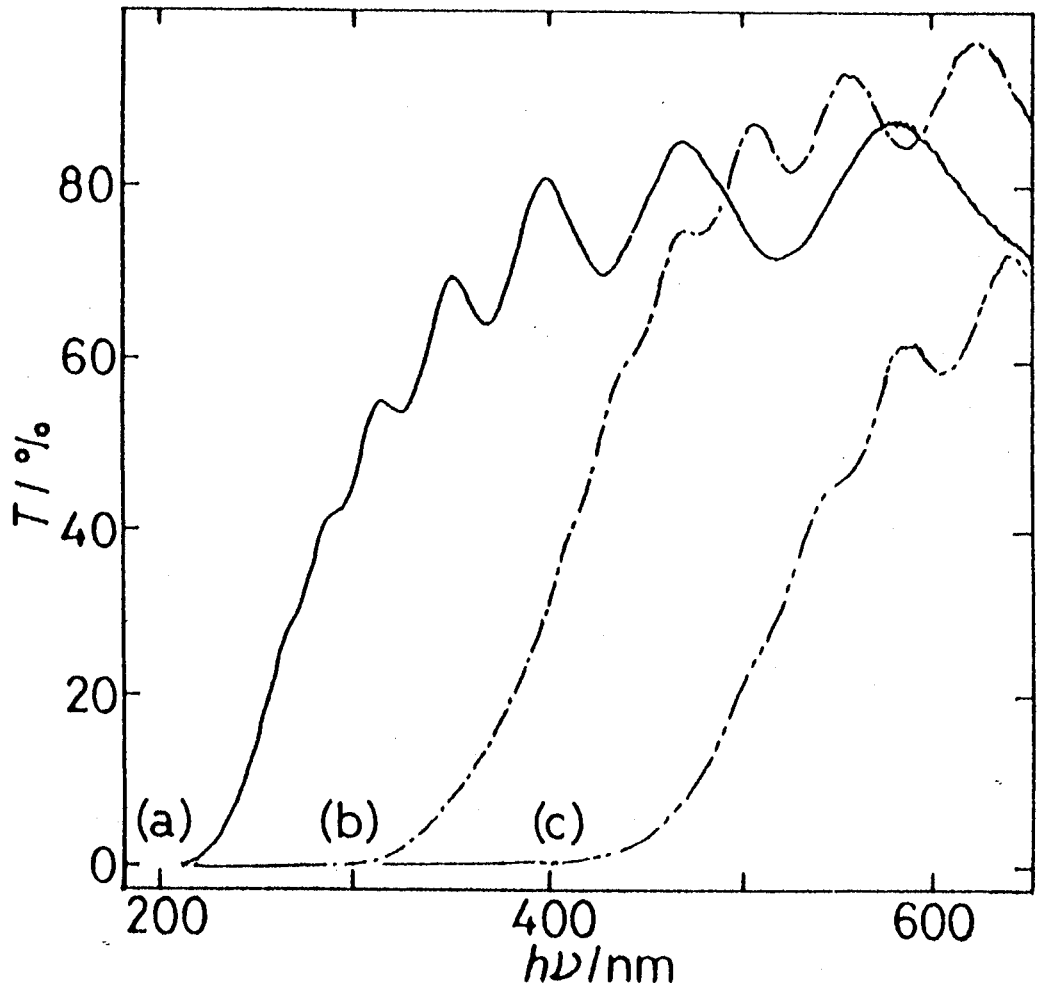

Fig. 4·2·1. UV Spectra for some of $Ti_{1-x}Al_xN$ solid solutions. (a) x=1.0, (b) x=0.90, and (c) x=0.83. The ordinate denotes transmittance, T.

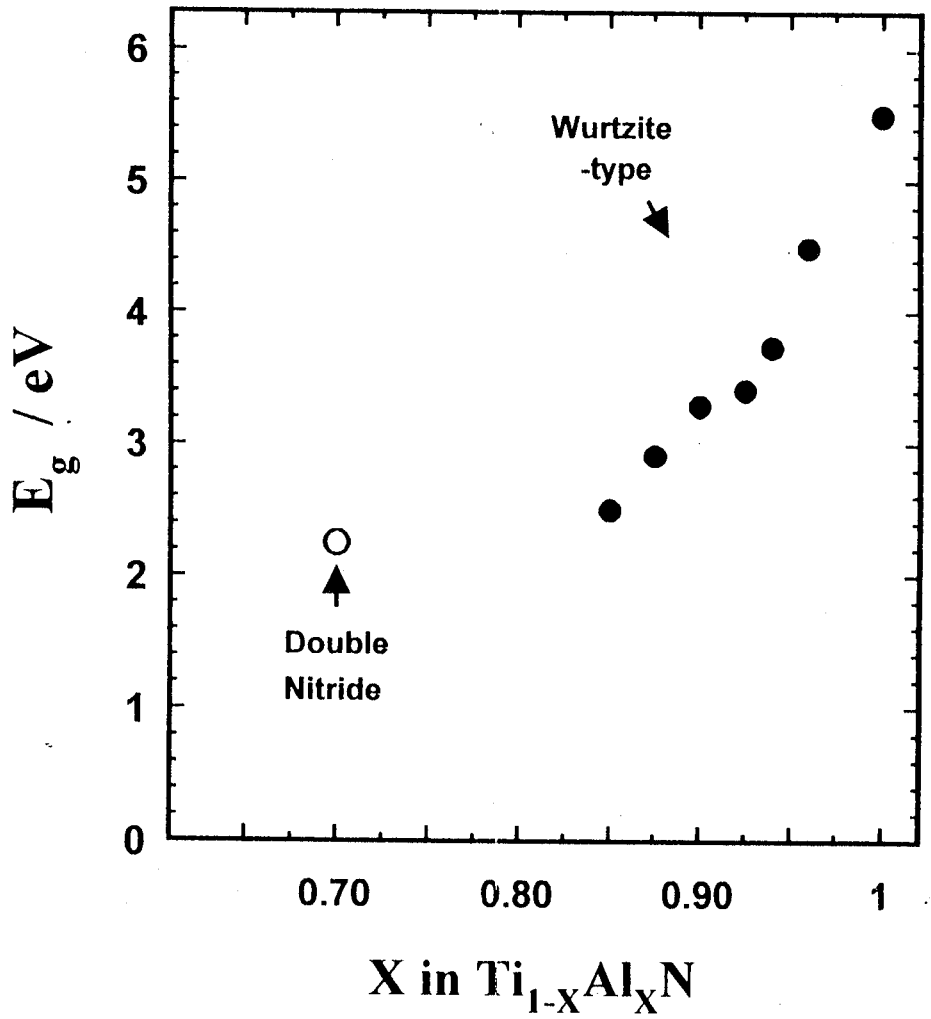

Fig. 4-2-2 **Band gap of $Ti_{1-x}Al_xN$ for the wurtzite-type solid solution and the new double nitride**

The DV-Xα MO calculations for several model clusters for $Ti_{1-x}Al_xN$ revealed the followings. The valence band of AlN consists of Al 3s, 3p and N 2p, and in the wurtzite-type solid solution, new levels composed of Ti 3d appear over the top of the band of AlN. As describing in the Chapter III-3-2, the offset of the first band in the low Eb side shifts to lower Eb side with an increase of Ti contents, i.e., with a decrease of x as shown in Fig.4-2-3. The shift of the offset does not contradict the result of the DV-Xα MO calculations. These observations disclose that the origins of the decrease of the band gap with a decrease of x are the formation of levels consisting of mainly Ti 3d with substituting Ti for Al as shown in Fig.4-2-3, and the decrease of inter-atomic distance as shown in Fig.3-2-2.

IV-3-3. Durability against oxidation

(1).Surface oxidation of $Ti_{1-x}Al_xN$ film in air at room temperature.

Fig.4-3-1(a) shows the Auger electron spectrum of the TiN film often exposing in air for a few days after preparing the film at a gas pressure ($Ar+N_2$) of 1 Pa.. The intensity of the oxygen KLL line is suitably high in comparing with the lines originated from titanium and nitrogen. This finding indicates that the surface of TiN film was vigorously oxidized. In order to check oxygen contamination inside the film, Auger electron spectrum was measured after etching the film surface by Ar sputtering in vacuum of $7x10^{-3}$Pa. after pre-evacuation of $7x10^{-6}$ Pa.. Just after etching the surface of the TiN film, the Auger electron spectrum of the film in the high vacuum of $7x10^{-6}$Pa. shows significant decrease in the intensity of oxygen KLL line though titanium LMM and nitrogen KLL peaks reserve its intensity as shown in Fig.4-3-1(b). The small signal of oxygen KLL line is still remained after etching because readsorption of oxygen on the film surface took place even in high vacuum as $7x10^{-6}$Pa..

The nitrogen KLL peak overlaps with the titanium LMM line of lower energy side. It was reported that the intensity ratio of titanium LMM peaks at 387 and 418eV is about 1.1 in a Ti film prepared by sputter deposition using a Ti target with purity of 99.99%. The intensity ratio $(Ti_{387}+N_{KLL})/Ti_{418}$ is given in Table 4-3-1, and the value indicates that atomic ratio of N to Ti in the TiN film is unity. These results of Auger electron spectroscopy before and after etching the TiN film surface indicate that the TiN film prepared under the sputtering condition mentioned above did not contain oxygen almost inside the film and that only surface of the film was severely oxidized by exposing the film to air.

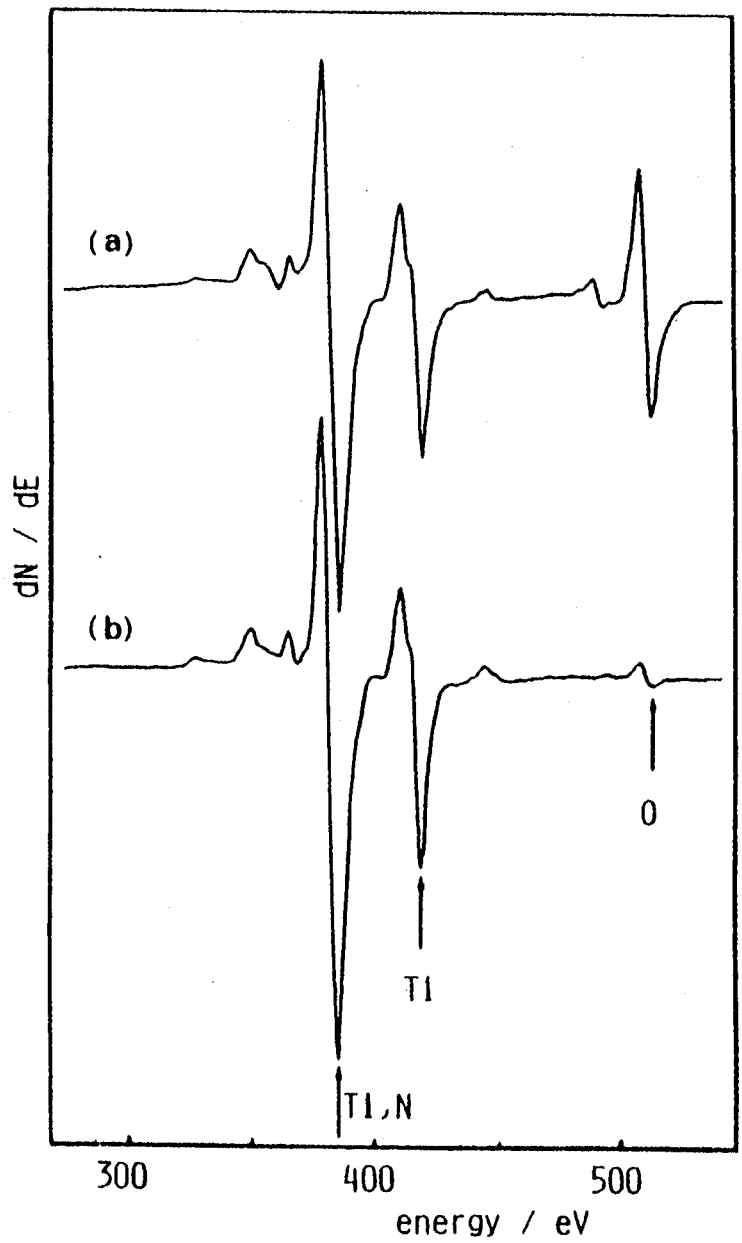

Fig. 4·3·1. Auger electron spectroscopy of the TiN film: (a) as-sputtered films, (b) after etching.

Titanium nitride is used a hard coating material, but has weak point that TiN is easily oxidized to TiO_2 above 550℃ in air. The recent investigations have been focused on the improvement for oxidation of TiN films by adding third elements. While, aluminum nitride is stable up to 1200℃ in air. Durability against oxidation of the solid solutions $Ti_{1-x}Al_xN$, therefore, is of interest because of a role of Al as a oxidation inhibitor.

Table 4-3-1. Amount changing of N and O (a) before and (b) after etching the TiN film surface.

	$(Ti_{387}+N_{KLL})/Ti_{418}$	O_{KLL}/Ti_{418}
(a)	1.66	0.69
(b)	2.03	0.03

The XPS spectra of the $Ti_{1-x}Al_xN$ films were measured in order to investigate more quantitatively oxidation of the surface of the films in air at room temperature. Fig.4-3-2 displays Ti2p bands in XPS spectra of TiN, NaCl-type $Ti_{0.65}Al_{0.35}N$ and orthorhombic $Ti_{0.3}Al_{0.7}N$ (new crystal phase), respectively. The peaks around 463eV and 457eV are assigned to the signals of Ti $2p_{1/2}$ and Ti $2p_{3/2}$, respectively. Furthermore, the broad and asymmetric peaks of both $2p_{3/2}$ and $2p_{1/2}$ indicate that each peak composes of at least two sub-bands. The sub-band of Ti $2p_{3/2}$ with higher

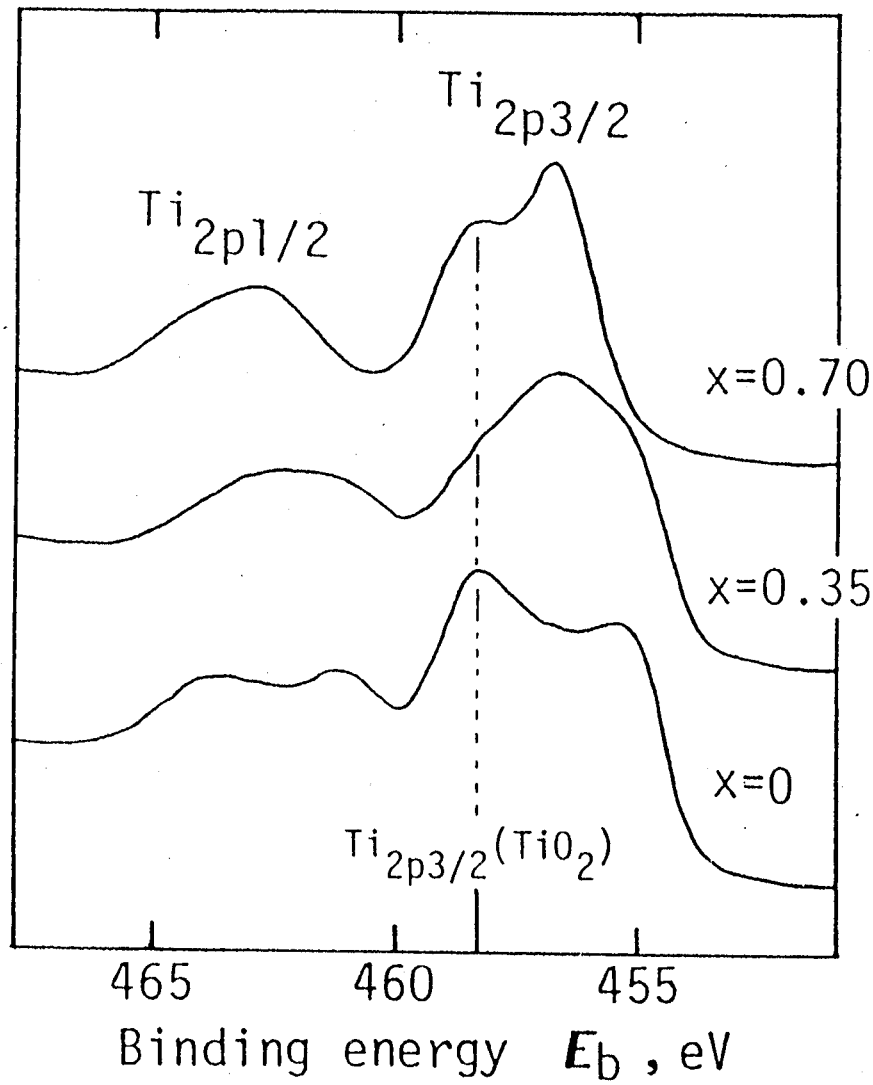

Fig. 4·3·2. Ti2p spectra in ESCA of TiN, NaCl-type $Ti_{0.65}Al_{0.35}N$ and new phase, $Ti_{0.3}Al_{0.7}N$.

binding energy (Eb), about 458eV, has same Eb value for all samples. Moreover the Eb value of these sub-bands agrees with that of TiO_2 reported by Sen et al.. These findings suggest that the Ti $2p_{3/2}$ sub-band with higher Eb was attributed to TiO_2 formed by oxidation of the surface of the films. While, the other Ti $2p_{3/2}$ sub-bands were assigned to the band corresponding to Ti bound to N, because the Ti $2p_{3/2}$ sub-band with lower Eb (around 458.5eV) in the spectrum of TiN film has the same value as Eb of TiN reported by Ramquist et al..

As shown in Fig.4-3-2, it is distinctly observed that the Ti $2p_{3/2}$ sub-bands corresponding to Ti-N bonding shift to higher energy side with increasing x. On the contrary, XPS spectrum of N 1s shifts toward lower energy side and that of Al 2p shifts also toward lower energy side compared with those of AlN. Those results seem to indicate that a part of electrons of Ti (maybe t_{2g}-electrons) transfers to N and/or Al atoms in the $Ti_{1-x}Al_xN$ solid solutions. Durability against oxidation of $Ti_{1-x}Al_xN$ may be related to the decrease of electrons on Ti, amount of which increase with increasing x. To confirm this model, DV-Xα MO calculation was carried out for the surface states of Ti_9N_9, $Ti_7Al_2N_9$ and $Ti_5Al_4N_9$ clusters as shown in Fig.4-3-5. The results shown in table 4-3-2 distinctly indicate that the bond orbital population of the Ti-N bond increase with increasing Al content. On the contrary, the bond orbital population of the Ti-O bond which is formed between Ti and O absorbed on the surface decrease with increase of Al content. These results of DV-Xα MO calculation indicate that durability against oxidation of $Ti_{1-x}Al_xN$ is related to the increase of the bond orbital population of Ti-N bond.

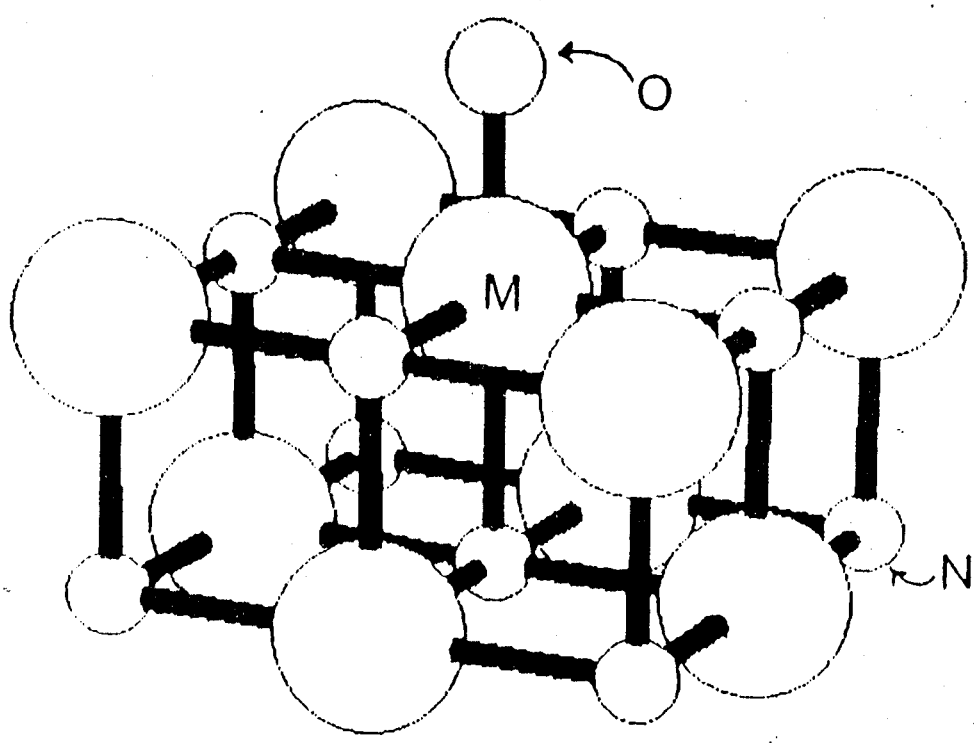

Fig. 4-3-5 Model Cluster($M_9N_9O^{2-}$) used in the calculations.

Table 4-3-2. Bond overlap populations and net charge for several model clusters.

	Ti_9N_9	$Ti_7Al_2N_9$	$Ti_5Al_4N_9$
Ti-N	0.61	0.74	0.84
	$Ti_9N_9O^{2-}$	$Ti_7Al_2N_9O^{2-}$	$Ti_5Al_4N_9O^{2-}$
Ti-O	0.16	0.01	0.04

(2). Stability of $Ti_{1-x}Al_xN$ films at high temperature.

(2)-1. Stability at high temperature under reducing atmosphere.

Heat treatment at 800 and 1000℃ in a mixed gas of N_2 (90%)and H_2 (10%) gases was carried out on $Ti_{1-x}Al_xN$ solid solutions, in order to investigate stability of the solid solutions at high temperature under reducing atmosphere. Fig.4-3-3 shows X-ray diffraction patterns of the NaCl-type solid solution with x=0.35 after heat treatment at each temperature. After heating at 800℃ , the sample had the same X-ray diffraction pattern and the same lattice constant as that annealed at 550℃ .

But, after heating the sample at 1000℃ , the X-ray diffraction pattern consists of diffraction lines of both NaCl-type and wurtzite-type phases. The diffraction lines assigned to NaCl-type phase remarkably shift to lower Bragg angle side as compared with those of the as-prepared sample, and the lattice constant of the NaCl-type phase agrees with that of the end member, TiN. The remaining diffraction peaks marked in Fig.4-3-

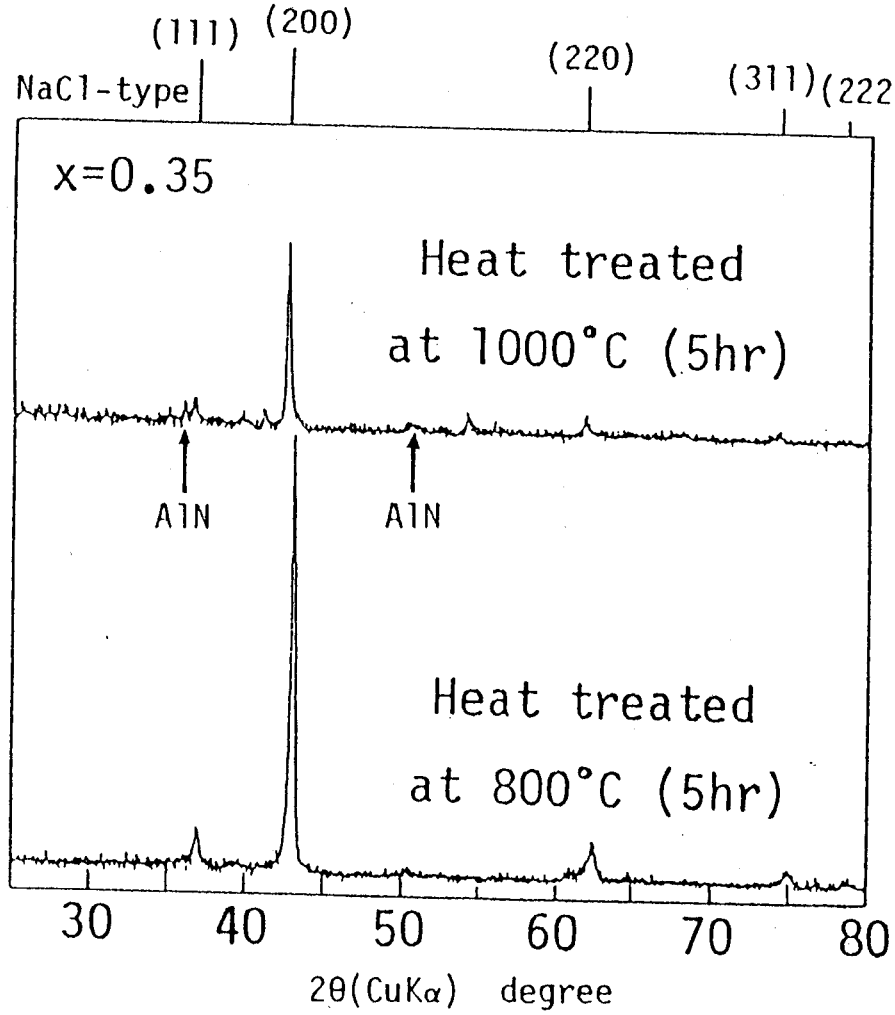

Fig. 4·3·3. X-ray diffraction pattern of the heat-treated Nacl-type $Ti_{0.65}Al_{0.35}N$.

3 are also assigned to another end member, AlN. This finding shows that in reducing atmosphere, the NaCl-type solid solution is stable below 800℃ , but decomposes to TiN and AlN at 1000℃ . This decomposition is closely related to oxidation of the solid solution above 1000℃ as described in the following session.

(2)-2 Durability against oxidation under oxidizing atmosphere.

In order to investigate durability against oxidation for $Ti_{1-x}Al_xN$ at high temperature in air, the isothermal weight change was measured in the temperature range from 600 to 900℃ using a thermo-gravimetry SINKU-RIKO TGD-5000RH. Some examples of the results are displayed in Fig.4-3-4, where the relations between weight change and heating time are shown at each temperature. The saturated value of the weight gain at 900℃ was defined as 100% weight gain for each sample. The TiN was perfectly oxidized and was converted to TiO_2 at 700℃ for 50min. Whereas, the weight gain was not observed for new double nitride $Ti_{0.3}Al_{0.7}N$, even at 800℃ for 5hr, but the double nitride was perfectly oxidized at 900℃ for 3hr. The X-ray diffraction pattern of the $Ti_{0.3}Al_{0.7}N$ after heat treatment at 900℃ , showed that the sample was a mixture of TiO_2, Al_2TiO_5, AlN and Al_2O_3. The results of isothermal gravimetry are summarized in table 4-3-3. The weight gain of the NaCl-type and wurtzite-type solid solutions was not observed below 800℃ , but was observed at 900℃ as similar to $Ti_{0.3}Al_{0.7}N$. Each sample after heat treatment at 900℃ was a mixture of four crystalline phases mentioned above.

Weight gain was not observed on an end member AlN even at 900℃ . In the other end member TiN, the weight gain observed above

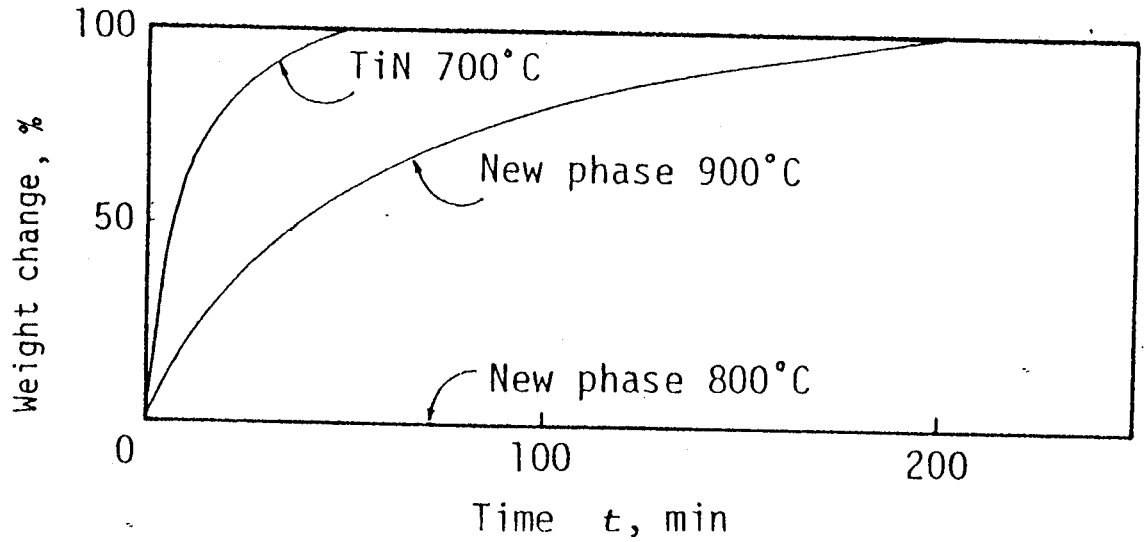

Fig. 4·3·4. Weight change of TiN and new phase with heating time at constant temperature in O_2 gas flow.

Table 4-3-3. Oxidation Isotherms Obtained for $Ti_{1-x}Al_xN$

Temperature (^{0}C)	TiN	NaCl-type solid solution	New double nitride	Wurtzite-type solid solution	AlN
	x = 0	x = 0.4	x = 0.7	x = 0.9	x = 1.0
600	O	U	U	U	U
700	O	U	U	U	U
800	O	U	U	U	U
900	O	O	O	O	U

O: Oxidation was detected, U: Oxidation was not detected.

600℃ showed that durability against oxidation of TiN was extremely lower than that of AlN. Durability against oxidation was confirmed to be decreased according to the order of AlN > the both solid solution and new double nitride > TiN.

Comparing weight gain vs heating time curves for the sample at high temperature under the oxidizing atmosphere with those under the reducing one, it is concluded that the oxidation reaction of the solid solutions and $Ti_{0.3}Al_{0.7}$ does not proceed until they decompose to end members, TiN and AlN, but take place immediately after decomposition of the sample to a mixture of TiN and AlN above 900℃ as indicated below.

$$Ti_{1-x}Al_xN \longrightarrow (1-x)TiN + x\ AlN, \qquad (1)$$

$$TiN + O_2 \longrightarrow TiO_2 + 1/2\ N_2, \qquad (2)$$

$$AlN + 3/4\ O_2 \longrightarrow 1/2\ Al_2O_3 + 1/2\ N_2, \qquad (3)$$

$$TiO_2 + Al_2O_3 \longrightarrow Al_2TiO_5, \qquad (4)$$

AlN produced by the above-mentioned phase separation (1) is very fine powder and is partially oxidized to yield a small amount of Al_2TiO_5 and Al_2O_3, though AlN is usually not oxidized below 1200℃ in air.

It is noticeable that not only wurtzite-type solid solution containing plenty of AlN but also NaCl-type solid solution with large amount of Ti as the main component has high durability against oxidation though structural type of NaCl-type solid solution is the same as TiN. Accordingly it is obvious that aluminum in the $Ti_{1-x}Al_xN$ solid solution plays an important role to prevent oxidation of the nitrides at high temperature.

As described above (IV-1), a part of d electrons of titanium atom in $Ti_{1-x}Al_xN$ transfers to nitrogen and aluminum atoms, resulting in the increase of the bond overlap populations in the Ti-N and the Al-N bonds of $Ti_{1-x}Al_xN$. The increase of these bond overlap populations caused reduction of the bond overlap populations of the Ti-O bond when absorbing oxygen on the surface of $Ti_{1-x}Al_xN$. It is suggested that the reduction of electron around titanium atom decreases the activity for titanium atom to react with oxygen accordingly increases durability against oxidation for the nitrides with NaCl-type structure. While, the aluminum titanate layer formed on the surface of the $Ti_{1-x}Al_xN$ films protect diffusion of Ti and O ions through the oxide layer. These phenomena are the reason why the durability against oxidation of $Ti_{1-x}Al_xN$ increase at high temperature in air.

IV-3-4. Durability against water

Aluminum nitride has high durability against oxidation, but is able to decompose in water, especially easily decomposed to aluminum hydroxide and NH_3 gas in the solution containing alkaline ions, even if it's content is very low level. It is interest to examine the effect of Ti addition on durability against hydrolysis of AlN.

In order to investigate durability against water of the solid solution in the TiN-AlN system, X-ray induced Auger electron spectrum (XAES) was measured. XAES of Al KLL was measured on the $Ti_{1-x}Al_xN$ solid solutions with various content of Ti, before and after soaking them in distilled water for 6 hours. As shown in Fig.4-4-1, Al KLL peak of AlN appears at about 1392 eV with a shoulder at the low energy side. Comparing with $Al(OH)_3$ and Al_2O_3, the shoulder was estimated to be attributed to the chemical bonding Al-OH.

The intensity of the shoulder remarkably decreases with increasing Ti content, and the shoulder disappears with addition of Ti more than 10 atomic percent. This result indicates that the durability against water of the $Ti_{1-x}Al_xN$ solid solution become higher by increasing Ti content replaced Al of AlN. By the way, the distinct shift of Al KLL peak toward high energy side is observed on the $Ti_{1-x}Al_xN$ solid solution as shown in Fig.4-4-1. As shown in Fig.4-4-2, the results of XPS indicated that the Ti $2p_{3/2}$ peak of wurtzite-type solid solution shifted toward higher energy side than that of TiN, and that both of N 1s and Al 2p of the solid solutions shifted toward lower energy side than that of AlN. As mentioned before also, this fact indicates that a part of electrons of Ti atom moves to N and

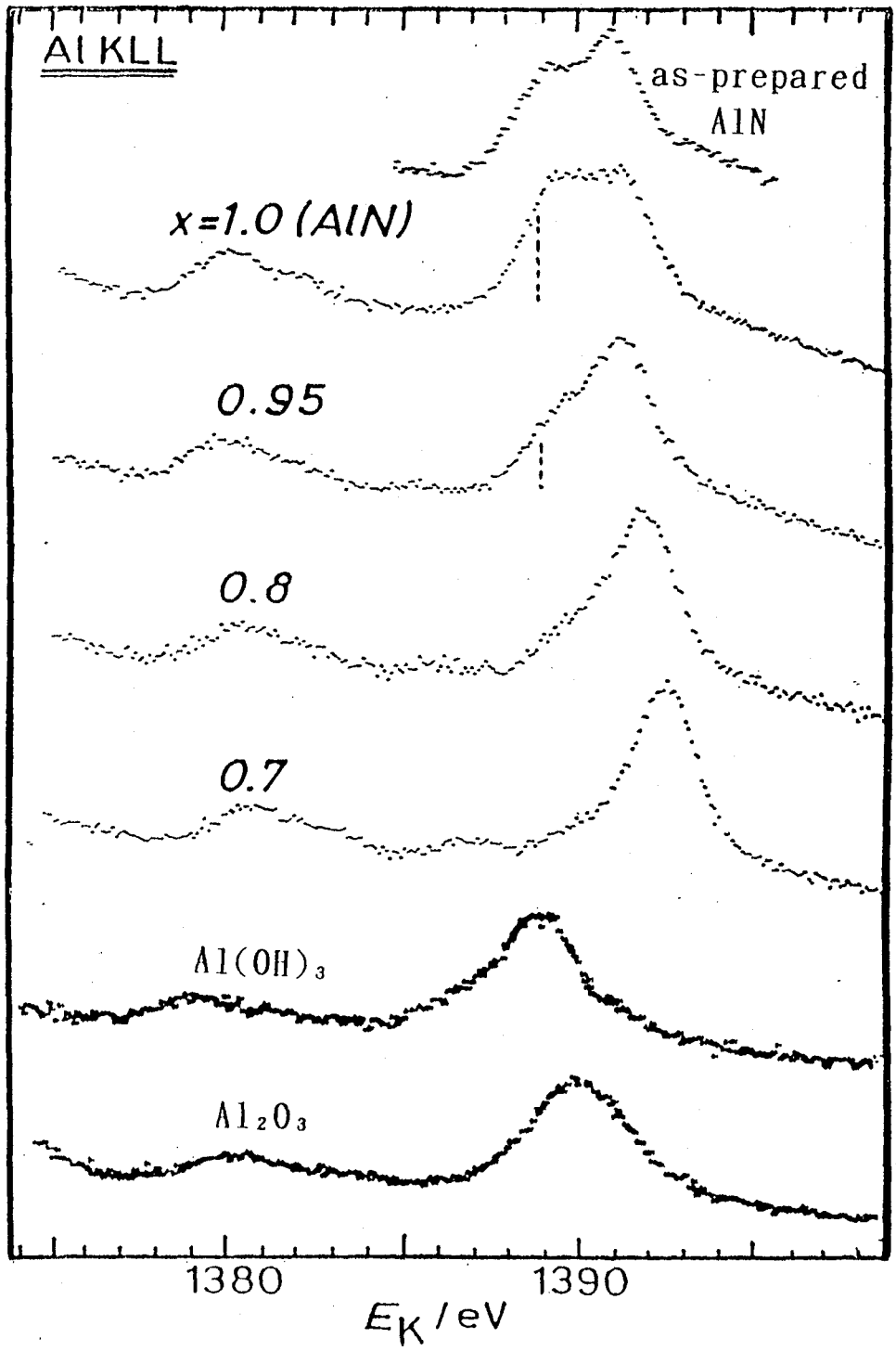

Fig. 4·4·1 XAES for $Ti_{1-x}Al_xN$

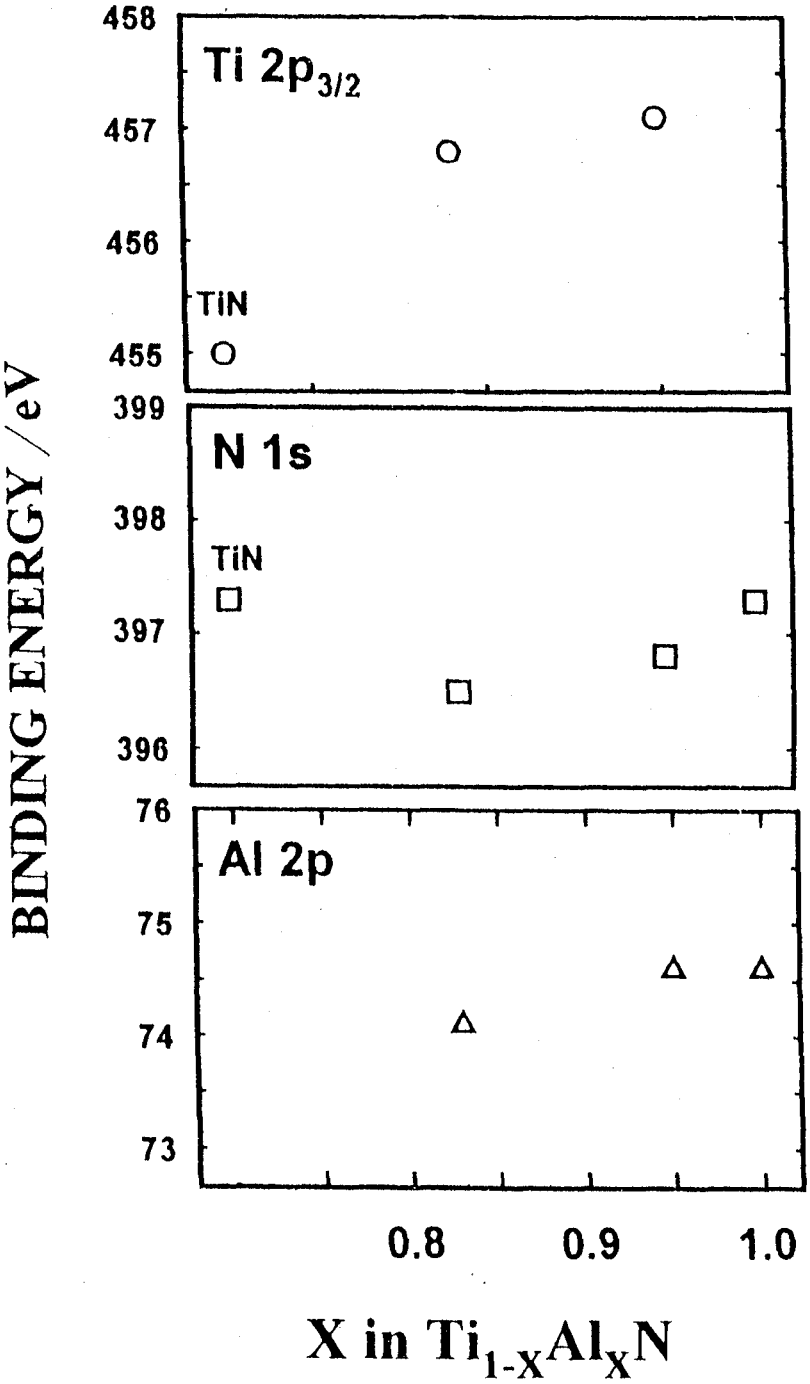

Fig. 4 4 2 **XPS of wurzite- type solid solution**

Al atoms, resulting in the increase of bond orbital populations in both the Ti-N and Al-N bonds in the solid solutions. High durability of the solid solutions is related to the increase of bond orbital population in the Al-N bond, which increases with increase of Ti content in the solid solutions.

Ⅳ-4. Conclusion

Synthesis of the double nitride, with atomic ratio of metal (Ti,Al) to nitrogen in unity, was examined by applying an rf-sputtering method which is non-equilibrium reaction process, and three crystal phases, two solid solutions and one new crystal phase, were prepared in the $Ti_{1-x}Al_xN$ system. The measurements of XPS and XAES of the $Ti_{1-x}Al_xN$ revealed that a part of electrons of Ti transfers to N and Al atoms with increasing Al content. The spectra of XPS in the valence band of TiN mainly consists of Ti 3d, N 2p and the Fermi level shifted toward lower energy side with increasing Al content in the composition range less than x=0.2, and the Fermi level disappeared in the composition range more than x=0.3, suggesting that the NaCl-type solid solution exhibit metallic conductivity in the composition range less than x=0.2, but semiconducting behavior in the composition range more than x=0.3.

The influence of chemical bonding in the $Ti_{1-x}Al_xN$ solid solutions on physical and chemical properties, i.e. the electric resistivity, the optical band gap and durabilities against oxidation and hydrated decomposition were described as follows.

1. Adding gradually AlN to TiN which exhibits metallic conductivity, the electric resistivity of NaCl-type solid solution became higher and a negative temperature coefficient of electrical resistivity became obvious, because the d electron in conduction band decreases by decrease of the average valence electron in the NaCl-type solid solution.

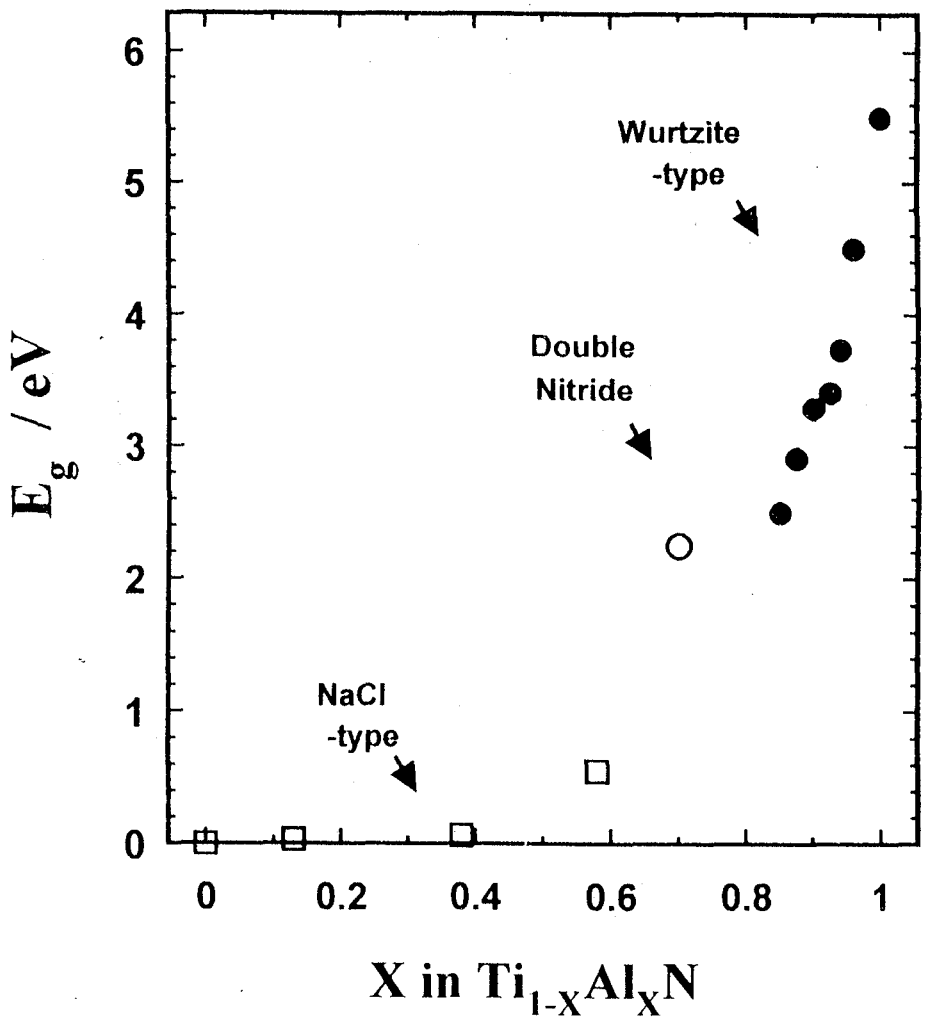

Fig.4-5-1. Band gap of $Ti_{1-x}Al_xN$

2. The band gap of $Ti_{1-x}Al_xN$ solid solution with wurtzite-type structure decreased from 5.5 to 2.5 eV with decreasing x. The change of band gap is suggested to depend on the change of local inter-atomic distance and of chemical bonding states which is due to partial electron transfer from Ti to Al-N, reduced partially replacing Al to Ti.

3. On the basis of the relation between electric resistivity and temperature, and UV absorption spectra, the change of band gap in the system of $Ti_{1-x}Al_xN$ was summarized in Fig.4-5-1. It can be said that the band gap is controlled in the wide range from 0 to 5.5 eV by forming solid solution in the TiN-AlN system.

4. The starting temperature for oxidation of TiN increased from 500 ℃ to 800～ 900℃ for the $Ti_{1-x}Al_xN$ solid solution film, i.e. the durability against oxidation for TiN was improved by adding Al.

5. The reason is the shift of chemical bonding which is the increase of the bond overlap populations of the Ti-N bond indicated by DV-Xα MO calculation. Oxidation of the $Ti_{1-x}Al_xN$ above 800℃ in air due to the thermal decomposition of $Ti_{1-x}Al_xN$ to TiN and AlN.

6. By the measurement of XAES's of Al KLL for the $Ti_{1-x}Al_xN$ solid solution, it was revealed that the intensity of shoulder attributed to the chemical bonding of Al-O and Al-OH decreased with increasing Ti content in the solid solution. It indicates that the durability against water of $Ti_{1-x}Al_xN$ solid solution become higher by increasing TiN content replaced Al

of AlN.

Chapter V. GENERAL DISCUSSION AND SUMMARY

Metal nitrides have a great variety of chemical bond natures such as metallic, covalent and ionic bondings corresponding to the countermetals of transition metals, IA and IIA metals and IIIB and IV metals, respectively. It is, therefore, expected to improve properties of metal nitrides and also to bring about new functions by controlling the chemical composition in solid solutions between nitrides with different bond natures.

Titanium nitride, having high hardness, has been spotlighted as a coating material. However, the durability against oxidation of TiN is much inferior to that of AlN with a strong covalent bond. TiN has a unfilled d-d band, resulting in metallic conductivity. On the contrast, AlN is a insulator with a wide band gap and exhibits high thermal conductivity. Therefore, AlN is a promising material as a substrate of LSI, but has a week point to decompose in water. It will be expected that the durability against oxidation and water of TiN and AlN is improved by adding Al and Ti, respectively, and also that the band gap varies in the rang from 0 to 6 eV depending upon the chemical composition if the solid solution of TiN and AlN could be found.

Titanium nitride has NaCl-type structure in which both Ti and N atoms have coordination numbers of 6. While, aluminum nitride has wurtzite-type structure with coordination number of 4 for both Al and N atoms. There are serious difference in crystal structure and chemical bond between TiN and AlN. Therefore, it is very difficult to form solid solution in the TiN and AlN system by applying conventional solid state reaction at high temperature. A little investigation of double metal nitrides in the TiN and AlN

system have been done so far expect Ti_2AlN, Ti_3AlN and $Ti_3Al_2N_2$, in which the atomic ratio of N to metal (Ti+Al)is not unity.

In the present study, synthesis of the double nitride, in which atomic ratio of metal (Ti,Al) to nitrogen in unity, was examined by applying an rf-sputtering method which is a non-equilibrium reaction process, and three crystal phases, two solid solutions and one new crystal phase, were prepared.

One of the solid solutions, $Ti_{1-x}Al_xN$, had NaCl-type structure and was produced in the composition range of $0<x<0.58$. The lattice constant linearly decreases with increasing Al content and satisfies Vegard's law. Accordingly the coordination number of Al was estimated as 6 by the crystal data. For sample with x greater than 0.5, a remarkable lattice distortion was observed but disappeared by heat treatment.

Another solid solution with the chemical composition in the range of $0.83 \leq x \leq 1.0$ had wurtzite-type structure. The lattice constant a of wurtzite-type solid solution linearly increases with increasing Ti content although the lattice parameter c is almost constant. The coordination number of Ti was estimated as 4 by the measurement of XAFS. For AlN the value of c/a, 1.60 is smaller than 1.63 for ideal wurtzite structure, and the value of c/a becomes further small with increasing Ti content i.e. the lattice distortion of the wurtzite-type solid solution becomes further larger in comparison with ideal wurtzite structure because of unusual coordination number of 4 for Ti in the wurtzite-type solid solution.

New double nitride $Ti_{0.3}Al_{0.7}N$ was crystallized in a orthorhombic system with a=0.560, b=0.955 and c=0.520nm. The coordination number of Ti was estimated as 4 by the measurement of XAFS.

Two solid solutions and $Ti_{0.3}Al_{0.7}N$ are considered to be metastable phases, because they easily decompose to both end members, TiN and AlN, above 900℃ in N_2 atmospher. Therefore, the present results indicate that a reaction sputtering method, which is a non-equilibrium reaction process, is a powerful synthetic method for preparation of metastable crystal phases combining between compounds with the different nature of chemical bonding and crystal structure.

In order to investigate the nature of chemical bond of the products, XPS and XAES were measured. The XPS spectra of Ti 2p, N 1s and Al 2p in $Ti_{1-x}Al_xN$ are shown in Fig.3-5-5.. In the NaCl-type solid solution the binding energy of Ti 2p increases, but that of N 1s decreases in comparison with TiN. By the way, the binding energy of Al 2p and N 1s in the wurtzite-type solid solution decrease with increase of Ti content. In the latter solid solution, the binding energy of Ti 2p is larger as compared with that of Ti 2p for TiN. These findings indicate that a part of d electrons of Ti transfers to N and Al atoms in $Ti_{1-x}Al_xN$. The spectra of XPS in the valence band of TiN mainly consists of Ti 3d, N 2P and the Fermi edge is definitely observed. But the Fermi edge decreased with increasing Al content, and then disappeared in the composition range between x=0.3 and 0.58, suggesting that the NaCl-type solid solution exhibits metallic conductivity in the composition range less than x=0.2, but semiconducting behavior in the composition range more than x=0.3, because the occupied electron in conduction band (t_{2g} band) disappears in the composition of $x \geq 0.3$, as the average valence electron decreases with increasing Al content.

The various properties such as the electric and optical properties and the durability against environment were affected by change in chemical

bonding described above. The temperature dependence of electric resistivity shows a positive temperature coefficient of electrical resistivity below x=0.13 but a negative one above x=0.38. It consists with results of XPS. In the optical absorption spectra, the band gap of $Ti_{1-x}Al_xN$ solid solution with wurtzite-type structure decrease from 5.5 to 2.5 eV with decreasing x, because the Ti 3d orbital superpose on the upper edge of valence band of AlN which consists of Al 3p and N 2p. It can be said that the band gap is controlled in the wide range from 0 to 5.5 eV by changing the atomic ratio of Ti to Al in the nitrides forming solid solution in the TiN-AlN system.

The results of thermal analysis and XPS indicate that the starting temperature for oxidation of $Ti_{1-x}Al_xN$ increased from 500℃ for TiN to the 800℃ for the $Ti_{1-x}Al_xN$ solid solution, but oxidation of the $Ti_{1-x}Al_xN$ takes place above 800℃ in air, which due to the thermal decomposition of $Ti_{1-x}Al_xN$ to stable end members, TiN and AlN. Improvement for the durability against oxidation for TiN due to the increase of the bond overlap populations in the Ti-N bond, which was caused by a partial d-electron transfer from Ti to N and Al atoms.

The XAES's Al KLL spectra of the wurtzite-type $Ti_{1-x}Al_xN$ solid solution indicate that the surface of AlN is easily hydrolyzed to form Al-O and Al-OH bonding, but the hydrolysis is depressed remarkably by adding Ti into AlN. The improvement of durability against water of $Ti_{1-x}Al_xN$ solid solution is also explained by the increase of the bond overlap populations in the Al-N and the Ti-N bonds in $Ti_{1-x}Al_xN$.

In conclusion, the NaCl-type and the wurtzite-type solid solutions and the new double nitride, $Ti_{0.3}Al_{0.7}N$ in the TiN and AlN system were first prepared in this study by applying a reaction sputtering method. the characterization of the three crystal phases were carried out systematically as a function of the chemical composition by measurements of XRD, AEM, XPS, AES and EELS. The electrical property of the $Ti_{1-x}Al_xN$ changes from metallic to semiconducting behaviors at about x=0.3, and the activation energy of electric conductivity of the NaCl-type solid solution with x larger than 0.3 increase from 0.2 to 0.5eV with an increase of x. The optical band gap of the wurtzite-type solid solution also increase with increasing x. Furthermore the durabilities against oxidation of TiN and against hydrolysis of AlN were remarkably improved with addition of Al and Ti atoms, respectively. It is concluded on the basis of DV-Xα MO calculations that these phenomena is attributed to the increase of the bond overlap populations of the Ti-N and the Al-N bond, which is caused by a partial electron transfer from Ti atom to N and Al atoms.

REFERENCES

1. A.F.Wells, Structural Inorganic Chemistry, Clarendon Press Oxford, 1982.
2. L.E.Toth, Transition Metal Carbides and Nitrides, Academic Press, New York, 1971.
3. W.D.Kingery, H.K.Bowen and D.R.Uhlmann, Introduction to Ceramics, A Wiley-Interscience Publication, 1975
4. NITROGEN CERAMICS
5. P.Drew, M.H.Lewis, J.Mater.Sci, 9 (1974) 261.
6. K.Yabe, M.Suzuki, Y.Igasaki and T.Yamashina, Shinku, 26 (1983) 557.
7. W.D.Sproul, P.J.Rudnik and C.A.Gogol, Thin Solid Films 171 (1989) 171.
8. H.Yoshihara and H.Mori, J. Vac. Sci. Technol., 16 (1979) 1007.
9. N.Biunno, J.Narayan, S.K.Hofmeister, A.R.Srivatsa, and R.K.Singh, Appl.Phys.Lett., 54 (1989) 1519.
10. D.H.Jang, J.S.Chun and J.G.Kim, Thin Solid Films, 169 (1989) 57.
11. S.Motojima and H.Mizutani, Appl.Phys.Lett., 54 (1989) 1104.
12. M.A.Eron'yan, R.G.Avarbeand T.N.Danisina, High Temp., 14 (1976) 359.
13. S.Nagakura, T.Kusuaki, F.Kaminoto and Y.Hirotsu, J. Appl. Crystallogr., 8 (1975) 65.
14. Glen A.Slack and T.F.Mcnelly, J.Crystal Growth, 34 (1976) 263.
15. F.Briegleb and A.Geuther, Ann.Chem. 123 (1862) 228.
16. E.Kauer and A.Rabenau, Z.Naturforsch. 12a (1957) 942.
17. G.A.Cox, D.O.Cummins, K.Kawabe and R.H.Tredgold, J.Phys.Chem. Solids, 28 (1967) 543.
18. C.O.Dugger, Mat.Res.Bull. 9 (1974) 331.
19. S.Horiuchi, T.Ishii and K.Asakura, J.Crystal Growth, 21 (1974) 17.
20. G.A.Slack and T.F.Mcnelly, J.Crystal Growth, 34 (1976) 263.
21. G.A.Slack and T.F.Mcnelly, J.Crystal Growth, 42 (1977) 560.
22. J.Pastrnak and L.Souckova, Phys. Status Solidi, 9 (1965) K73
23. T.L.Chu, D.W.Ing and A.J.Noreika, Solid State Electron. 10

(1967) 1023.
24. A.J.Noreika and D.W.Ing, J.Appl.Phys. 39 (1968) 5578.
25. H.M.Manasevit, F.M.Erdmann and W.I.Simpson, J.Electrochem.Soc., 118 (1971) 1864.
26. W.M.Yim, E.J.Stofko, P.J.Zanzucchi, J.I.Pankove, M.Ettenberg and S.L.Gilbert, J.Appl.Phys. 44 (1973) 292.
27. M.P.Callaghan, E.Patterson, B.P.Richards and C.A.Wallace, J. Cryst.Growth, 22 (1974) 85.
28. J.Bauer, L.Biste and D.Bolze, Phys.Stat.Sol. A39 (1977) 173.
29. J.K.Liu, K.M.Lakin and K.L.Wang, J.Appl.Phys. 46 (1975) 3703.
30. M.Morita, N.Uesugi, S.Isogai, K.Tsubouchi and N.Mikoshiba, Jpn.J.Appl.Phys. 20 (1981) 17.
31. M.Morita, S.Isogai, N.Shimizu, K.Tsubouchi and N.Mikoshiba, Jpn.J.Appl.Phys. 20 (1981) L173.
32. M.Morita, K.Tsubouchi and N.Mikoshiba, Jpn.J.Appl.Phys. 21 (1982) 723.
33. A.J.Noreika, M.H.Francombe and S.a.Zeitman, J.Vac.Sci.Technol. 6 (1969) 194.
34. A.J.Shuskus, T.M.Receder and E.L.Paradis, Appl.Phys.Lett. 24 (1974) 155.
35. F.Takeda and T.Hata, Jpn.J.Appl.Phys. 19 (1980) 1001.
36. J.A.Kovacich, J.Kasperkiewicz, D.Lichtman and C.R.Aita, J.Appl. Phys. 55 (1984) 2935.
37. C.G.Olson, J.H.Sexton, D.W.Lynch, A.J.Bevolo, H.R.Shanks, B.N.Harmon, W.Y.Ching and D.M.Wieliczka, Solid State Commun. 56 (1985) 35.
38. L.Xinjiao, X.Zechuan, H.Ziyou, C.Huazhe, S.Wuda, C.Zhongcai, Z.Feng and W.Enguang, Thin Solid Films, 139 (1986) 261.
39. J.Pastrnak and L.Roskovcova, Phys.Stat.Sol. 26 (1968) 591.
40. V.V.Michailin, V.E.Oranovskii, S.Pacesova, J.Pastrnak and A.S.Salamatov, Phys.Stat.Sol. B55 (1973) K51.
41. H.Yamashita, K.Fukui, S.Misawa and S.Yoshida, J.Appl.Phys. 50 (1979) 896.
42. S.Yoshida, S.Misawa and A.Itoh, Appl.Phys.Lett. 26 (1975) 461.
43. S.Yoshida, S.Misawa Y.Fujii, S.Takada, H.Hayakawa, S.Gonda and A.Itoh, J.Vac.Sci.Technol. 16 (1979) 990.
44. W.M.Yim, E.J.Stofko, P.J.Zanzucchi, J.I.Pankove, M.Ettenberg and S.L.Gilbert, J.Appl.Phys., 44(1973)292.
45. W.Y.Ching and B.N.Harmon, Phis.Rev.B, 34 (1986) 5305.

46. B.Hejda and K.Hauptmanova Phys.Status Solidi, 36 (1969) K95.
47. S.Bloom, J.Phys.Chem.Solids, 32 (1971) 2027.
48. D.Jones and A.H.Lettington,Solid State Commun.,11 (1972) 701.
49. A.Kobayashi, O.F.Sankey, S.M.Volz and J.D.Dow, Phys.Rev.B, 28 (1983) 935.
50. M.Z.Haung and W.Y.Ching, J.Phys.Chem.Solids, 46 (1985) 977.
51. J.C.Schuster and J.Bauer, J. Solid State Chem., 53 (1984) 260
52. A.Michalski, J. Mater. Sci. Lett., 4 (1985) 251.
53. Kiyotaka Wasa and Shigeru Hayakawa, Thin Solid Films, 10 (1972) 367.
54. G.Beensh-Marchwicka, L.Krol-Stepniewska and W.Posadowski, Thin Solid Films, 82 (1981) 313.
55. O.Knotek and T.Leyendecker, J. Solid State Chem., 70 (1987) 318.
56. S.Inamura, K.Nobugai and F.Kanamaru, J. Solid State Chem., 68 (1987) 124.
57. S.Inamura, K.Nobugai, F.Kanamaru and S.Emura, Chem. Express 2(1987)539.
58. W.Posadowski, L.Krol-Stepniewska and Z.Ziolowski, Thin Solid Films, 62 (1979) 347.
59. G.Johansson, J.Hedman, A.Berndtsson, M.Klasson and R.Nilsson, J.Electron Spectrosc.Relat.Phenom.,**2**(1973)295.
61. E.O.Ristolainen, J.M.Molarius, A.S.Korhonen and V.K.Lindroos, J.Vac.Sci.Technol., **A5** (1987) 2184.
62. L.E.Toth, Transition Metal Carbides and Nitrides, (Academic Press, New York, 1971), p.7.
63. S.Nagakura, T.Kusumoki, F.Kakimoto and Y.Hirotsu, J.Appl.Cryst., **8** (1975) 65.
64. J.E.Sundgren, B.O.Johansson, S.E.Karlsson and H.T.G.Hentzell, Thin Solid Films, **105** (1983) 367.
65. W.B.Pearson, A Handbook of Lattice Spacing and Structure of Metals and Alloys, (1958) p999.
66. KITTEL, Introduction to Solid StatePhysics (6th. edition). For original ref.,
67. M.Nakahira, 'Kessho-kagaku' Kodansha, p44.
68. W.B.Pearson, Crystal chemistry and physics of metal and alloys,

Wiley,(1972)
69. T.Ishida, S.Kimura, N.Kamijo, O.Tabata, H.Naito and M.Shimizu, Shinku, **26** (1983) 516.
70. T.Ito, M.Iwami and A.Hiraki, J.Phys.Soc.Jpn.,50(1981)1978.
71. A.Koma and K.Enari, Proc. 14th Intern. Conf. Phys. Semiconductors Edinburgh (Page Brothers Ltd., Norwich, 1979) p.895.
72. T.Ito, M.Iwami and A.Hiraki, J.Phys.Soc.Jpn.,50(1981)106.
73. L.I.Johansson, Phys.Rev.B24(1981)1883.
74. A.J.Noreika and D.W.Ing, J.Appl.Phys. 39 (1968) 5578.
75. R.A.Smith, Semiconductor, Cambridge Univ. Press, London (1968)
76. W.M.Yim, E.J.Stofko, P.J.Zanzucchi, J.I.Pankove, M.Ettenberg and S.L.Gilbert, J.Appl.Phys., 44(1973)292.
77. P.B.Perry and R.F.Rutz, Appl.Phys.Lett., 33(1978)319.
78. J.Bauer, L.Biste and D.Bolze, Phys.Stat.Sol. A39 (1977) 173.
79. J.K.Liu, K.M.Lakin and K.L.Wang, J.Appl.Phys. 46 (1975) 3703.
80. S.Inamura, M.Takahashi, K.Nobugai, F.Kanamaru and H.Miyamoto, J. Soc. Mater. Sci. Jpn.,37(1988)83
81. D.McIntyre, J.E.Greene, G.Hakansson, J.E.Sundgren and W.D.Munz, J.Appl.Phys., 67(1990) 1542.
82. M.Morita, K.Tsubouchi and N.Mikoshiba, Jpn. J. Appl. Phys. 21 (1982) 723.
83. A.J.Noreika, M.H.Francombe and S.a.Zeitman, J. Vac. Sci. Technol. 6 (1969) 194.
84. A.J.Shuskus, T.M.Receder and E.L.Paradis, Appl.Phys.Lett. 24 (1974) 155.
85. Y.Igasaki and H.Mitsuhashi, J.Appl.Phys., 54(1983) 836.
86. J.A.Kovacich, J.Kasperkiewicz, D.Lichtman and C.R.Aita, J.Appl. Phys. 55 (1984) 2935.
87. C.G.Olson, J.H.Sexton, D.W.Lynch, A.J.Bevolo, H.R.Shanks, B.N.Harmon, W.Y.Ching and D.M.Wieliczka, Solid State Commun. 56 (1985) 35.
88. L.Xinjiao, X.Zechuan, H.Ziyou, C.Huazhe, S.Wuda, C.Zhongcai, Z.Feng and W.Enguang, Thin Solid Films, 139 (1986) 261.
89. J.Pastrnak and L.Roskovcova, Phys.Stat.Sol. 26 (1968) 591.
90. V.V.Michailin, V.E.Oranovskii, S.Pacesova, J.Pastrnak and A.S.Salamatov, Phys.Stat.Sol. B55 (1973) K51.
91. J.Laimer, H.Stori and P.Rodhammer, J.Vac.Sci.Tecnol., A7(1989)2952. 1000-3300, CVD

92. S.Schiller, G.Beister, J.Reschke and Hoetzsch J.Vac.Sci.Tecnol., A5(1987)2180. 3200, sputter
93. M.V.Kuznetsov, M.V.Zhuravlev, E.V.Shalayeva and V.A.Gubanov, Thin Solid Films, 215(1992)1
94. E.O.Ristolainen, J.M.Molarius, A.S.Korhonen and V.K.Lindroos, J.Vac.Sci.Tecnol. A5(1987)2184
95. C.Ernsberger, J.Nickerson, T.Smith, A.E.Miller and D.Banks, J.Vac.Sci.Technol., A4(1986)2784.
96. N.C.Saha and H.G.Tompkins, J.Appl.Phys.72(1992)3072.
97. C.Ernsberger, J.Nickerson, T.Smith, A.E.Miller and D.Banks, J.Vac.Sci.Tecnol., A4(1986)2784.
98. N.Kumar, J.T.McGinn, K.Pourrezaei, B.Lee and E.C.Douglas, J.Vac.Sci.Technol.,A6(1988)1602.
99. J.Laimer, H.Stori and P.Rodhammer, J.Vac.Sci.Technol. A7(1989)2952.
100. S.Jiang, D.Peng, X.Zhao, L.Xie and Q.Li, Appl. Surface Sci. 84(1995)373.
101. S.Hofmann, Thin Solid Films, 193/194(1990)648.
102. T.Ikeda and H.Satoh, Thin Solid Films, 195(1991)99

LIST OF PUBLICATION

[Related paper]

1. "The Preparation of NaCl-type $Ti_{1-x}Al_xN$ Solid Solution"
   S. Inamura, K. Nobugai, F. Kanamaru, Journal of Solid State Chemistry **68**, 124-127(1987)
2. "Preparation of wurtzite-type $Al_{1-x}Ti_xN(0 \leqq x \leqq 0.17)$ Thin Films by Rf-sputtering and Their Optical Absorption" S. Inamura, K. Nobugai, F. Kanamaru and S. Emura, Chemistry Express **2**, 539-542 (1987)
3. "Structural Chemical Study on Band Gap of $Ti_{1-x}Al_xN$ Solid Solution" M. Takahashi, S. Inamura, K. Nobugai, F. Kanamaru, J. Jpn. Soc. Powder and Powder Met., **34**, 502 (1987)
4. "Resistance against Oxidation of $Ti_{1-x}Al_xN$ Films Prepared by RF-Sputtering Method" S. Inamura, M. Takahashi, K. Nobugai, F. Kanamaru, H. Miyamoto, J. Soc. Mat. Sci., Japan, **37**, 83 (1988)
5. "Durability Against Oxidation for $Ti_{1-x}Al_xN$ Thin Films"
   M. Takahashi, S. Inamura, K. Nobugai, F. Kanamaru
   MRS Int'l. Mtg. on Adv. Mats. Vol. 4 c1989 Materials Research Society.
6. "Investigation of Oxidation for $Ti_{1-x}Al_xN$ Thin Films by XPS"
   S. Inamura, M. Takahashi and F. Kanamaru, to be submitted J. Mat. Sci.
7. "Investigation of Crystal Structure of $Ti_{0.3}Al_{0.7}N$ by XANES
   S. Inamura, M. Takahashi,... and F. Kanamaru, in preparation

[Other paper]

1. "Electron Microscopy Study of the "Cubic" Perovskite Phase $SrFe_{1-x}V_xO_{2.5+x}$ $(0.05 \leq x \leq 0.1)$ "
   N. Nakayama, M. Takano, S. Inamura, N. Nakanishi and K. Kosuge
   Journal of Solid State Chemistry **71**, 403-417(1987)
2. "Preparation of Al_2O_3 Ceramics by Low Pressure Injection Molding Method"
   K. Miyamoto, Y. Takahashi, S. Inamura, and H. Miyamoto,
   J. Jpn. Soc. Powder and Powder Met., **34**, 378(1987)
3. "Oxygen Deficiency of $Ba_2YCu_3O_{7-\delta}$ and Superconductivity"
   H. Miyamoto, K. Miyamoto, S. Inamura and Y. Takahashi,
   J. Jpn. Soc. Powder and Powder Met., **34**, 617(1987)
4. "Preparation of $BiSrCaCu_2O_x$ and Its Superconductivity"
   H. Miyamoto, K. Miyamoto, S. inamura and Y. Takahashi,
   J. Jpn. Soc. Powder and Powder Met., **34**, 617(1987)
5. "Preparation of Superconductive Ceramics of Bi-Sr-Ca-Cu-O System and Its Superconductivity"
   H. Miyamoto, K. Miyamoto, S. Inamura and Y. Takahashi,
   J. Jpn. Soc. Powder and Powder Met., **35**, 927(1988)

6. "Preparation of Si_3N_4 Ceramics by Low Pressure Injection Molding Method"
K. Miyamoto, H. Miyamoto, S. Inamura and Y. Takahashi,
J. Jpn. Soc. Powder and Powder Met., **35**, 633 (1988)
7. "Preparation of Si_3N_4 Ceramics by Low Pressure Injection Molding Method(II)"
K. Miyamoto, H. Miyamoto, S. Inamura and Y. Takahashi,
J. Jpn. Soc. Powder and Powder Met., **36**, 192 (1989)
8. "Preparation of Single Phese of Bi System Superconducting Ceramics"
H. Miyamoto, K. Miyamoto, S. Inamura and Y. Takahashi,
J. Jpn. Soc. Powder and Powder Met., **36**, 482(1989)
9. "Preparation of Superconductive Ceramics of $Bi_2Sr_2Ca_2Cu_3O_x$ by Sol-Gel Method"
H. Miyamoto, K. Miyamoto, S. Inamura and Y. Takahashi,
J. Jpn. Soc. Powder and Powder Met., **36**, 485(1989)
10. "Growth of Thin Plates of BGO($Bi_{12}GeO_{20}$) Single crystal by EFG Method"
K. Miyamoto, Y. Takahashi, S. Inamura and H. Miyamoto,
J. Jpn. Soc. Powder and Powder Met. **37**, 31(1990)
11. "Synthesis of Ti-Al Intermetallic Compounds by HIP-reaction Sintering"
A. Kakitsuji, M. Tanihara, H. Miyamoto, Y. Takahashi, M. Mori, K. Miyamoto, and S. Inamura,
J. Jpn. Soc. Powder and Powder Met. **37**, 665(1990)
12. "Low Pressure Injection Molding and HIP Sintering of Al_2O_3 of High Purity"
K. Miyamoto, S. Inamura, Y. Takahashi and H. Miyamoto,
J. Jpn. Soc. Powder and Powder Met. **38**, 782, (1991)
13. "HIP Sintering of the Fine Powder in the System ZrO_2(3Y)-Al_2O_3"
S. Inamura, K. Miyamoto, Y. Takahashi and H. Miyamoto,
J. Jpn. Soc. Powder and Powder Met., **39**, 1072(1992)
14. "Formation, Transformation and Sintering of ZrO_2-MgO Composition Prepared from Alkoxides"
J. Saiki, K. Hirota, O. Yamaguchi, S. Inamura, H. Miyamoto, N. Shiokawa, K. Tsuji,
Br. Ceram. Trans., **92**, 161 (1993)
15. "High Fracture Toughness of ZrO_2 Solid-solution Ceramics with Nanometre Grain Size in the System ZrO_2-Al_2O_3"
S. Inamura, H. Miyamoto, Y. Imaida, M. Takagawa, K. Hirota, O. Yamaguchi
J. Mat. Sci. Lett., **12**, 1368 (1993)
16. "Metastable Zirconia Phases Prepared from Zirconium Alkoxide and Yttrium Acetylacetonate. Part 1: Formation and Characterization of Metastable Zirconia Solid Solutions"
S. Fujii, M. Tamamaki, S. Inamura, H. Miyamoto, and S. Kume,
Mat. Res. Bull., **28**, 877(1993)
17. "Formation of Alkoxy-derived Yttrium Aluminates in the Al_2O_3-rich Region"
K. Hirota, O. Yamaguchi, S. Inamura, and H. Miyamoto,
J. Jpn. Soc. Powder and Powder Met., **40**, 789(1993)

18. "Formation of Zirconia Solid Solutions Containing Alumina Prepared by New Preparation Method"
K. Ishida, K. Hirota, O. Yamaguchi, H. Kume, S. Inamura and H. Miyamoto
J. Am. Ceram. Soc., **77**, 1391-95, (1994)

19. "Formation and Sintering of Yttria-Doped Tetragonal Zirconia with 50 mol% Alumina Prepared by the Hydrazine Method"
S. Kimoto, K. Hirota, O. Yamaguchi, H. Kume, S. Inamura and H. Miyamoto
J. Am. Ceram. Soc., **77**, 1694-96, (1994)

20. "Formation of Alumina/Zirconia(3mol% Yttria) Composite Powders Prepared by the Hydrazine Method"
K. Yamakata, K. Hirota, O. Yamaguchi, H. Kume, S. Inamura and H. Miyamoto,
J. Am. Ceram. Soc., **77**, 2207-208, (1994)

21. "Hot Isostatic Pressing of Tetragonal ZrO_2 Solid-solution Powders Prepared from Acetylacetonates in the system ZrO_2-Y_2O_3-Al_2O_3"
H. Watanabe, K. Hirota, O. Yamaguchi, S. Inamura, H. Miyamoto, N. shiokawa, and K. Tsuji,
J. Mat. Sci., **29**, 3719-3723(1994)

22. "Formatin and Hot Isostatic Pressing of ZrO_2 Solid Solution in the System ZrO_2-Al_2O_3"
S. Inamura, H. Miyamoto, Y. Imaida, M. Takagawa, K. Hirota, and O. Yamaguchi,
J. Mat. Sci., **29**, 4913-4917(1994)

23. "Metastable Zirconia Phases Prepared from Zirconium Alkoxide and Yttrium Acetylacetonate Part 2: Hot Isostatic Pressing of Tetoragonal Zirconia Solid Solution Powders"
M. Shimazaki, K. Hirota, O. Yamaguchi, S. Inamura, H. Miyamoto, N. Shiokawa, and K. Tsuji,
Mat. Res. Bull., **29**, 277(1994)

24. "Sintering and Characterization of Yttoria-stabilized Cubic Zirconia with Alumina Derived from Solid Solution"
M. Fukuya, K. Hirota, O. Yamaguchi, H. Kume, S. Inamura, H. Miyamoto, N. Shiokawa, and R. Shikata,
Mat. Res. Bull., **29**, 619(1994)

25. "Fabrication and Mechanical Properties of Yttria-Doped Ceramics Containing Alumina"
J. Jpn. Soc. Powder and Powder Met., **41**, 790(1994)
H. Watanabe, K. Hirota, O. Yamaguchi, H. Kume, S. Inamura and H. Miyamoto

26. "Formation and HIP Sintering of ZrO_2 Solid Solution in the System ZrO_2-Al_2O_3"
S. Inamura, H. Kume, H. Miyamoto, Y. Imaida, K. Hirota, O. Yamaguchi, N. Shiokawa and K. Tsiji,
J. Jpn. Soc. Powder and Powder Met., **41**, 955(1994)

27. "Sintering of Alumina-Zirconia Composite Powders Prepared from Aluminum Sulfate and Zirconium"
H. Kume, S. Inamura, and H. Miyamoto
Isopropoxide" J. Soc. Mat. Sci., Japan, **43**, 1042(1994)

ACKNOWLEDGEMENTS

The author would like to express his sincere thanks to Professor F.Kanamaru for the encouragement and simulating discussions. It is indeed a great pleasure for the author to have two supervisors for this thesis, Professor K.Kushi and T.Kawai of Faculty of Science and The Institute of Scientific and Industrial Reseach of Osaka university, respectively. The author expresses his thanks to Dr.K.Nobugai and Dr.M.Takahashi for helpful discussions and advices during the course of this study. Thanks are due to Dr.K.Koto, Dr.H.Horiuchi and Dr.S.Kikkawa for their helpful discussions and encouragement. The author would like to thank people in Kanamaru Lab. in ISIR Osaka University.